

**Development of a Simple Model for Estimating
Evapotranspiration Using Remote Sensing
(Sim-ReSET)**

January 2008

Zhigang SUN

**Development of a Simple Model for Estimating
Evapotranspiration Using Remote Sensing
(Sim-ReSET)**

**A Dissertation Submitted to
the Graduate School of Life and Environmental Sciences,
the University of Tsukuba
in Partial Fulfillment of the Requirements
for the Degree of Doctor of Philosophy in Science
(Doctoral Program in Integrative Environmental Sciences)**

Zhigang SUN

Acknowledgements

First and foremost, I would like to thank my parents and my young sister for all the supports they have given me throughout my education. Their encouragements got me through my stressful times. No doubt, this dissertation would not have been possible without them.

I gratefully acknowledge the financial sponsorship of the Asia-Pacific Environmental Innovation Strategy (APEIS) project launched by the Ministry of Environment, Japan. It funded me through a research assistant fellowship in the National Institute for Environmental Studies, Japan (NIES). Special thanks go to Dr. Qinxue Wang (Director of Asian Water Environment Section, NIES) and Professor Masataka Watanabe (Keio University) for insights, encouragements and supports at NIES. I cannot say enough about what I have learned both academically and professionally from Dr. Qinxue Wang and Professor Masataka Watanabe.

I cannot thank enough Professor Takehiko Fukushima and Assistant Professor Bunkei Matsushita for being such great advisors. I have learned from them much more than what is in this thesis. I have always appreciated the focus they have provided to this study but at the same time allowed me the freedom to explore the world. Professor Michiaki Sugita and Assistant Professor Kenlo Nishida have supported me in my graduate education, too. I am incredibly grateful that I had the opportunity to get advises and comments from them. Their contributions have made my work better.

Operating a field experiment in the Yucheng Experimental Station (YES, a national field experimental station of Chinese Academy of Sciences) in China required helps and dedications from local individuals. Lots of thanks are given to Professor Zhu Ouyang (Director of the YES) for providing intensive data and good comments on my work. Mr. Zhenmin Liu maintained the field experiment all the time. His superior work made my job easier and my thesis better.

Throughout my graduate studies in the University of Tsukuba, I had an incredible time and I will be sad to leave. The friends I have developed while I was here can take all the credit. I thank Dr. Shigeru Mizugaki, Dr. Kazuki Nanko, Mr. Yoshifumi Wakiyama, Mr. Hiroaki Mikami, Mr. Luki Subehi, Ms. Akane Ito, Ms. Yuna Otsuki, Ms. Asami Furuya, Mr. Fan YANG and Mr. Ralph Estal for getting me away from my thesis. I thank the people of Dr. Youichi Oyama, Dr. Zhao Zhang, Dr. Hiroaki Kato, Dr. Medeok Han, Mr. Koichi Kamiya and Ms. Hitomi Yoshida for all the stimulating conversations, friendship and help they gave me. The experience truly enriched my time at the university.

Last but not least, I thank our research team (Asian Water Environment Section, NIES) led by Dr. Qinxue Wang. I thank Dr. Chen Liu, Dr. Makoto Ooba, Dr. Tonghua Wu and Dr. Qinan Xiao for their kind helps. I will never forget the good time with them in NIES.

Contents

Acknowledgements.....	i
Contents.....	iii
Abstract.....	v
List of tables.....	ix
List of figures.....	x
List of abbreviations.....	xiv
List of symbols.....	xvi
Chapter 1 Introduction.....	1
1.1 Evapotranspiration and its vital role.....	1
1.2 Review of <i>ET</i> estimation methods using remote sensing data.....	2
1.3 Study purpose, structure and content in this dissertation.....	12
Chapter 2 Evaluation of a Previous Evapotranspiration Model over Winter Wheat Fields in North China Plain (MOD16).....	25
2.1 Introduction.....	25
2.2 Description of MOD16 algorithm.....	26
2.3 Study area and data used.....	29
2.4 Results and discussions.....	32
2.5 Conclusion.....	47

Chapter 3	Development of a Simple Remote Sensing Evapotranspiration Model (Sim-ReSET model): Algorithm and Parameterizations	53
3.1	Introduction	53
3.2	Algorithm of Sim-ReSET model	53
3.3	Parameterizations in Sim-ReSET model	56
3.4	Conclusion	61
Chapter 4	A New Method to Obtain “Dry and Wet Points” for Sim-ReSET Model Using Subpixel Information	64
4.1	Introduction	64
4.2	Methods	66
4.3	Results	73
4.4	Discussions	79
4.5	Conclusion	83
Chapter 5	Mapping <i>ET</i> from satellite data by Sim-ReSET model and <i>in situ</i> Validation	88
5.1	Introduction	88
5.2	Mapping <i>ET</i> from satellite data by the Sim-ReSET model	88
5.3	Sensitivity analysis and validation	91
5.4	Conclusions	101
Chapter 6	General Conclusions	103

Abstract

Evapotranspiration (*ET*) is a combination of evaporation and plant transpiration from land surface to atmosphere. It is one important component of the terrestrial surface water and energy balances, and thus *ET* is essential for understanding the water cycle, climate dynamics and terrestrial ecosystem productivity. Many water and land managements require land surface *ET* information from a range of spatial and temporal scales. Compared with limited ground observation networks, remote sensing (RS) can provide unprecedented coverage data for *ET* estimation on a global scale. Many studies have proposed models to estimate *ET* using RS data. However, these models still depend on the ground data or the reanalyzed meteorological data, which blocks regular and real-time *ET* retrieval.

The purpose of this study is to develop a new *ET* model based solely on RS data. Firstly, a previous RS-*ET* model (MOD16) was evaluated. Secondly, a new *ET* model (Sim-ReSET) was developed independent of ground data. Thirdly, a new method was proposed to obtain “dry & wet points” for the Sim-ReSET model. Finally, *ET* was mapped from satellite data by the Sim-ReSET model, and validation was carried out using ground data.

(1) Evaluation of a previous ET model (MOD16)

MOD16 developed by Nishida et al. (2003) was a practical *ET* model for global MODIS *ET* mapping, which minimized the use of ground data. MOD16 was validated in USA, and it was reported that the maximum estimation error occurred in the crop ecotype. In this study, intensive ground data were used to validate the MOD16 model in winter wheat fields of the North China Plain (NCP) in 2002. It was found that accurate estimations of canopy resistance and aerodynamic

resistance still depended on the ground data. Without the support of ground data, canopy resistance and aerodynamic resistance were essentially underestimated in MOD16. If canopy resistance was estimated using ground data and if aerodynamic resistance was estimated using sophisticated equations and ground data, evaporation fraction (EF) and ET became more consistent with both observations from the eddy covariance system and estimations from the Penman-Monteith method. This result shows that although MOD16 performs well when mapping ET , the ground data are still required.

(2) Development of Sim-ReSET model: algorithm & parameterizations

In order to obtain ET based solely on RS data, a dry point (dry bare soil without ET) was introduced to remove the requirement of aerodynamic resistance. Requirement of canopy resistance was also avoided by estimating ET as a residual of the land surface energy balance. Therefore, input requirements for the Sim-ReSET model were only net radiation, soil heat flux, canopy height, surface temperature (T_s), air temperature, and parameters related to the dry point of which all could be obtained from RS observations in the model. For examples, net radiation can be estimated by the scheme of Bisht et al. (2005); bare soil heat flux can be estimated using a scaled temperature; and canopy height can be obtained from a look-up table based on the IGBP classification in this study. The dry point and air temperature can be obtained from the VI- T_s diagram (2D plot of vegetation index (VI) and T_s).

(3) A new method to obtain “dry & wet points” for Sim-ReSET model

In the VI- T_s diagram, the dry point is defined as a pixel with maximum T_s and minimum VI, and the wet point is defined as a pixel with minimum T_s and maximum VI. Air temperature is close to T_s of the wet point. If both dry and wet

points can be obtained, a right triangle of VI-Ts diagram can be readily defined. The traditional method cannot define a correct VI-Ts diagram in both cases of rainy season and narrow range of VI. A new method based on subpixel information of MODIS Ts was proposed to define the VI-Ts diagram in this study. Firstly, MODIS Ts was decomposed into surface temperatures for vegetation and soil. Secondly, minimum vegetation Ts and maximum soil Ts were used to determine wet and dry points, respectively. This method was tested in a 30 km×30 km area in the NCP through 2003 using ground data and MODIS RS data. Wet and dry points obtained from my proposed method were compared with those obtained using the ground data. The results showed that my proposed method could define correct VI-Ts diagrams throughout the whole year, even for both cases of rainy season and narrow range of VI.

(4) Mapping *ET* from satellite data by Sim-ReSET model and *in situ* validation

A dry point experiment was conducted in the NCP in 2006. This experiment was designed for sensitivity analysis and the model's validation without using RS data. The advantage of validation without using RS data is that the potential error of RS data is not brought into the evaluation of model's mechanism. The result showed that the Sim-ReSET model could obtain *ET* with a root mean square error (RMSE) of 48.94 W/m² over a cotton field. In addition, the results of sensitivity analysis showed that the most sensitive variables were temperatures, and that vegetation canopy height had a negligible effect on the model. The Sim-ReSET model and the original MOD16 model were used to map *ET* over the NCP through 2003 using MODIS products. Pixel-based *ET* was validated using the ground flux data obtained from the eddy covariance system. Results showed that the accuracy of the Sim-ReSET model was close to those of other models or algorithms depending on

ground data. RMSE of *ET* estimated by the Sim-ReSET model was 58.74 W/m² while RMSE of *ET* estimated by the original MOD16 model was 65.48 W/m². Because atmospheric stratification corrections were ignored, *ET* showed a little overestimation, especially when solar radiation and air temperature were high. In order to remain the simplicity of Sim-ReSET model, the neutral atmospheric stratification was adopted, although some accuracies of the model were lost.

In summary, the previous *ET* models could obtain good results if intensive ground data were given. The Sim-ReSET model was developed with the purpose of mapping *ET* only by RS data. The accuracy of the Sim-ReSET model mainly depended on the accuracies of wet and dry points, which were determined effectively by using subpixel information of surface temperature. In this study, the accuracy of Sim-ReSET model was consistent with the accuracies obtained by previous studies. On cloudy days, surface temperature cannot be observed by satellite sensors. Solar radiation is not readily estimated on cloudy days, too. Therefore, the Sim-ReSET method can only be used on cloud-free days.

Keywords: evapotranspiration, remote sensing, surface temperature, vegetation index, VI-Ts diagram, wet and dry points, MOD16 model, Sim-ReSET model

List of tables

Table 2-1 Results of VI-Ts diagram analysis.....	31
Table 2-2 Winter wheat physiological temperatures for the canopy resistance mode in MOD16 and in its different growing phases in NCP.....	36
Table 3-1 The look-up table for vegetation canopy height based on the IGBP land cover classifications.....	60
Table 4-1 Statistics of the ASTER and MODIS datasets related to Ts and NDVI on May 9 2003.....	69
Table 4-2 Statistics of MODIS_NDVI and MODIS_Ts on 12 cloud-free days in 2003.....	71
Table 4-3 Comparisons of MODIS_T _{veg} and MODIS_T _{soil} with the normalized 90m-ASTER-Ts of pure vegetation and soil on May 9 2003.....	74
Table 4-4 Surface temperatures of dry and wet points from the ground data, the proposed and the traditional methods using MODIS data.....	78
Table 5-1 Results of sensitivity analyses for the input variables in Sim-ReSET model.....	96

List of figures

Fig.1-1	The diagram of vegetation index (VI) and surface temperature (Ts).....	9
Fig.2-1	The VI-Ts diagram used in MOD16.....	28
Fig.2-2	The study area, a 20 km × 20 km square area, in the North China Plain. YES locates at the center of the study area. Its main land use is irrigated cropland, shown as grey on the map.....	30
Fig.2-3	The estimation and observation of solar shortwave radiation when the Terra satellite passed over the Yucheng Experimental Station (YES) from DOY1 to DOY161, 2002, every 16 days.....	33
Fig.2-4	Albedo at 10:30, 11:00, 11:30 (YES, 2003). Here, albedo is calculated as the ratio of observational upward shortwave radiation to downward shortwave radiation at YES in 2003.....	34
Fig.2-5	Sensitivity of $f_l(T_a)$ for the different growing phases to winter wheat physiological temperatures (minimum, optimal and maximum). Phase definition is based on Gao (1995).....	36
Fig.2-6	Seasonal variations of LAI and canopy resistance estimated in MOD16 and by the modified method.....	37
Fig.2-7	Comparisons of estimated wind speed and aerodynamic resistance above the vegetation surface with the observations at 10 m height at 11:00 am. a is estimated directly by the original MOD16 algorithm; b is estimated by the modified algorithm; c is observations from the standard meteorological station. Solid and dashed lines represent wind speed and aerodynamic resistance, respectively.....	41
Fig.2-8	Flow chart of aerodynamic resistance estimation over vegetation surface, where ω is used to control the quality of wind speed estimation over bare soil surface.....	42

Fig.2-9	Comparison of MOD16 original and modified vegetation EF , P-M calculated EF and eddy covariance measured EF .	43
Fig.2-10	Sensitivity analysis of air temperature, canopy resistance (r_c) and aerodynamic resistance (r_a) to EF of vegetation. Assuming r_c and r_a in the possible range of 5-400 s/m, r_c / r_a is within 0.0125-80.	44
Fig.2-11	Comparison of air temperatures observed and estimated by MOD16 with the VI-Ts method.	45
Fig.2-12	Seasonal variations in ET estimated from the original and modified (this study; Modified) MOD16, P-M calculations based on in-situ measurement variables (P-M) and eddy covariance measurements (Eddy) over a winter wheat field.	46
Fig.2-13	Comparisons of ET estimated by the original MOD16 algorithm and modified algorithm to ET calculated by the P-M method.	46
Fig.3-1	The upper boundary of atmospheric surface layer used to remove r_a calculation.	54
Fig.3-2	Seasonal variations of leaf area index (LAI) and the ratio of soil heat flux to net radiation in Yucheng Experimental Station in 2006.	58
Fig.3-3	Seasonal variations of soil water content (SWC) and the ratio of soil heat flux to net radiation observed over bare soil in Yucheng Experimental Station in 2006.	58
Fig.3-4	Linear relationships between crops' canopy heights and LAI.	60
Fig.4-1	The concept of a VI-Ts diagram. Point A is called the dry point, and Point C is called the wet point in the VI-Ts diagram.	66
Fig.4-2	Study area. On the right is the ASTER false-color image (UTM-N50, WGS-84, 15 m, Band 3, 2, 1). The red part is vegetation, mainly winter wheat.	67

Fig.4-3	Comparisons of the MODIS-Ts with (a) the 1 km-ASTER-Ts and (b) the normalized 1 km-ASTER-Ts.....	69
Fig.4-4	Procedure scheme of identifying the ASTER 90 m-pixels of pure soil and vegetation and obtaining Ts of pure soil and vegetation within a pixel with 1 km resolution.....	70
Fig.4-5	The trapezoidal VI-Ts diagram for obtaining surface temperatures of soil and vegetation.....	73
Fig.4-6	The VI-Ts diagrams on May 9 2003 (a) defined using the 90m-ASTER-Ts of pure vegetation and soil, (b) defined by the proposed method using MODIS data, and (c) defined by the traditional method using MODIS data. In Fig. 4-5a and 4-5b, yellow and green points are component Ts of soil and vegetation, respectively. In Fig. 4-5c, yellow circles (o) are pixels for defining the dry edge.....	75
Fig.4-7	The VI-Ts diagrams defined by the proposed (black) and traditional (red) methods using MODIS data through 2003. The horizontal axis is vegetation cover fraction, and the vertical axis is surface temperature in°C.....	77
Fig.4-8	Daily rainfall within the half month just before Jul. 26 (a), and Sep. 21 (b) in 2003.....	79
Fig.4-9	Description of several dry points in the same VI-Ts diagram.....	81
Fig.5-1	Flowchart of the Sim-ReSET model.....	89
Fig.5-2	Net radiation map over the North China Plain on DOY133 of 2003.....	90
Fig.5-3	Soil heat flux map over the North China Plain on DOY133 of 2003.....	90
Fig.5-4	Evapotranspiration map over the North China Plain on DOY133 of 2003.....	90

Fig.5-5	Evaporation fraction map over the North China Plain on DOY133 of 2003.	91
Fig.5-6	Dry point experiment design.	92
Fig.5-7	Time series of net radiation and soil heat flux.	92
Fig.5-8	Time series of surface temperature.	93
Fig.5-9	Time series of soil surface water content.	93
Fig.5-10	The APEIS-Flux station in the cotton field.	94
Fig.5-11	Relationship between the height of the upper boundary of the ASL and the sensible heat transfer function. One line of $f(H)$ was estimated using the dataset at 11:30 of one day from DOY263-319.	94
Fig.5-12	Comparison of ET between the measurements by the eddy covariance system and the estimations using the ground data.	95
Fig.5-13	Sensitivity analyses of the input variables in Sim-ReSET model. X-axis is ET estimations without any changed variable. Y-axis is ET estimations while only one variable is changed.	97
Fig.5-14	Comparison of net radiation estimated by Sim-ReSET model and that measured on the ground.	98
Fig.5-15	Comparison of soil heat flux estimated by Sim-ReSET model and that measured on the ground.	99
Fig.5-16	Comparison of ET estimated by Sim-ReSET model (a) and by the MOD16 model (b) using the measured ET on the ground.	100
Fig.5-17	Comparison of EF estimated by the Sim-ReSET model (a) and by the MOD16 model (b) using the measured EF on the ground.	100

List of abbreviations

APEIS	Asia-Pacific Environmental Innovation Strategy Project
AML	Atmospheric mixed layer
ASL	Atmospheric surface layer
ASTER	Advanced Spaceborne Thermal Emission Reflection Radiometer
ATSR	Along track scanning radiometer
AVHRR	Advanced very high resolution radiometer
CO ₂	Carbon dioxide
EF	Evaporation fraction
EOS	Earth Observation System
ET	Evapotranspiration
EVI	Enhanced vegetation index
GOES	Geostationary Operational Environmental Satellites
LAI	Leaf area index
MAE	Mean absolute error
METEOSAT	Meteorological satellite
MODIS	MODerate-resolution Imaging Spectroradiometer
MOS	Monin-Obukhov similarity
NASA	National Aeronautics and Space Administration
NCP	North China Plain
NDVI	Normalized difference vegetation index
NOAA	National Oceanic and Atmospheric Administration, USA
P-M	Penman-Monteith equation
P-T	Priestley-Taylor equation
RMSE	Root mean square error
SEBAL	Surface energy balance algorithm for land

SEBS	Surface energy balance system
Sim-ReSET	Simple remote sensing evapotranspiration model
SSM/I	Special Sensor Microwave/Imager
SVAT	soil-vegetation-atmospheric transfer
TM	Thematic mapper
VI	Vegetation index
VPD	Vapor pressure deficit
YES	Yucheng Experimental Station

List of symbols

H	sensible heat flux, W/m^2
ET	latent heat flux or evapotranspiration, W/m^2
EF	evaporation fraction, 0-1
R_n	net radiation, W/m^2
G	soil heat flux, W/m^2
Q	available energy ($R_n - G$), W/m^2
f_{veg}	vegetation cover fraction, 0-1
ρ	air density, kg/m^3
C_p	heat capacity of air at constant pressure, J/kg/K
e	water vapor pressure, Pa
e_{sat}	saturated water vapor pressure, Pa
Δ	the slope of the curve relating saturated water vapor pressure to air temperature, Pa/K
γ	the psychrometric constant, Pa/K
T_s	surface temperature, $^{\circ}\text{C}$
T_a	air temperature, $^{\circ}\text{C}$
r_a	aerodynamic resistance for heat transfer, s/m
r_{excess}	excess resistance, s/m
r_s	canopy surface resistance, s/m
k	von Karman constant, 0.4
A	the height of the upper boundary of atmospheric surface layer, m
z	reference height, m
z_{0m}	roughness length for momentum, m

z_{0h}	roughness length for heat, m
u	wind speed at reference height, m
u^*	friction velocity, m/s
d_0	zero plane displacement height, m
L	Monin–Obukhov length, m
ψ_M	stratification correction function for momentum
ψ_H	stratification correction function for heat
R_S^\downarrow	downward shortwave radiation, W/m ²
R_S^\uparrow	upward shortwave radiation, W/m ²
R_L^\downarrow	downward long wave radiation, W/m ²
R_L^\uparrow	upward long wave radiation, W/m ²
α	land surface albedo
ε_a	air emissivity
ε_s	land surface emissivity
S_0	solar constant at the atmospheric top, 1367 W/m ²
θ	solar zenith angle
σ	Stephan-Bolzmann constant, 5.67×10^{-8} W/m ² /K ⁴
e_0	vapor pressure at screen level, Pa
Γ	the ratio of soil heat flux to net radiation
a	the Priestley-Taylor parameter, 1.26

Chapter 1

Introduction

1.1 Evapotranspiration and its vital role

Evapotranspiration (*ET*) is a sum of evaporation and transpiration from land surface to atmosphere. Evaporation accounts for the movement of water to the air from sources such as soil, canopy interception, and water bodies. Transpiration accounts for the movement of water within a plant and the subsequent loss of water as vapor through stomata in its leaves (Allen et al., 1998). *ET* is a very important component of the terrestrial surface water balance which also includes precipitation, runoff, streamflow and soil water storage (Rivas and Caselles, 2004; Mu et al., 2007), thus *ET* is essential for understanding water cycle, climate dynamics and terrestrial ecosystem productivity (Willmott et al., 1985; Potter et al., 1993; Churkina et al., 1999; Nemani et al., 2002, Mu et al., 2007). About 64% of the precipitation on the continents is evapotranspired on a global scale, of which about 97% is evapotranspired from land surface, and 3% is evaporated from open-water (Rivas and Caselles, 2004). In some specific zones of the world such as semiarid and arid regions, approximately 90% of the precipitation can be evapotranspired (Varni et al., 1999). Therefore, many water resource, agricultural and forest management applications, such as agricultural water distribution, crop growth monitoring, drought detection and assessment, desert restoration, and deforestation, require the knowledge of surface *ET* from a range of spatial and

temporal scales (Allen et al., 1998; Dodds et al., 2005; Keane et al., 2002; Kustas & Norman, 1996; Meyer, 1999; McVicar and Jupp, 1998; Rango and Shalaby, 1998; Raupach, 2001).

The ground observation networks cover only a small portion of global land surface, thus the regular measurements and calculations at point scale cannot meet the requirements for *ET* estimation over a large scale. Satellite remote sensing provides unprecedented global coverages of critical hydrological, vegetation, soil and topographic data which are logistically and economically impossible to obtain from ground-based observation networks. Remote sensing has been considered as the most promising tool for *ET* estimation in the large spatial scale. With the unceasing efforts by many researches, *ET* has been estimated from the regional scale (*e.g.*, Ambast et al., 2002; Cleugh, 2007; Holwill et al., 1992; Matsushima, 2007; Seguin et al., 1989; Seguin et al., 1994) to the global scale (*e.g.*, Mu, 2007). However, these studies still depend on the ground measurements or the reanalyzed meteorological data. In order to obtain the regional, even global *ET*, some attempts were done to reduce the use of ground data in *ET* algorithms (Nishida et al., 2003a, b; Qiu et al., 1998; Qiu et al., 2006; Venturini et al, 2007). Following these efforts, the purpose in this study is to develop a simple remote sensing *ET* model fully independent of the ground measurement.

1.2 Review of *ET* estimation methods based on remote sensing

For the field scale, *ET* can be directly measured using lysimeter, evaporation pan, Bowen ratio system and eddy covariance system. If intensive ground micrometeorological data are ready, *ET* can also be calculated using some sophisticated equations, such as the Penman-Monteith equation. For larger scales, however, *ET* is usually estimated using remote sensing data. From previous studies, *ET* estimation methods based on remote sensing can be divided into 6 groups:

- (1) *ET* as an output of simulation models;
- (2) Empirical methods;
- (3) Methods related to Penman-Monteith equation (P-M);
- (4) Land surface energy balance methods while *ET* is estimated as a residual in the land surface energy balance equation;
- (5) Priestley-Taylor method and its revised versions (P-T);
- (6) *ET* estimated from the relationships of VI-Ts or Ts-Albedo.

1.2.1 *ET* as an output of simulation models

ET estimation is an important component in many simulation models (Running et al., 1989). Many researchers used simulation models to map *ET* while remote sensing data were taken as a part of input data. Olioso et al. (1999) estimated *ET* and photosynthesis by combining remote sensing data into a soil-vegetation-atmosphere transfer model (SVAT). Ridder (2000) obtained energy and water transfers at the land-atmosphere interface by combining a land surface model and two remotely sensed variables, vegetation cover fraction (f_{veg}) estimated from AVHRR/NDVI and soil moisture retrieved from the SSM/I polarization difference temperature. Houborg and Soegaard (2004) simulated the regional ecosystem CO₂ and water vapor exchange for an agricultural land using the two-leaf model (De Pury and Farquhar, 1997; Wang and Leuning, 1998) and NOAA/AVHRR and Terra/MODIS data. Chen et al. (2005) mapped *ET* using a distributed hydrological model and remote sensing data. Except for meteorological, topographical and soil data, the model utilized Landsat TM data to characterize the distributions of vegetation types and LAI. Zhang and Wegehenkel (2006) integrated MODIS data into a simple grid-based soil water balance model for the spatial simulations of soil water content and *ET*. The same character of all the above simulation models is that these models have good performances to estimate

ET , but depend on intensive ground data.

1.2.2 Empirical methods for ET estimation

The energy source of ET comes from available energy, and the drive force of ET comes from the vapor pressure gradient or air temperature gradient. Some empirical methods for ET estimation using remote sensing data were developed based on the simple relations between ET and its drive factors. [Seguin et al. \(1994\)](#) proposed a simplified equation suggested by [Jackson et al. \(1977\)](#) to estimate daily ET with an error of ± 1 mm/day using NOAA/AVHRR and METEOSAT data,

$$ET_d = R_n + a - b(T_s - T_a) \quad (1-1)$$

where a and b were constants depending on local situations; T_s was retrieved from the NOAA/AVHRR and METEOSAT data; and net radiation and air temperature were measured on ground. [Rivas and Caselles \(2004\)](#) divided the P-M equation into three terms, a radiation term, a surface temperature term, and an aerodynamic term. They found that the latter two items were much stable throughout the whole year, so they defined $ET = aT_s + b$, but a and b must be estimated for a given area using meteorological data. Their results indicated that the error of ET estimates was ± 0.6 mm/day. Using the relations between ET , EVI and T_a , an empirical equation was proposed by [Nagler et al. \(2005a, b\)](#),

$$ET = a(1 - e^{-bEVI})(c / (1 + e^{-(T_a - d)/e})) + f \quad (1-2)$$

where coefficients were determined by the regression analyses between ET and the independent variables.

The above empirical methods can be concluded that ET is a function of some constant coefficients and one or two variables which are readily obtained from remote sensing or ground data. These coefficients should be determined using the

intensive ground measurements when these methods are used for another area or time, which hamper their application at large scales.

1.2.3 ET estimation methods based on Penman-Monteith equation (P-M)

By comparing different methods of *ET* estimation, [Jensen et al. \(1990\)](#) and [Kite and Droogers \(2000\)](#) found that the Penman-Monteith ([Monteith, 1965](#)) equation could provide the most accurate values.

$$ET_{P-M} = \frac{\Delta(R_n - G) + \rho C_p (e_{sat} - e) / r_a}{\Delta + \gamma(1 + r_s / r_a)} \quad (1-3)$$

[Cleugh et al. \(2007\)](#) estimated regional *ET* using MODIS data and the P-M equation where a surface conductance algorithm was proposed only with leaf area index, and vapor pressure deficit (VPD) was estimated from air temperature. Compared with the observational data from two flux towers in Australia, *ET* was obtained with a good accuracy (RMSE=27W/m², R²=0.74). [Mu et al. \(2007\)](#) extended the algorithm proposed by [Cleugh et al. \(2007\)](#) to a global *ET* algorithm based on MODIS and global meteorological data by (1) adding VPD and minimum air temperature constraints on stomatal conductance; (2) using leaf area index as a scalar for estimating canopy conductance; (3) replacing NDVI with EVI thereby changing the equation for calculation of f_{veg} ; and (4) adding a calculation of soil evaporation to the algorithm proposed by [Cleugh et al. \(2007\)](#). By comparing *ET* estimates with observations from the flux towers, the results of [Mu et al. \(2007\)](#) were better than those of [Cleugh et al. \(2007\)](#). The P-M equation provides a robust approach to estimate land surface *ET*, but it requires many input variables that include wind speed, humidity, air temperature, solar radiation as well as roughness length and vegetation properties, such as canopy height, LAI and canopy resistance ([Choudhury, 1997](#)). Hence, the P-M method is not applicable at large scale if the ground observations are not ready. In order to approach the purposes of both near

truth and minimal use of the ground data, Nishida et al. (2003a, b) developed a dual-source model of ET and evaporation fraction (EF) using remote sensing data, named as MOD16 model. This model used the complementary relationship of the actual (the P-M method) and the potential ET (the P-T method) to obtain the equation of EF for vegetation in which canopy resistance was used to describe vegetation physiology. The relationship of remotely sensed vegetation index and surface temperature (VI-Ts diagram) was used to estimate EF for bare soil. The main input in MOD16 model came from remote sensing data except some parameters for the calculations of canopy and aerodynamic resistances. Because the MOD16 model was based on the well-known P-M equation, and almost independent of the ground data, MOD16 was taken as an example for evaluation using intensive ground data in this dissertation.

1.2.4 ET as a residual based on the land surface energy balance equation

As a residual of the land surface energy balance equation, ET is obtained after H is estimated while R_n and G can be relatively easy to obtain from remote sensing data. Hence, the key point of ET estimation is to calculate H ,

$$ET = R_n - G - H = R_n - G - \rho C_p \frac{T_s - T_a}{r_a} \quad (1-4)$$

In equation (1-4), all variables can be obtained from remote sensing data except r_a because the value of r_a depends on wind speed which can not be readily retrieved from satellite data. Therefore, this method must depend on the auxiliary ground observations, especially wind speed (e.g., Ambast et al., 2002; French et al., 2005; Gao, 1995; Gao et al., 1998; Melesse and Nangia, 2005; Mallick et al., 2007; Matsushima, 2007; Norman et al., 1995; Zhang et al., 1995).

Aiming to reduce or avoid the r_a calculation, some researches used a reference site to estimate the regional ET . Kustas et al. (1994) extrapolated ET estimates from

one location containing near-surface meteorological data to other areas using an energy balance model which relied primarily on remotely sensed inputs. In SEBAL model (Bastiaanssen et al., 1998a; Bastiaanssen et al., 1998b; Bastiaanssen, 2000), dry land surface elements determined by the albedo- T_s relationship (albedo- T_s diagram) were used to estimate the area-effective momentum flux and friction wind speed, thus regional ET . In SEBS model (Su, 2002; Jia et al., 2003), EF was estimated by means of the sensible and latent heat flux information under two extreme conditions, dry and wet land surfaces. Loheide II and Gorelick (2005) used a scaled value between air temperature and dry surface temperature to estimate ET , and dry surface temperature was estimated using the meteorological data while assuming $ET=0$. The above studies required one or two reference conditions whose determinations still depend on the ground observation. In order to avoid r_a calculation, Qiu et al. (1998; 2006) developed a simple model for soil evaporation using a scaled temperature in which r_a was assumed to be equal to r_a over the dry soil. This model involved only 5 variables all can be obtained from remote sensing,

$$ET = (R_n - G) - \frac{T_s - T_a}{T_{sd} - T_a} (R_n - G)_d \quad (1-5)$$

For applications, this model is not practicable because this model is only for soil. In this dissertation, a new Simple Remote Sensing Evapotranspiration model was developed based solely on remote sensing data, named as Sim-ReSET model, which is applicable not only for soil but also for vegetation canopy.

1.2.5 The Priestley-Taylor method and its revised versions (P-T)

The Priestley-Taylor method can be considered as a simplified version of more theoretical Penman equation (Priestley and Taylor, 1972),

$$ET_{P-T} = a \frac{\Delta}{\Delta + \gamma} (R_n - G) \quad (1-6)$$

Equation (1-6) includes only 5 variables. Δ and γ can be obtained using air temperature. Among these variables, a is the most important one, which is related to EF and Bowen ratio (Bastiaanssen et al., 1996; Crago, 1996; Wang et al., 2006). Over moist surfaces, a approximates 1.26. For dry surfaces, a may be much less than 1.26, which relates to surface moisture, wind speed and air temperature (Davies and Allen, 1973; Komatsu, 2003). Some studies simply used the relationship between remotely sensed vegetation index and surface temperature to determine a (Jiang and Islam, 2001; Batra et al., 2006; Wang et al., 2006). Venturini et al. (2007) proposed a formulation based on Granger's (1989) complementary relationship and the P-T equation, which could be considered as a modified version of the P-T model,

$$ET_{P-T}^F = a \left(\frac{F\Delta}{F\Delta + \gamma} \right) (R_n - G) \quad (1-7)$$

where F is a dimensionless coefficient varying from 0 to 1, where 0 corresponds to $ET = 0$ and 1 to potential ET . F is empirically determined using air temperature, surface temperature, dew point temperature, actual air vapor pressure, and saturated surface vapor pressure, all of which can be obtained from MODIS land and atmospheric products. Therefore, the P-T method and its modified version may be suitable to map EF and ET from remote sensing data without the ground supports, but the empirical determinations of a and F may increase uncertainties and errors.

1.2.6 ET estimated from the relationships of VI-Ts or Albedo-Ts

Some researches defined EF using a scaled temperature in the albedo-Ts diagram, and then ET can be partitioned from available energy (Roerink et al., 2000; Gómez

et al., 2005; Sobrino et al., 2005; Verstraeten et al., 2005; Fan et al., 2007). Compared with the albedo-Ts diagram, the VI-Ts diagram was widely used for *ET* estimation (e.g., Boegh et al., 1999; Gillies et al., 1997; Nishida et al., 2003a; Venturini et al., 2004; Yang et al., 1997). Here, studies related to the VI-Ts diagram were simply reviewed.

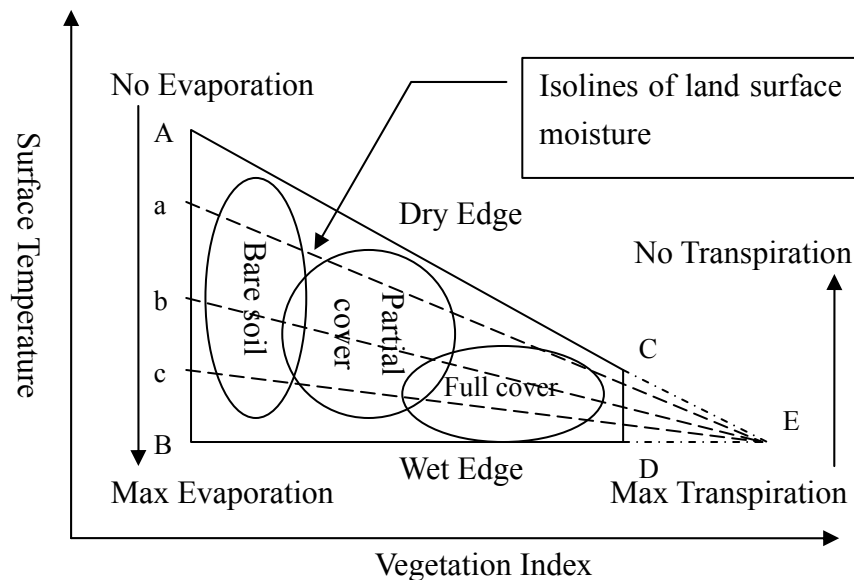


Fig.1-1 The diagram of vegetation index (VI) and surface temperature (Ts) (after Goward and Hope, 1989; Nemani et al., 1993; Lambin and Ehrlich, 1996; Sandholt et al., 2002)*.

*Over bare soil, variations of radiant surface temperature are highly correlated with variations of surface water content. Thus, point A and B respectively represent dry bare soil (low VI, high Ts) and wet bare soil (low VI, low Ts), and point A is called dry point in the VI - Ts diagram. As the vegetation cover increases, the surface temperature decreases. Point C corresponds to the continuous vegetation canopies with a high resistance to evapotranspiration (high VI, relatively high Ts), e.g., due to a low soil water availability. Point D corresponds to the continuous vegetation canopies with a low resistance to evapotranspiration (high VI, low Ts), e.g., a well-watered surface. However, if vegetation is dense enough, it can be considered that land surface is wet enough because there must be enough soil water in the root zone to keep dense vegetation growing naturally. Then, both AC and BD are concentrated into point E, which changes the trapezoid into a triangle. The upper edge in the VI - Ts diagram, AC, represents a no-evapotranspiration line, called dry edge. The lower edge, BD, represents the line of potential evapotranspiration, called wet edge. The dashed lines, including AC and BD, are the isolines of land surface moisture, all of which are concentrated into point E (wet point).

A clear negative relationship between the remotely sensed vegetation index and land surface temperature has been widely observed except in the winter season or in cold areas such as tundra ecosystems (Hope et al., 2005). When the sampling window for defining a VI-Ts diagram is relatively small, and the land surface moisture status within the sampling window is relatively homogenous, the near-linear relationship of VI-Ts can be observed by using optical and thermal remote sensing data (e.g., Nemani and Running, 1989; Smith and Choudhury, 1991; Hope and McDowell, 1992; Moran et al., 1994; Prihodko and Goward, 1997). When the sampling window is large enough to have the full ranges of vegetation cover fraction (f_{veg} , 0-1) and land surface moisture status (from fully wet to fully dry), the shape of an ideal VI-Ts diagram represents a triangle or trapezoid (Fig.1-1) (Nemani et al., 1993; Carlson et al., 1995b; Venturini et al., 2004). This shape can also be simulated by some models (Hope et al., 1986; Smith and Choudhury, 1991; Gillies et al., 1997; Goward et al., 2002), or determined using the ground meteorological data (Moran et al., 1994; Zhang et al., 2005). This negative relationship in the VI-Ts diagram is driven by several mechanisms that include vegetation cover fraction, evapotranspiration, thermal properties of the surface, atmospheric forcing, and surface roughness (Lambin and Ehrlich, 1996; Nemani and Running, 1997; Goward et al., 2002; Sandholt et al., 2002).

Except for the *ET* estimation, the VI-Ts diagram can be also used to retrieve surface moisture status (e.g., Smith and Choudhury, 1991; Nemani et al., 1993; Moran et al., 1994; Carlson et al., 1995b; Gillies et al., 1997; Sandholt et al., 2002), or to classify the land covers (Lambin and Ehrlich, 1996; Nemani and Running, 1997). Additionally, canopy resistance has a high correlation with the slope of Ts / VI over well-covered vegetation areas (Nemani and Running, 1989). With a hypothesis that the bulk temperature of an infinitely thick vegetation canopy is close to the ambient air temperature, air temperature can be directly estimated from the VI-Ts diagram (Carlson et al., 1995a; Prihodko and Goward, 1997). In all the applications of the VI-Ts diagram, a reasonable VI-Ts diagram is required while

the atmospheric forcing should be homogeneous, which is defined with the whole boundaries (Gillies et al., 1997; Sandholt et al., 2002). Generally, the construction of whole boundaries requires the full ranges of land surface moisture and VI, which needs a large sampling window. However, the condition of homogeneous atmospheric forcing over the sampling window limits the sampling window size. In practice, therefore, an ideal VI-Ts diagram may not be determined easily and correctly from remote sensing data if the size of sampling window is not suitable. In Fig. 1-1, the dry edge is a key line to define the VI-Ts diagram. If assuming the minimum vegetation temperature equals to the minimum soil temperature, the VI-Ts diagram can be defined only using the dry edge. Previously, the VI-Ts diagram was defined by either manual screening or automation detecting based on pixel information. Nemani and Running (1989) selected pixels for defining the VI-Ts relationship while excluding cloud-water contamination by hand. Goward and Hope (1989) used a visual best fit, and Carlson et al. (1990) used an arch diagram (standard deviation of surface temperature versus the absolute value of radiometric surface temperature within a pixel subset) to define the VI-Ts relationship. The manual methods were uncertain and inefficient. In order to efficiently define the VI-Ts relationship, Nemani et al. (1993) developed an automated approach in which the algorithm can find the stable slope of Ts/NDVI using an iterative process. Sandholt et al. (2002) determined dry edges using the pixels with maximum temperatures observed for small intervals of NDVI. These automatic methods defined the dry edge within a sampling window, and this sampling window should cover the full ranges of VI and land surface moisture, at least covers the driest bare soil and moisture vegetation. At the 1×1 km pixel scale, such as MODIS and AVHRR, it is difficult to ensure the full ranges of VI and land surface moisture in a limited sampling window. However, if the sub-pixel

information can be obtained, there will be more possibilities to find the driest bare soil and moisture vegetation. In this dissertation, a method was proposed to obtain the component surface temperatures of vegetation and soil to define the VI-Ts diagram at sub-pixel scales. In addition, the VI-Ts diagram was used to obtain the dry bare soil and wet vegetation for my developed Sim-ReSET model.

1.3 Study purpose, structure and content in this dissertation

In this dissertation, the purpose study was to estimate *ET* only using remote sensing data, and the work was divided into two steps. Firstly, a previous algorithm of *ET* and evaporation fraction (*EF*) estimations (MOD16) was evaluated, which was robust and almost independent of the ground observations. Secondly, aiming at estimating *ET* without the ground data support, a new model was developed, the Sim-ReSET model. In this model, subpixel information was used to define the VI-Ts diagram that was used for the determinations of dry and wet points. Here, the dry point corresponds to driest bare soil without any evaporation, and wet point corresponds to moisture vegetation. The dry point was used to remove r_a , and the wet point was used to determine air temperature in the model. The study area of all my work was located in the North China Plain (NCP), China.

Followed the sequence of my work, the detailed structure and content of this dissertation were given as:

Chapter 1 -- Review the previous studies about *ET* estimation based on remote sensing data, and show the purpose of my study;

Chapter 2 -- Evaluate the MOD16 model using the MODIS data and ground measurements in the NCP;

Chapter 3 -- Develop the Sim-ReSET model;

Chapter 4 -- Propose a simple method to define the VI-Ts diagram using subpixel information, and then identify the dry and wet points for the Sim-ReSET model using the VI-Ts diagram;

Chapter 5 -- Map *EF* and *ET*, then validate the Sim-ReSET model using the ground data and MODIS data;

Chapter 6 -- Conclusions of the whole studies in this dissertation.

Reference

- Allen, R. G., Pereira, L. S., Raes, D., & Smith, M. (1998). Crop evapotranspiration - Guidelines for computing crop water requirements, FAO Irrigation and drainage paper 56,
<http://www.fao.org/docrep/X0490E/x0490e00.HTM>
- Ambast, S. K., Keshari, A. K., & Gosain, A. K. (2002). An operational model for estimating regional evapotranspiration through surface energy partitioning (RESEP). *International Journal of Remote Sensing*, 23(22), 4917-4930.
- Bastiaanssen, W. G. M., Pelgrum, H., Meneti, M. A., & Feddes, R. A. (1996). Estimation of surface resistance and Priestley-Taylor α -parameter at different scales. In Stewart. J., Engman, E., Feddes, R., & Kerr, Y. (Ed.), *Scaling up in hydrology using remote sensing* (pp93-111). New York: John Wiley and Sons.
- Bastiaanssen, W. G. M., Menenti, M., Feddes, R. A., & Holtslag, A. A. M. (1998a). A remote sensing surface energy balance algorithm for land (SEBAL) 1. Formulation. *Journal of Hydrology*, 212-213, 198-212.
- Bastiaanssen, W. G. M., Pelgrum, H., Wang, J., Ma, Y., Moreno, J. F., Roerink, G. J., & van der Wal, T. (1998b). A remote sensing surface energy balance algorithm for land (SEBAL) 2. Validatin. *Journal of Hydrology*, 212-213, 213-229.
- Bastiaanssen, W. G. M. (2000). SEBAL-based sensible and latent heat fluxes in the irrigated Gediz Basin, Turkey. *Journal of Hydrology*, 229, 87-100.
- Boegh, E., Soegaard, H., Hanan, N., Kabat, P., & Lesch, L. (1999). A remote sensing study of the NDVI-Ts relationship and the transpiration from sparse vegetation in the Sahel based on high-resolution satellite data. *Remote Sensing of Environment*, 69 (3), 224-240.
- Brutsaert, W. (1982). Evaporation into the atmosphere: Theory, History, and Applications. D. Reidel Publishing Company, Dordrecht, Holland.

- Carlson, T. N., Perry, E. M., & Schmugge, T. J. (1990). Remote estimation of soil moisture availability and fractional vegetation cover for agricultural fields. *Agricultural and Forest Meteorology*, 52, 45-69.
- Carlson, T. N., Capehart, W. J., & Gillies, R. R. (1995a). A new look at the simplified method for remote sensing of daily evapotranspiration. *Remote Sensing of Environment*, 54, 161-167.
- Carlson, T. N., Gillies, R. R., & Schmugge, T. J. (1995b). An interpretation of methodologies for indirect measurement of soil water content. *Agricultural and Forest Meteorology*, 77, 191-205.
- Chen, J. M., Chen, X., Ju, W., & Geng, X. Distributed hydrological model for mapping evapotranspiration using remote sensing inputs. *Journal of Hydrology*, 305, 15-39.
- Choudhury, B. J. (1997). Global patten of potential evaporation calculated from the Penman-Monteith equation using satellite and assimilated data. *Remote Sensing of Environment*, 62, 64-81.
- Churkina, G., Running, S. W., Schloss, A. L., & the Participants of the Potsdam NPP Model Intercomparison. (1999). Comparing global models of terrestrial net primary productivity (NPP): The importance of water availability. *Global Change Biology*, 5(suppl.1), 46-55.
- Cleugh, H. A., Leuning, R., Mu, Q., & Running, S. W. (2007). Regional evaporation estimates from flux tower and MODIS satellite data. *Remote Sensing of Environment*, 106, 285-304.
- Crago, R. D. (1996). Comparison of the evaporative fraction and the Priestley-Taylor a for parameterizing daytime evaporation. *Water Resources Research*, 32 (5), 1403-1409.

- Davies, J. A., & Allen, C. D. (1973). Equilibrium, potential and actual evaporation from cropped surface in southern Ontario. *Journal of Applied Meteorology*, *12*, 649-657.
- De Pury, D. G. G., & Farquhar, G. D. (1997). Simple scaling of photosynthesis from leaves to canopy without the errors of big-leaf models. *Plant, Cell and Environment*, *20*, 537-557.
- Dodds, P., Meyer, W., & Barton, A. (2005). A review of methods to estimate irrigated reference crop evapotranspiration across Australia. *Technical Report 04/05, CRC for irrigation futures and CSIRO land and water, Adelaide, South Australia*.
- Fan, L., Liu, S., Bernhofer, C., Liu, H., & Berger, F. H. (2007). Regional land surface energy fluxes by satellite remote sensing in the Upper Xilin River Watershed (Inner Mongolia, China). *Theoretical and Applied Climatology*, *88*, 231-245.
- French, A. N., Jacob, F., Anderson, M. C., Kustas, W. P., Timmermans, W., Gieske, A., Su, Z., Su, H., McCabe, M. F., Li, F., Prueger, J., & Brunsell, N. (2005). Surface energy fluxes with the Advanced Spaceborne Thermal Emission and Reflection radiometer (ASTER) at the Iowa 2002 SMACEX site (USA). *Remote Sensing of Environment*, *99*, 55-65.
- Gao, W. (1995). Parameterization of subgrid-scale land surface fluxes with emphasis on distributing mean atmospheric forcing and using satellite-derived vegetation index. *Journal of Geophysical research*, *100*, 14 305-14 317.
- Gao, W., Coulter, R. L., Lesht, B. M., Qiu, J., & Wesely, M. L. (1998). Estimating clear-sky regional surface fluxes in the Southern Great Plains atmospheric radiation measurement site with ground measurements and satellite observations. *Journal of Applied Meteorology*, *37*, 5-22.

- Gillies, R. R., Carlson, T. N., Cui, J., Kustas, W. P., & Humes, K. S. (1997). A verification of the “triangle” method for obtaining surface soil water content and energy fluxes from remote measurements of the Normalized Difference Vegetation Index (NDVI) and surface radiant temperature. *International Journal of Remote Sensing*, 18(15), 3145- 3166.
- Goward, S. N., & Hope, A. S. (1989). Evapotranspiration from combined reflected solar and emitted terrestrial radiation: Preliminary FIFE results form AVHRR data. *Advances in Space Research*, 9 (7), 239-249.
- Goward, S. N., Xue, Y., & Czajkowski, K. P. (2002). Evaluating land surface moisture conditions from the remotely sensed temperature / vegetation index measurements: An exploration with the simplified simple biosphere model. *Remote Sensing of Environment*, 79, 225-242.
- Granger, R. J. (1989). A complementary relationship approach for evaporation from nonsaturated surfaces. *Journal of Hydrology*, 111, 31-38.
- Holwill, C. J., & Stewart, J. B. (1992). Spatial variability of evaporation derived from aircraft and ground-based data. *Journal of Geophysical Research*, 97(D17), 18, 673-680.
- Hope, A. S., Petzold, D. E., Goward, S. N., & Ragan, R. M. (1986). Simulated relationships between spectral reflectance, thermal emissions, and evapotranspiration of a soybean canopy. *Water Resources Bulletin*, 22 (6), 1011-1019.
- Hope, A. S., & McDowell, T. P. (1992). The relationship between surface temperature and a spectral vegetation index of a tallgrass prairie: effects of burning and other landscape controls. *International Journal of Remote Sensing*, 13 (15), 2489-2683.

- Hope, A., Engstrom, R., & Stow, D. (2005). Relationship between AVHRR surface temperature and NDVI in Arctic tundra ecosystems. *International Journal of Remote Sensing*, 26 (8), 1771-1776.
- Jackson, R. D., Reginato, R. J., & Idso, S. B. (1977). Wheat canopy temperature: A practical tool for evaluating water requirements. *Water Resource Research* 13(3), 651-656.
- Jensen, M. E., Burman, R. D., & Allen, R. G. (1990). Evaporation and irrigation water requirement, *ASCE Manual and Reports on Engineering Practices*. New York, American Society of Civil Engineers, 70, 332.
- Jia, L., Su, Z., van den Hurk, B., Menenti, M., Moene, A., De Bruim, H. A. R., Yrisarry, J. J. B., Ibanez, M., & Cuesta, A. (2003). Estimation of sensible heat flux using the surface energy balance system and ATSR measurements. *Physics and Chemistry of the Earth*, 28, 75-88.
- Jiang, L., & Islam, S. (2001). Estimation of surface evaporation map over southern Great Plains using remote sensing data. *Water Resource Research* 37 (2), 329–340.
- Keane, R. E., Ryan, K. C., Veblen, T. T., Allen, C. D., Logan, J., & Hawkes, B. (2002). Cascading effects of fire exclusion in Rocky Mountain ecosystems: A literature review. *USDA forest service gen. tech. report RMRS-GTR-91* 24pp.
- Kite, G. W., & Droogers, P. (2000). Comparing evapotranspiration estimates from satellites, hydrological models and field data. *Journal of Hydrology*, 229, 3-18.
- Komatsu, T. S. (2003). Toward a robust phenomenological expression of evaporation efficiency for unsaturated soil surface. *Journal of Applied Meteorology*, 42, 1330-1334.

- Kustas, W. P., Perry, E. M., Doraiswamy, P. C., & Moran, M. S. (1994). Using satellite remote sensing to extrapolate evapotranspiration estimates in time and space over a semiarid rangeland basin. *Remote Sensing of Environment*, *49*, 275-286.
- Kustas, W. P., & Norman, J. M. (1996). Use of remote sensing for evapotranspiration monitoring over land surface. *Hydrological Sciences Journal des Sciences Hydrologiques*, *41*, 495-516.
- Lambin, E. F., & Ehrlich, D. (1996). The surface temperature-vegetation index space for land cover and land-cover change analysis. *International Journal of Remote Sensing*, *17*, 463-487.
- Loheide II, S. P., & Gorelick, S. M. (2005). A local-scale, high-resolution evapotranspiration mapping algorithm (ETMA) with hydroecological applications at riparian meadow restoration site. *Remote Sensing of Environment*, *98*, 182-200.
- Mallick, K., Bhattacharya, B. K., Chaurasia, S., Dutta, S., Nigam, R., Mukherjee, J., Banerjee, S., Kar, G., Rao, V. U. M., Gadgil, A. S., & Parihar, J. S. (2007). Evapotranspiration using MODIS data and limited ground observations over selected agroecosystems in India. *International Journal of Remote Sensing*, *28* (10), 2091-2110.
- Matsushima, D. (2007). Estimating regional distribution of surface heat fluxes by combining satellite data and a heat budget model over the Kherlen River Basin, Mongolia. *Journal of Hydrology*, *333*, 86-99.
- McVicar, T. R., & Jupp, D. L. B. (2002). Using covariates to spatially interpolate moisture availability in the Murray-Darling Basin: A novel use of remotely sensed data. *Remote Sensing of Environment*, *79*, 199-212.

- Melesse, A. M., & Nangia, V. (2005). Estimation of spatially distributed surface energy fluxes using remotely-sensed data for agricultural fields. *Hydrological Processes*, 19 (14), 2653-2670.
- Meyer, W. (1999). Standard reference evaporation calculation for inland, south eastern Australia. *Technical report 35/98* Adelaide, South Australia: SCIRO Land and Water.
- Monteith, J. L. (1965). Evaporation and environment. *19th Symposia of the Society for Experimental Biology*. University Press, Cambridge, 19:205-234.
- Moran, M. S., Clarke, T. R., Inoue, Y., & Vidal, A. (1994). Estimating crop water deficit using the relation between surface-air temperature and spectral vegetation index. *Remote Sensing of Environment*, 49, 246-263.
- Mu, Q., Heinsch, F. A., Zhao, M., & Running, S. W. (2007). Development of a global evapotranspiration algorithm based on MODIS and global meteorology data. *Remote Sensing of Environment*, doi: 10.1016/j.rse.2007.04015.
- Nagler, P. L., Scott, R. L., Westenburg, C., Cleverly, J. R., Glenn, E. P., & Huete, A. R. (2005a). Evapotranspiration on western U.S. rivers estimated using the enhanced vegetation index from MODIS and data from eddy covariance and Bowen ratio flux towers. *Remote Sensing of Environment*, 97, 337-351.
- Nagler, P. L., Cleverly, J. R., Glenn, E., Lampkin, D., Huete, A., & Wan, Z. (2005b). Predicting riparian evapotranspiration from MODIS vegetation indices and meteorological data. *Remote Sensing of Environment*, 94, 17-30.
- Nemani, R. R., & Running, S. W. (1989). Estimation of regional surface resistance to evapotranspiration from NDVI and thermal-IR AVHRR data. *Journal of Applied Meteorology*, 28, 276-284.
- Nemani, R. R., Pierce, L., Running, S. W., & Goward, S. (1993). Developing satellite-derived estimates of surface moisture status. *Journal of Applied Meteorology*, 32 (3), 548-557.

- Nemani, R. R., & Running, S. W. (1997). Land cover characterization using multi-temporal red, near-IR and thermal-IR data from NOAA / AVHRR. *Ecological Applications*, 7 (1), 79-90.
- Nemani, R. R., White, M. A., Thornton, P., Nishida, K., Reddy, S., Jenkins, J. & Running, S. W. (2002). Recent trends in hydrologic balance have enhanced the carbon sink in the United States. *Geophysical Research Letter*, 29(10),1468. DOI: 10.1029/2002GL014867.
- Nishida, K., Nemani, R. R., & Running, S. W. (2003a). An operational remote sensing algorithm of land surface evaporation. *Journal of Geophysical Research*, 108(D9), 4270. DOI: 10.1029/2002JD002062.
- Nishida, K., Nemani, R. R., Glassy, J. M. & Running, S. W. (2003b). Development of an evapotranspiration index from Aqua/MODIS for monitoring surface moisture status. *IEEE Transactions on Geoscience and Remote Sensing*, 41(2), 1-9.
- Norman, J. M., Kustas, W. P., & Humes, K. S. (1995). Source approach for estimating soil and vegetation energy fluxes in observations of directional radiometric surface temperature. *Agricultural and Forest Meteorology*, 77, 263-293.
- Olioso, A., Chauki, H., Courault, D., Wigneron, J. P. (1999). Estimation of evapotranspiration and photosynthesis by assimilation of remote sensing data into SVAT models. *Remote Sensing of Environment*, 68, 341-356.
- Potter, C. S., Randerson, J. T., Field, C. B., Matson, P. A., Vitousek, P. M., Mooney, H. A., & Klooster, S. A. (1993). Terrestrial ecosystem production: a process model based on global satellite and surface data. *Global Biogeochemical Cycles*, 7, 811-841.

- Priestley, C. H. B., & Taylor, R. J. (1972). On the assessment of surface heat flux and evaporation using large-scale parameters. *Monthly Weather Review*, *100*, 81-92.
- Prihodko, L., & Goward, S. N. (1997). Estimation of air temperature from remotely sensed surface observations. *Remote Sensing of Environment*, *60* (3), 335-346.
- Qiu, G. Y., Yano, T., & Momii, K. (1998). An improved methodology of measure evaporation from bare soil based on comparison of surface temperature with a dry soil surface. *Journal of Hydrology*, *210*, 93-105.
- Qiu, G. Y., Shi, P., & Wang, L. (2006). Theoretical analysis of a remotely measurable soil evaporation transfer coefficient. *Remote Sensing of Environment*, *101*, 390-398.
- Rango, A., & Shalaby, A. I. (1998). Operational applications of remote sensing in hydrology: Success, prospects and problems. *Hydrological Sciences Journal des Sciences Hydrologiques*, *43*, 947-968.
- Raupach, M. R. (2001). Combination theory and equilibrium evaporation. *Quarterly Journal of the Royal Meteorological Society*, *127*, 1149-1181.
- Rivas, R., & Caselles, V. (2004). A simplified equation to estimate spatial reference evaporation from remote sensing-based surface temperature and local meteorological data. *Remote Sensing of Environmental*, *93*, 68-76.
- Roerink, G. J., Su, Z., & Meneni, M. (2000). S-SEBI: A simple remote sensing algorithm to estimate the surface energy balance. *Physics and Chemistry of the Earth*, *25* (2), 147-157.
- Running, S. W., Nemani, R. R., Peterson, D. L., Band, L. E., Potts, D. F., Pierce, L. L., & Spanner, M. A. (1989). Mapping regional forest evapotranspiration and photosynthesis by coupling satellite data with ecosystem simulation. *Ecology*, *70*, 1090-1101.

- Sandholt, I., Rasmussen, K., & Andersen, J. (2002). A simple interpretation of the surface temperature/vegetation index space for assessment of surface moisture status. *Remote Sensing of Environment*, *79*, 213-224.
- Seguin, B., Assad, E., Freaud, J. P., Imbernon, J. P., Kerr, Y., & Lagouarde, J. P. (1989). Use of meteorological satellite for rainfall and evaporation monitoring. *International Journal of Remote Sensing*, *10*, 1001-1017.
- Seguin, B., Courault, D., & Guérf, M. (1994). Surface temperature and evapotranspiration: Application of local scale methods to regional scales using satellite data. *Remote Sensing of Environment*, *49*, 287-295.
- Smith, R. C. G., & Choudhury, B. J. (1991). Analysis of normalized difference and surface temperature observations over southeastern Australia. *International Journal of Remote Sensing*, *12* (10), 2021-2044.
- Sobrino, J. A., Gómez, M., Jiménez-Muñoz, J. C., Oliso, A., & Chehbouni, G. (2005). A simple algorithm to estimate evapotranspiration from DAIS data: Application to the DAISEX campaigns. *Journal of Hydrology*, *315*, 117-125.
- Su, Z. (2002). The surface energy balance system (SEBS) for estimation of turbulent heat fluxes. *Hydrology and Earth System Sciences*, *6* (1), 85-99.
- Varni, M., Usunoff, E., Weinzettel, P., & Rivas, R. (1999). The groundwater recharge in the Azul aquifer, central Buenos Aires Province, Argentina. *Physics and Chemistry of the Earth*, *24*(4), 349-352.
- Venturini, V., Bisht, G., Islam, S., & Jiang, L. (2004). Comparison of evaporative fractions estimated from AVHRR and MODIS sensors over South Florida. *Remote Sensing of Environment*, *93*, 77-86.
- Venturini, V., Islam, S., & Rodriguez, L. (2007). Estimation of evaporative fraction and evapotranspiration from MODIS products using a complementary based model. *Remote Sensing of Environment*, doi: 10.1016/j.rse.2007.04.014.

- Verstraeten, W. W., Veroustraete, F., & Feyen, J. (2005). Estimating evapotranspiration of European forests from NOAA-imagery at satellite overpass time: Towards an operational processing chain for integrated optical and thermal sensor data products. *Remote Sensing of Environment*, *96*, 256-276.
- Wang, K., Li, Z., & Cribb, M. (2006). Estimation of evaporative fraction from a combination of day and night land surface temperature and NDVI: A new method to determine the Priestley-Taylor parameter. *Remote Sensing of Environment*, *102*, 293-305.
- Wang, Y. P., & Leuning, R. (1998). A two-leaf model for canopy conductance, photosynthesis and partitioning of available energy: 1. Model description and comparison with a multi-layered model. *Agricultural and Forest Meteorology*, *91*, 89-111.
- Willmott, C. J., Rowe C. M., & Mintz, Y. (1985). Climatology of the terrestrial seasonal water cycle. *Journal of Climatology*, *5*, 589-606.
- Yang, X., Zhou, Q., & Melville, M. (1997). Estimating local sugarcane evapotranspiration using Landsat TM image and a VITT concept. *International Journal of Remote Sensing*, *18* (2), 453-459.
- Zhang, L., Lemeur, R., & Goutorbe, J. P. (1995). A one-layer resistance model for estimating regional evapotranspiration using remote sensing data. *Agricultural and Forest Meteorology*, *77*, 241-261.
- Zhang, R. H., Sun, X. M., Wang, W. M., Xu, J. P., Zhu, Z. L., & Tian, J. (2005). An operational two-layer remote sensing model to estimate surface flux in regional scale: Physical background. *Science in China, Ser. D: Earth Sciences*, *48* (Supp. I), 225-244.
- Zhang, Y., & Wegehenkel, M. (2006). Integration of MODIS data into a simple model for the spatial distributed simulation of soil water content and evapotranspiration. *Remote Sensing of Environment*, *104*, 393-408.

Chapter 2

Evaluation of a Previous Evapotranspiration Model over Winter Wheat Fields in North China Plain (MOD16)

2.1 Introduction

MOD16 developed by [Nishida et al. \(2003a, b\)](#) is a simple dual-source model for ET and evaporation fraction (EF) estimations using remote sensing data. A pixel is simplified as a mixture of bare soil and vegetation in MOD16, which is much closer to natural conditions than the assumption of pure pixel. Here, EF ([Shuttleworth et al., 1989](#)) is defined as ET divided by available energy Q that equals net radiation R_n minus soil heat flux G , or sensible heat flux H plus latent heat flux ET , whose units are all W/m^2 ,

$$EF = \frac{ET}{Q} = \frac{ET}{R_n - G} = \frac{ET}{H + ET} \quad (2-1)$$

EF has frequently been found to be remarkably steady between about 9:00 am and 4:00 pm, which was also validated using the eddy covariance data (not shown), although a graph of EF over time displayed a slightly concave shape during the daytime ([Crago, 1996](#)). Therefore, EF provides an approach to extrapolate ET from an instantaneous value to a daily average value ([Sugita and Brutsaert, 1991](#); [Brutsaert and Sugita, 1992](#)).

The MOD16 algorithm uses the complementary relationship of the actual and the potential ET to deduce the equation of EF for vegetation in which the canopy resistance is used to describe vegetation physiology. On the other hand, the VI-Ts diagram is used for EF estimation for bare soil. MOD16 is practicable for global

MODIS ET mapping, which minimizes the uses of ground observations. This is the reason why MOD16 was selected for evaluation in this study. The MOD16 algorithm was validated with test datasets of 13 flux sites in USA, whose results showed that there were different errors in 10 ecotypes over the 13 flux sites. The maximum error (more than 0.25 for EF , root mean square error) occurred in the crop ecotype. It seems that MOD16 is not suitable for applications to all kinds of ecotypes because several biophysical and meteorological parameters are considered constants, whereas they actually vary with time and space.

In this study, the MOD16 algorithm was taken as an example of previous remote sensing - based ET models, and the purpose is to understand the potential problems of previous remote sensing - based models. In this study, MOD16 was evaluated in winter wheat fields using APEIS-Flux datasets (Wang et al., 2005) collected at the Yucheng Experimental Station (YES) and MODIS datasets from DOY 1 to DOY 161 of 2002 with a 16-day interval, where DOY stands for day of year. This covers most of the winter wheat growing period.

2.2 Description of MOD16 algorithm

2.2.1 Evaporation fraction for vegetation

The formulation of vegetation EF is expressed as,

$$EF_{veg} = \frac{\alpha\Delta}{(\Delta + \gamma) + \gamma r_s / 2r_a} \quad (2-2)$$

Δ and γ are calculated using air temperature T_a . Although γ also depends on atmospheric pressure, its influence is generally low. MOD16 applies the canopy resistance r_s to describe vegetation physiological characters. It is estimated using the Jarvis method (1976),

$$1/r_s = f_1(T_a) f_2(PAR) f_3(VPD) f_4(\Psi) f_5(CO_2) / r_{cMIN} + 1/r_{cuticle} \quad (2-3)$$

where PAR is photosynthetic active radiation ($\mu\text{mol}/\text{m}^2/\text{s}$); VPD is the vapor pressure deficit (Pa); Ψ is leaf-water potential (Pa); r_{cMIN} and $r_{cuticle}$ are the minimum resistance (s/m) and the canopy resistance related to diffusion through the cuticle layer of leaves, 100000(s/m), respectively. Among the environmental

factors in equation (2-3), only air temperature and PAR can be estimated from satellite remote sensing and radiation transfer calculation, whereas VPD , Ψ and CO_2 concentration are difficult to estimate from satellite data. Therefore, the terms of VPD , Ψ and CO_2 are dropped from equation (3), and only T_a and PAR are used. The following equations (Jarvis, 1976) are adopted to estimate $f_1(T_a)$ and $f_2(PAR)$,

$$f_1(T_a) = \left(\frac{T_a - T_n}{T_o - T_n} \right) \left(\frac{T_x - T_a}{T_x - T_o} \right)^{[(T_x - T_o)/(T_o - T_n)]} \quad (2-4)$$

$$f_2(PAR) = \frac{PAR}{PAR + A} \quad (2-5)$$

where T_n , T_o and T_x are minimum, optimal and maximum temperatures for stomata activity, respectively; and A is the parameter of photon absorption efficiency at low light intensity, $152 \mu\text{mol}/\text{m}^2/\text{s}$.

Aerodynamic resistance r_a is given by the empirical formula,

$$1/r_a = 0.003U_{1m}, \text{ for grassland and cropland} \quad (2-6)$$

where U_{1m} is wind speed at 1.0 m height above ground (m/s), and is estimated from U_{50m} using the logarithmic profile of wind speed,

$$U_{1m} = U_{50m} \frac{\ln(1/z_{0m})}{\ln\left(\frac{50 - d_0}{z_{0m}}\right)} \quad (2-7)$$

where d_0 is a function of canopy height; and z_{0m} is assumed to be 0.005 m for bare surface and 0.01 m for grassland.

2.2.2 Evaporation fraction for bare soil

The equation for bare soil EF is expressed as,

$$EF_{soil} = \frac{Q_{soil \max}}{Q_{soil}} \times \frac{T_{soil \max} - T_{soil}}{T_{soil \max} - T_a} \quad (2-8)$$

where $Q_{soil \max}$ is the available energy over dry bare soil surface (W/m^2); Q_{soil} is available energy over bare soil surface (W/m^2); $T_{soil \max}$ is the maximum estimated bare soil surface temperature. Air temperature, soil surface temperature and maximum temperature are all estimated using the VI-Ts diagram (Fig. 2-1).

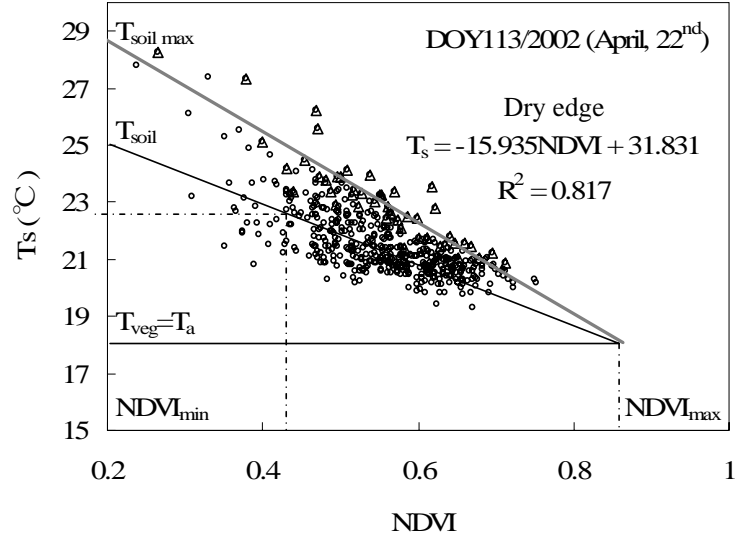


Fig.2-1 The VI-Ts diagram used in MOD16. It consists of a scatter plot (\circ) of $NDVI$ and T_s (MODIS, DOY113 of 2002, YES) in a $20 \text{ km} \times 20 \text{ km}$ sampling window, where \triangle are selected from \circ to retrieve the “dry edge” using the method proposed in MOD16. T_a and $T_{soil \max}$ is obtained by extrapolating the dry edge (the upper envelope line of the scatter plot) to the maximum $NDVI$ and minimum $NDVI$ respectively. T_{soil} is obtained by extrapolating the straight line via $(NDVI_{\max}, T_a)$ and $(NDVI, T_s)$ to the minimum $NDVI$.

2.2.3 A simple dual-source model (MOD16)

MOD16 simplifies a landscape to a mixture of vegetation and bare soil. The proportion of vegetation is denoted by the fractional vegetation cover f_{veg} whose value is between 0 and 1. The normalized difference vegetation index (NDVI) was not linear to f_{veg} (Jiang et al., 2006). In this study, the second-order scaled NDVI was used to calculate f_{veg} (Choudhury et al., 1994; Gillies and Calson, 1995; Calson and Ripley, 1997),

$$f_{veg} = \left(\frac{NDVI - NDVI_{\min}}{NDVI_{\max} - NDVI_{\min}} \right)^2 \quad (2-9)$$

where $NDVI_{\max}$ and $NDVI_{\min}$ are the normalized difference vegetation index (NDVI) of full vegetation ($f_{veg} = 1$) and bare soil ($f_{veg} = 0$). Based on the analysis of MODIS-NDVI data during the whole winter wheat growing season in my study

area in 2002, $NDVI_{max}$ is given as 0.85 instead of 0.75 used in the original MOD16 algorithm while $NDVI_{min}$ is the same to the original 0.20. Steven et al. (2003) have inter-calibrated the vegetation indices from different sensor systems. They found that MODIS-NDVI has linear relationship with AVHRR-NDVI, $MODIS-NDVI = 1.103 * AVHRR-NDVI + 0.004$. Hence, 0.20 for $NDVI_{min}$ and 0.75 for $NDVI_{max}$ in NOAA-AVHRR are changed to 0.22 and 0.83 in MODIS, respectively. The maximum MODIS-NDVI is close to the observation (0.82-0.88) for canopy-saturated vegetation in FIFE (Prihodko and Goward, 1997). Assuming that a coupled energy transfer between vegetation and bare soil is negligible, ET for a pixel is described as a linear combination of ET values for vegetation and bare soil,

$$ET = f_{veg} ET_{veg} + (1 - f_{veg}) ET_{soil} \quad (2-10)$$

The subscripts “veg” and “soil” denote vegetation and bare soil, respectively. Combining equation (2-1) and (2-10), therefore, the EF of a pixel is,

$$EF = \frac{ET}{Q} = f_{veg} \frac{Q_{veg}}{Q} EF_{veg} + (1 - f_{veg}) \frac{Q_{soil}}{Q} EF_{soil} \quad (2-11)$$

All the above are the basic algorithms for MOD16, which is used to estimate only EF up to now (Nishida et al., 2003a, b). If ET is required, it can be calculated with a simple formula, $ET = Q \times EF$.

2.3 Study area and data used

2.3.1 Study area

My study area, a square of 20 km × 20 km, is located in North China Plain (NCP), China. The Yucheng Experimental Station (YES) at 36°50’N latitude, 116°35’E longitude, and 26 m elevation above sea level, an integrated agricultural experiment station of Chinese Academy of Sciences (CAS), is at the center of the study area (Fig. 2-2). The main land use in the NCP is irrigated cropland. The study area has a representative climate and agricultural cropping system characteristic of the NCP. The yearly mean air temperature is 13.1°C, and annual precipitation is 610 mm, of which about 70% falls between June and August. The soil is sandy loam, and the cropping system is mainly a rotation of winter wheat

and summer maize. Generally, winter wheat is seeded in the first ten days of October and harvested in the first ten days of June the following year, while the summer maize growing period is between June and October, immediately following the winter wheat harvest.

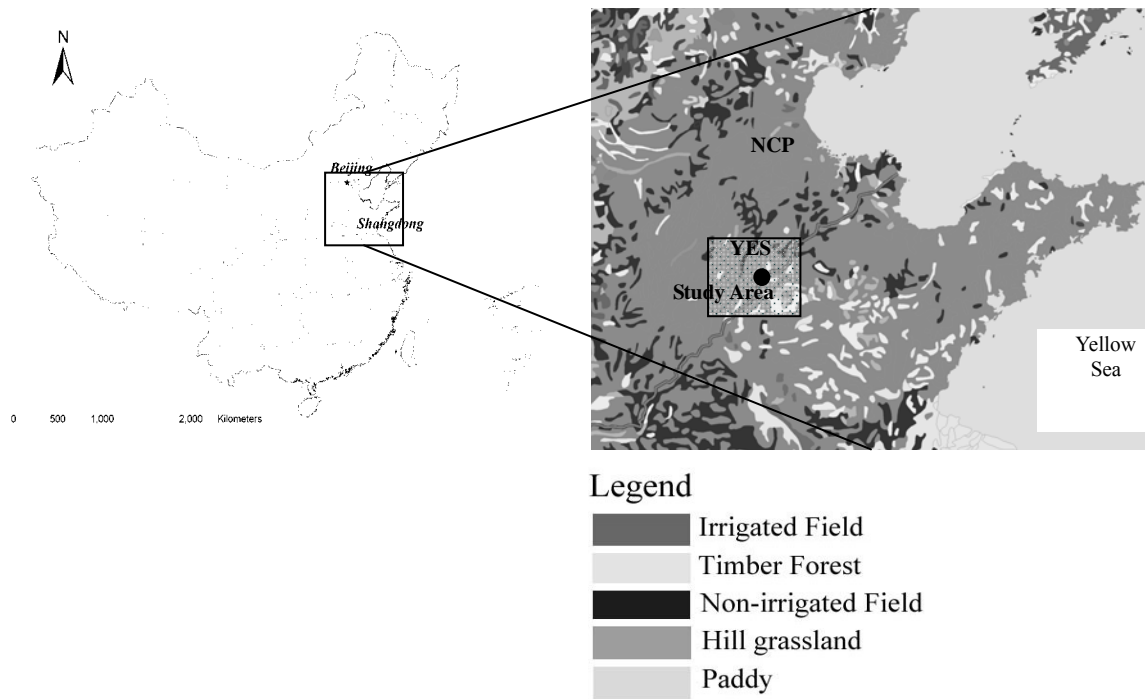


Fig.2-2 The study area, a 20 km × 20 km square area, in the North China Plain, China. Yucheng Experimental Station locates at the center of the study area. Its main land use/cover is irrigated cropland, shown as grey on the map.

2.3.2 Remote sensing data

Two kinds of data were used in this study - MODIS data and ground observational data. The MODIS science team of NASA (http://modis.gsfc.nasa.gov/sci_team/) has developed many MODIS products, including atmosphere, land and ocean. In this study, two data products were used, MOD11- land surface temperature (Ts) and emissivity, and MOD13 - vegetation indices (VIs) with the spatial resolution of 1 km. The daily MOD11 value has been validated in more than 20 clear-sky cases with in-situ measurement data collected in field studies from 2000 to 2002. The MOD11 is within 1°C accuracy when the land surface temperature ranges from -10 to 50 °C (Wan et al., 2004). MOD13 provides the 16-day maximum compositing vegetation index (van Leeuwen et al., 1999). Two vegetation indices

(VIs) have been produced globally. One is the standard normalized difference vegetation index (NDVI), which is referred to as the continuity index for the existing NOAA-AVHRR-derived NDVI. The other is an enhanced vegetation index (EVI) with improved sensitivity to high biomass regions and improved vegetation monitoring through an uncoupling of the canopy background signal and a reduction in atmosphere influences. The 16-day compositing NDVI was used in this study so as to be consistent with MOD16.

In the growing season of winter wheat, it can be assumed that NDVI of winter wheat field does not vary significantly during 16 days because LAI of winter wheat during such a period changes with only small amplitude. The study area can be considered as a mixture of winter wheat, bare soil, villages and small cities. However, villages and cities only cover a small portion, and can be assumed as a bare soil surface with higher roughness length. The 16-day compositing MOD13-NDVI data paired with 16-day instantaneous Ts/MOD11 were used to obtain the “dry edge” in the VI-Ts diagram from DOY 1 to DOY 161, 2002, which covered the majority of the growing season of winter wheat. [Table 2-1](#) is the result of the VI-Ts diagram analysis when the method is proposed in MOD16.

Table 2-1 Results of VI-Ts diagram analysis.

DOY	Time	Slope	Intercept	R ²	T _{veg}	T _{soilmax}
1	10:52	-2.88	8.75	0.23	6.61	8.17
17	11:00	-1.32	7.96	0.02	6.5	7.75
33	11:23	-17.09	16.77	0.65	9.5	13.35
49	11:00	-16.76	22.1	0.66	13.46	18.75
65	11:01	-11.5	23.43	0.61	16.01	21.13
81	10:59	-8.07	23.03	0.6	16.89	21.42
97	10:58	-11.07	24.91	0.63	17.01	22.7
113	10:52	-15.94	31.83	0.82	20.5	28.64
129	11:12	-6.93	29.85	0.63	24.4	28.46
145	10:48	-7.3	34.59	0.49	29.22	33.13
161	11:18	-4.86	32.7	0.25	30.39	31.73

Time is Terra satellite overpassing time (LST). Slope, Intercept and R² are regression analysis results of the “dry Edge”. T_{veg} is the surface temperature of vegetation, and T_{soilmax} is the maximum surface temperature of bare soil.

2.3.3 Ground observations

The ground data were collected from the APEIS-Flux / YES from DOY 97 to DOY 161, 2002. This dataset includes air temperature, humidity, wind speed, components of radiation balance, soil heat flux, latent heat flux and sensible heat flux at half-hour intervals measured by the eddy covariance system (Wang et al., 2005). The closure ratio, defined as $(H+ET)/(R_n-G)$, of the eddy covariance system at the YES site was about 80% in the daytime, based on the 30-minute flux data (not shown). The other ground data from DOY 1 to 161, with the exception of latent heat flux and sensible heat flux, were also collected from the micrometeorological station near a flux tower. Thus, the actual ET and EF were calculated using the Penman-Monteith (P-M, equation (1-3)) method, which is usually used as the standard for comparison for other methods (Irmak et al., 2003), as an additional evaluation dataset. The estimations using the P-M method were compared with the observations from the eddy covariance system, and it was found that they were consistent with an average absolute error of 29.05 W/m^2 . Meanwhile, LAI of winter wheat was measured using LAI2000 (LI-COR, Inc., Lincoln, USA). My observation site was surrounded by a large area of winter wheat field, so the measurements at this site can be used to validate pixel-based estimation of MOD16. The Terra Satellite overpass time over the study area was close to 11:00 am (LST), time details are listed in Table 2-1. Therefore, the averages of observational data from 10:30 to 11:30 were used for validation.

2.4 Results and discussions

Firstly, the parameterizations of MOD16 were compared and evaluated, such as the radiation budget on the land surface, canopy resistance, wind speed and aerodynamic resistance using the observations. Then, the EF and ET values estimated directly by the original MOD16 algorithm and by the modified algorithm were compared with the observations.

2.4.1 Parameterizations and evaluations

In order to obtain EF and ET , estimates of the radiation budget on the land surface, canopy resistance, wind speed and aerodynamic resistance are required firstly. In this section, how to estimate these terms using the MOD16 algorithm, and then how to validate them by comparing them with observed data were described. Then, the algorithms were modified accordingly.

2.4.1.1 Radiation budget on the land surface

The radiative transfer scheme of [Kondo \(2000\)](#) was used to estimate the shortwave radiation budget in MOD16 while assuming 0.03 for turbidity, 0.20 for albedo, 60% for relative humidity and 1013 hPa for standard atmospheric pressure. When the sky was cloud-free (DOY 1, 33, 65 and 81), the downward shortwave radiation estimation was similar to the observed data ([Fig. 2-3](#)). PAR is estimated by multiplying downward shortwave radiation by a transfer coefficient of 2.05 mmol/W. The downward long wave radiation is estimated by assuming that the effective temperature of sky radiation is 20°C lower than T_a ([Kondo, 1994](#)). The upward long wave radiation is estimated using surface temperature T_s and assumed emissivities of 0.98 for vegetation and 0.95 for bare soil respectively. The ground heat flux is considered as a set ratio to net radiation.

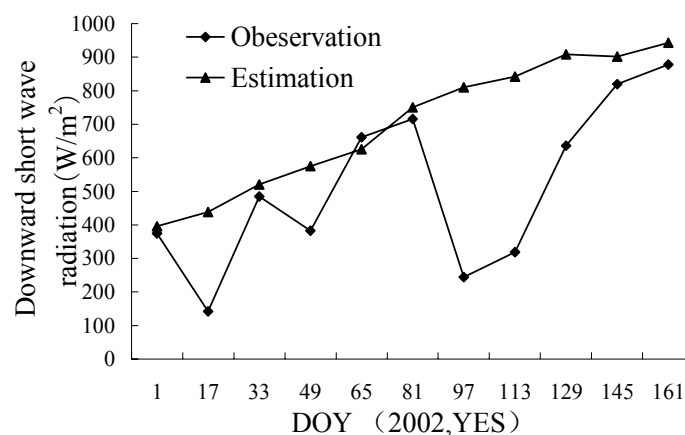


Fig.2-3 The estimation and observation of solar shortwave radiation when the Terra satellite passed over the Yucheng Experimental Station (YES) from DOY1 to DOY161, 2002, every 16 days.

When estimating the radiation budget of each pixel in the remote sensing image, gridded albedo, emissivity and the ratio of ground heat flux to net radiation are required. It was considered that each of their values was a linear combination of the values of the full vegetation canopy and the entirely bare soil surface by the fractional vegetation cover f_{veg} in this study, whose formula structure was the same as that of equation (2-10). The albedo of cropland surface in the NCP ranges from about 0.1 for full vegetation canopy to about 0.2 for bare soil, except for surfaces covered with snow (Fig. 2-4). Generally, the field surface is fully covered with vegetation from April to May with winter wheat and July to September with summer maize due to high LAI in the NCP. In the whole winter and the period from wheat harvest to maize seeding soil is almost bare. The emissivities of the vegetation canopy and bare soil are the same to those in the MOD16 algorithm. Boegh's (2002) simple method was used to parameterize the ground heat flux while assuming the ratio of ground heat flux to net radiation for full vegetation and bare soil as 0.1 and 0.5, respectively, based on the observed data (not shown).

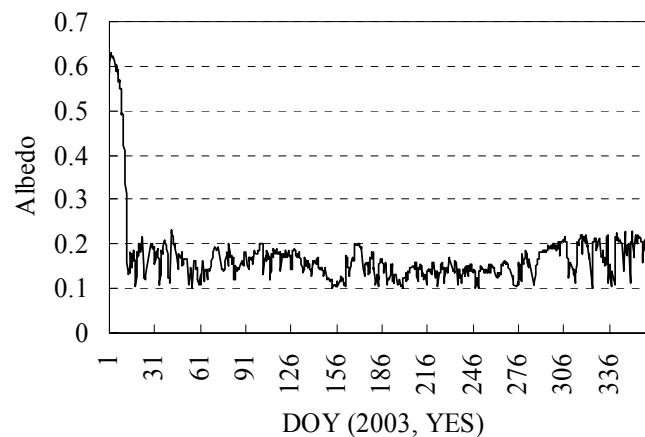


Fig.2-4 Albedo at 10:30, 11:00, 11:30 (YES, 2003). Here, albedo is calculated as the ratio of observational upward shortwave radiation to downward shortwave radiation at 10:30, 11:00 and 11:30 every day at YES in 2003.

In the radiation budget sub-model, the main error is in the estimation of downward shortwave radiation. When the sky is entirely clear, the downward shortwave radiation is consistent with the observations, but such sky condition is rare,

especially in the middle and low latitude areas. During this study the in-situ downward shortwave and long wave radiation were used instead of estimates in MOD16 when the sky was cloudy. This was acceptable because downward radiation was almost homogenous over my small study area with an area of only $20 \text{ km} \times 20 \text{ km}$. The MODIS science team provides atmospheric data from individual images taken by the MODIS sensors aboard the Terra and Aqua satellite platforms. [Van Laake and Sanchez-Azofeifa \(2005\)](#) computed instantaneous *PAR* from MODIS atmospheric data. Compared to field observations, the daily integrated *PAR* values were shown to have average errors on the order of 5–8%. Thus, MODIS atmospheric products can be expected to improve the estimation accuracy of the downward shortwave radiation sub-model in MOD16.

2.4.1.2 Canopy resistance

The [Jarvis \(1976\)](#) formula was used to estimate canopy resistance using T_a , *PAR* and other physiological temperatures of vegetation (equation (2-3) - (2-5)). Winter wheat is sensitive to air temperature. It has different physiological temperatures in different growing phases. However, these temperatures used in MOD16 are considered as constants. Canopy resistance obtained using the parameters provided by MOD16 was far different from the one based on the local winter wheat physiological temperatures ([Table 2-2](#)), which indicated that $f_1(T_a)$ was sensitive to physiological temperatures ([Fig. 2-5](#)). Furthermore, the minimum canopy resistance was not considered to vary with the different stages of crop growth, but was defined as a constant in MOD16. Canopy resistance can be considered as a summation of the stomatal resistance of individual leaves, which are assumed to contribute in parallel. Generally, the leaf stomatal resistance of dense, green and unstressed canopy is low, ranging from 50 to 200 s/m ([Verseghy et al., 1993](#)). It differs among crop varieties and crop management techniques, and usually increases when the crop ages and begins to ripen. There is, however, a lack of consolidated information on changes in stomatal resistance over time for different crops and different growth stages of crops. The information available in the

literature on stomatal resistance is often oriented toward physiological or ecophysiological studies. Canopy resistance is calculated by using minimum stomatal resistance divided by LAI, instead of the 33 s/m proposed in MOD16, where the minimum stomatal resistance is 100 s/m according to field measurements (Shen et al., 2002).

Table 2-2 Winter wheat physiological temperatures for the canopy resistance mode in MOD16 and in its different growing phases in NCP.

	Growing phase	Tn Minimum temperature	To Optimal temperature	Tx Maximum temperature
MOD16 (Nishida et al., 2003a)	--	2.7	31.1	45.3
Winter wheat in North China	Phase 1	1	16	32
	Phase 2	3	13	30
Plain (Gao, 1995)	Phase 3	8	17	35
	Phase 4	10	22	35

Phase 1 -- Sowing to beginning of leaf growth after winter (8th Oct. ~ 4th Mar.)

Phase 2 -- Leaf and stem growing period (4th Mar. ~ 19th Apr.)

Phase 3 -- Ear growing period (19th Apr. ~ 15th May)

Phase 4 -- End of ear growth to harvest (15th May ~ 10th Jun.)

The detailed date of each phase depends on the cumulative temperature from sowing. Here, the approximate dates are given according to the observations at YES.

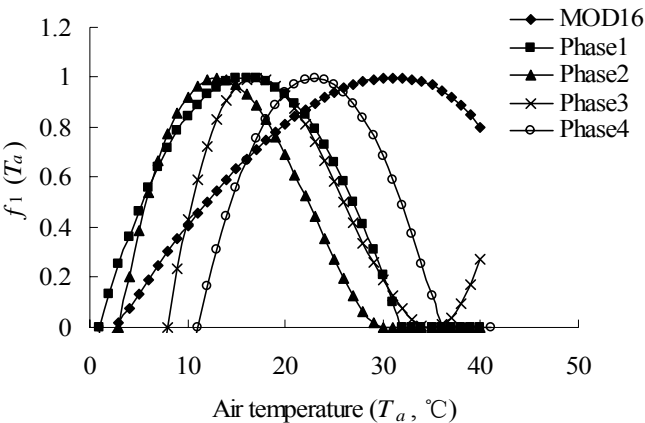


Fig.2-5 Sensitivity of $f_1(T_a)$ for the different growing phases to winter wheat physiological temperatures (minimum, optimal and maximum). Phase definition is based on Gao (1995). MOD16 is based on Nishida et al. (20003a).

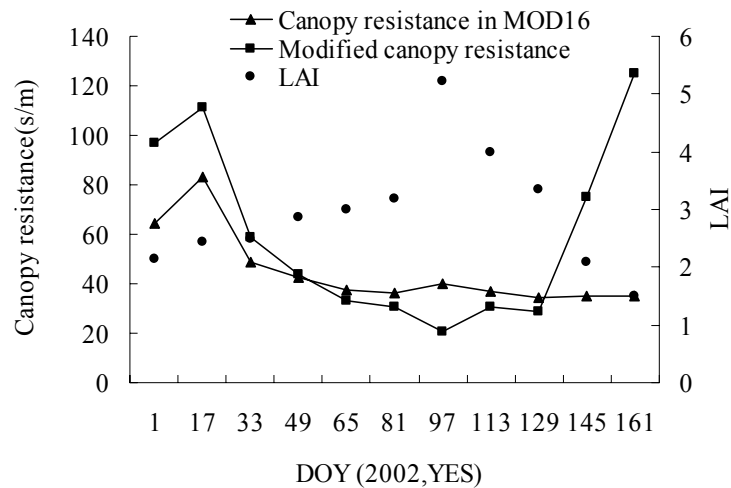


Fig.2-6 Seasonal variations of *LAI* and canopy resistance estimated in MOD16 and by the modified method.

As shown in Fig. 2-6, it was found that the difference between the MOD16 estimate and the modified canopy resistance was very large when LAI was less than 2.5, especially when winter wheat was near harvest. The canopy resistance was larger on DOY1 and DOY17 because low air temperature decreased the plants' physiological activities, while on DOY 145 and DOY161, LAI decreases because winter wheat leaves were aging.

Among the simulations of stomata conductance, the Jarvis model (Jarvis, 1976) and the Ball-Berry model (Ball et al., 1987) are two typical methods. The Jarvis model is an empirical model that is characterized by multiplying a series of correction coefficients, each of which represents an environmental factor. The Ball-Berry model, a semi-empirical model, has a solid experimental basis with a linear relationship between photosynthesis and stomatal conductance. It takes into account a feedback interaction between the photosynthetic rate and stomatal conductance, so an iteration of calculations is required. The Jarvis model is more widely applied to studies on evapotranspiration, land surface processes and the biogeochemical cycle (e.g., Hanan and Prince, 1997; Cox et al., 1998) because of its simple structure and practical performance. Canopy resistance estimated by the Jarvis model is sensitive to minimum canopy resistance and plant physiological temperatures (minimum, optimum and maximum), which vary with plant growth.

The minimum canopy resistance can be estimated from the leaf area index and leaf maximum assimilation rate, which are determined from observed data (Bhaskar and Nicolo, 1998). Sakai et al. (1997) presented an empirical linear regression method to estimate canopy resistance using NDVI and *PAR*-albedo. This contributes to the estimation of canopy resistance using remote sensing data. The look-up table (LUT) method is widely used in remote sensing research (e.g., Combal et al., 2003; Bertrand and Royer, 2004; Chander et al., 2004; Mobley et al., 2005). NDVI and LAI have been obtained successfully using remote sensing images. This provides a promising method to predict regional vegetation phenology (Jolly et al., 2005; Cook et al., 2005). Based on land use/cover maps, vegetation phenology and the ground-based observational canopy resistance, LUTs can be produced. Hence, when applying LUTs and parameters retrieved from remote sensing, such as NDVI, albedo and *PAR*, there will be a practical method to estimate canopy resistance in remote sensing-based *ET* research independent of real-time ground observations.

2.4.1.3 Aerodynamic resistance

Once T_a , $T_{soil\ max}$ are estimated using the VI-Ts diagram (Fig. 2-1), aerodynamic resistance for dry bare soil $r_{a\ bare\ max}$ can be obtained by solving the following equation while assuming that the latent heat flux over dry bare soil surface is close to 0,

$$r_{a\ bare\ max} = \rho C_p \frac{T_{soil\ max} - T_a}{Q_{soil\ max}} \quad (2-12)$$

Then, $r_{a\ bare\ max}$ is converted to wind speed using equation (2-6), meanwhile, the coefficient 0.003 for cropland is replaced by 0.0015 for bare soil. Equation (2-7) is used to convert U_{1m} above bare soil to U_{50m} while assuming 0.005 m for the roughness length and 0 m for the surface zero plane displacement. Finally, r_a for vegetation is obtained (equation (2-6), (2-7)), but when considering errors in MOD16, one of the largest sources of error lies in the estimation of wind speed

(Nishida et al., 2003a). In this study, the surface layer Monin-Obukhov similarity (MOS) theory was used to estimate wind speed and aerodynamic resistance, and then evaluate the algorithm of wind speed estimation in MOD16.

Based on the MOS theory, the wind speed profile in the atmospheric boundary layer is a well-known logarithmic curve,

$$U = \frac{u^*}{k} \left[\ln\left(\frac{z-d_0}{z_{0m}}\right) - \Psi_M\left(\frac{z-d_0}{L}\right) + \Psi_M(z_{0m}/L) \right] \quad (2-13)$$

$\Psi_M(z_{0m}/L)$ is usually close to 0. Under strictly neutral conditions, $\Psi_M\left(\frac{z-d_0}{L}\right)$ equals 0. Under the non-neutral conditions, based on field and laboratory experiment data and applications of Businger et al. (1971) and Dyer (1974)'s functions, modified Dyer functions (Hogstrom, 1988) are used for unstable conditions, which usually occurs above dry bare soil in the daytime,

$$\Psi_M(\xi) = 2 \ln[(1+x)/2] + \ln[(1+x^2)/2] - 2 \tan^{-1} x + \pi/2 \quad (2-14)$$

$$\Psi_H(\xi) = \Psi_W(\xi) = 2 \ln[(1+x^2)/2] \quad (2-15)$$

while $\xi < 0$, where $x = [1 - 15.2\xi]^{1/4}$, $\xi = z/L$. L has to be solved using an iterative procedure. For practical applications, this is inconvenient. Byun (1990) and Launiainen (1995) gave a series of empirical expressions for z/L as a function of Ri_b (bulk Richardson number). In this study, Launiainen's solution was used to parameterize L for an unstable region,

$$\xi = z/L = \left(\frac{(\ln z/z_{0m})^2}{\ln z_{0m}/z_{oh}} - 0.55 \right) Ri_b \quad (2-16)$$

Tests in conditions of z_{0m} from 10^{-5} to 10^{-1} m and z_{0m}/z_{oh} from 0.5 to 7.3 were shown to generally yield estimates within a few percent of those found using iteration (Launiainen, 1995).

Near the ground surface, the potential temperature is close to air temperature or surface temperature, so Ri_b is also expressed as,

$$Ri_b = \frac{g[z - (d_0 + z_{0m})]}{T_0} \frac{T_z - T_s}{u^2} \quad (2-17)$$

where T_0 is mean absolute temperature, and approximates air temperature at

reference height or surface temperature (K); $T_z - T_s$ is the difference of temperature between surface and reference height.

Considering the surface layer thermal stratification functions and the roughness lengths for momentum and heat respectively, the aerodynamic resistance is then

$$r_a = \frac{1}{k^2 U} \left[\ln\left(\frac{z-d_0}{z_{oh}}\right) - \psi_h\left(\frac{z-d_0}{L}\right) \right] \left[\ln\left(\frac{z-d_0}{z_{om}}\right) - \psi_m\left(\frac{z-d_0}{L}\right) \right] \quad (2-18)$$

where z_{oh} is estimated using the values of kB^{-1} and z_{om} . $kB^{-1} = \ln\left(\frac{z_{om}}{z_{oh}}\right)$ is fairly constant (~ 2) for many vegetated surfaces, but varies significantly for bluffly rough surfaces that contain impermeable obstacles for wind flow. An empirical approach evaluated over a semiarid area by [Kustas et al. \(1989\)](#) and tested in this watershed by [Moran et al. \(1991\)](#) is used to estimate kB^{-1} ,

$$kB^{-1} = \ln\left(\frac{z_{om}}{z_{oh}}\right) = S_{kB} U (T_s - T_a) \quad (2-19)$$

where S_{kB} is constant, approximately 0.17.

Above the bare soil surface, equation (2-12), (2-14)-(2-19) were then combined to obtain the wind speed at 1 m height instead of empirical equation (2-6). However, the value of wind speed can not be obtained directly because an irrational function presented in the solving process. According to the observations, wind speed at about 2 m/s occurs above the land surface with higher frequency, hence the initial value of wind speed, 2 m/s, was applied to equation (2-17) and (2-19). This effectively improved the solving process. The average of 2 m/s and the result of the above calculations was taken as the wind speed at 1 m height above the bare soil surface. This process can be repeated if greater accuracy is required. Wind speed at 10 m height was then derived using equation (2-13), which was closer to the observations than the estimate from the MOD16 algorithm ([Fig. 2-7](#)).

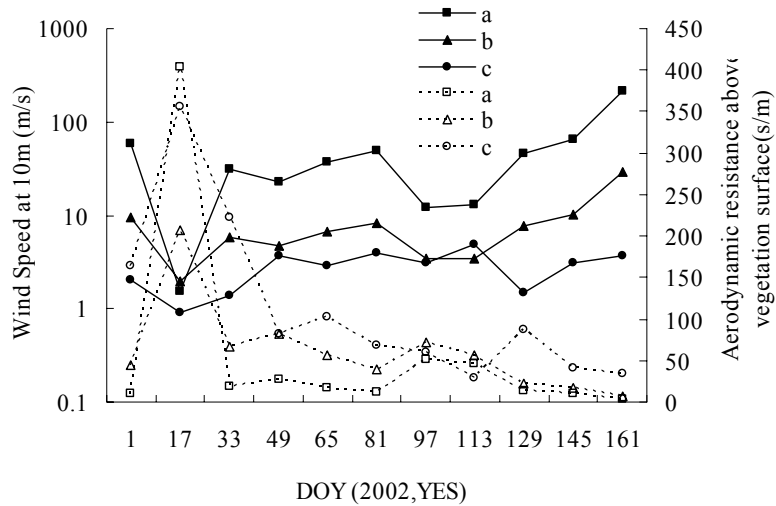


Fig.2-7 Comparisons of estimated wind speed and aerodynamic resistance above the vegetation surface with the observations at 10 m height at 11:00 am. a is estimated directly by the original MOD16 algorithm; b is estimated by the modified algorithm; c is observations from the standard meteorological station. Solid and dashed lines represent wind speed and aerodynamic resistance, respectively.

After the wind speed at 1 m height above the bare soil surface was obtained, the wind speed at 1 m height over the vegetation-covered field was estimated using equation (2-13) and the intermediate variable of wind speed at 50 m height U_{50m} , while assuming 0.005 m as the roughness length for momentum and 0 m as the zero plane displacement for the bare soil surface. $0.13 h$ as the roughness length for momentum and $0.63 h$ as the zero plane displacement for vegetation surface were also assumed, where h is the crop canopy height (m). h was measured in this study, but can also be estimated using land use/cover map and vegetation phenological information. Above the vegetation surface, the atmospheric thermal stratification stability is considered as a neutral condition because surface temperature is close to air temperature. By using equation (2-18) and considering the kB^{-1} as constant 2, the aerodynamic resistance above the vegetation surface was estimated. The whole process is shown in the flow chart (Fig.2-8). As shown in Fig. 2-7, the modified aerodynamic resistance is closer to the values estimated using the observational wind speed and canopy height than those estimated directly by MOD16.

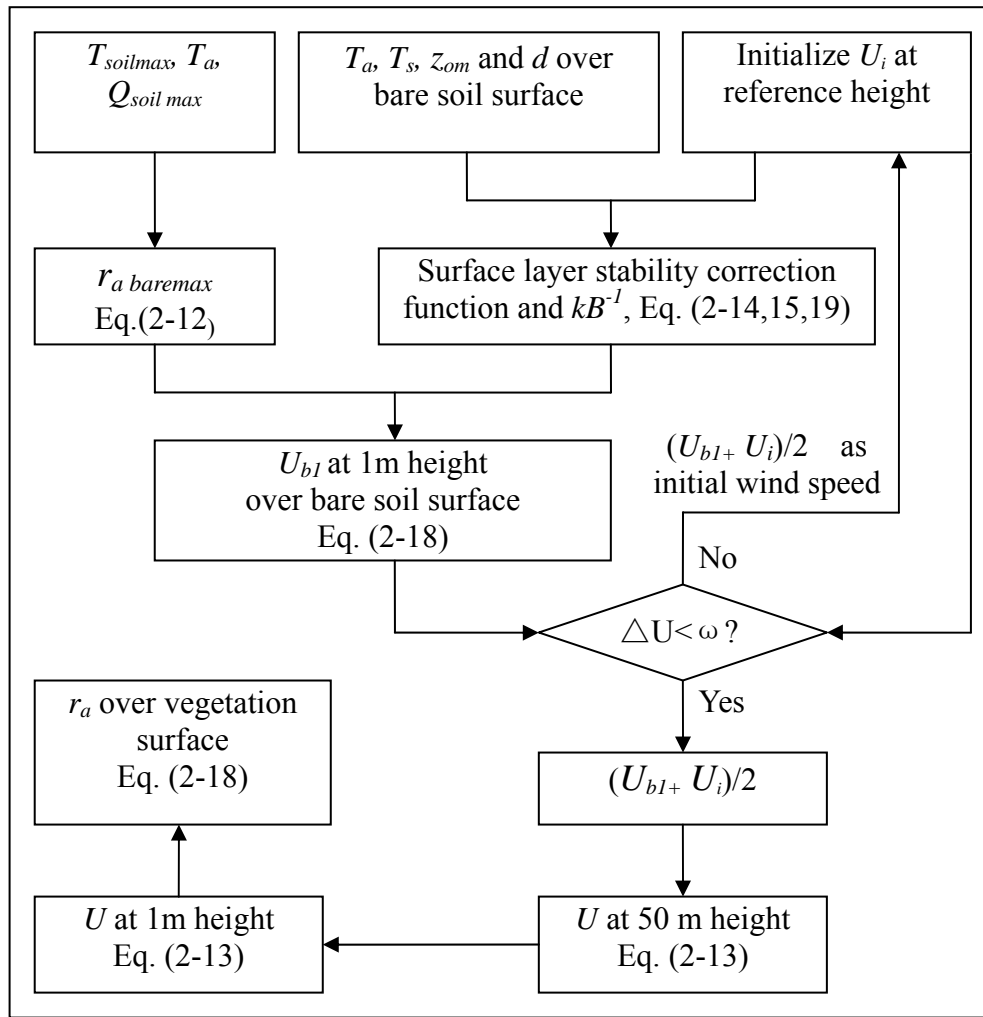


Fig.2-8 Flow chart of aerodynamic resistance estimation over vegetation surface, where ω is used to control the quality of wind speed estimation over bare soil surface.

Aerodynamic resistance, a key parameter in vegetation EF estimation, is determined by wind speed and land surface aerodynamic parameters, such as zero plane displacement and roughness length. In MOD16, aerodynamic resistance is given only as an empirical function of wind speed. This results in overestimation of wind speed above the bare soil surface with the maximum surface temperature in the sampling window and underestimation of aerodynamic resistance above the vegetation surface. There is a strong unstable thermal stratification above such bare soil surface because the surface temperature and the temperature near the land surface are higher than the upper air temperature, or $\frac{\partial T}{\partial z} < 0$. Considering this factor and kB^{-1} , the estimates of wind speed and aerodynamic resistance are consistent with the observations.

2.4.2 EF and ET

Based on the above analyses and calculations, EF for bare soil surface by equation (2-8), EF for vegetation by equation (2-2) and EF for the whole pixel by equation (2-11) were calculated. Here, the averaged values of five pixels were used for comparisons with the YES observations, where the middle pixel was corresponding to YES, and the others were the geographically closest to YES. Because the dataset used for the P-M calculation was collected from a winter wheat field and the results of the P-M calculation represented EF and ET of winter wheat, the original MOD16 estimated EF for vegetation was compared with EF calculated using the P-M method that was consistent with the eddy covariance measurements. It was found that its mean absolute error was 0.13, mean relative error was 40%, and the correlation coefficient was 0.62. After the sub-models of MOD16 were modified as described in section 4.1, the results were improved (Fig. 2-9). Comparison of the MOD16 modified EF with the P-M calculated EF showed that its mean absolute error was 0.1, mean relative error was 26% and the correlation coefficient was 0.88.

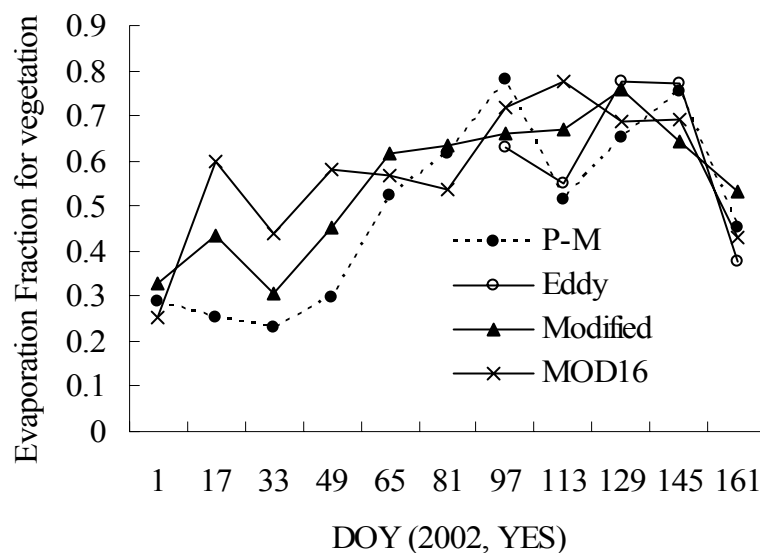


Fig.2-9 Comparison of MOD16 original and modified vegetation EF , P-M calculated EF and eddy covariance measured EF .

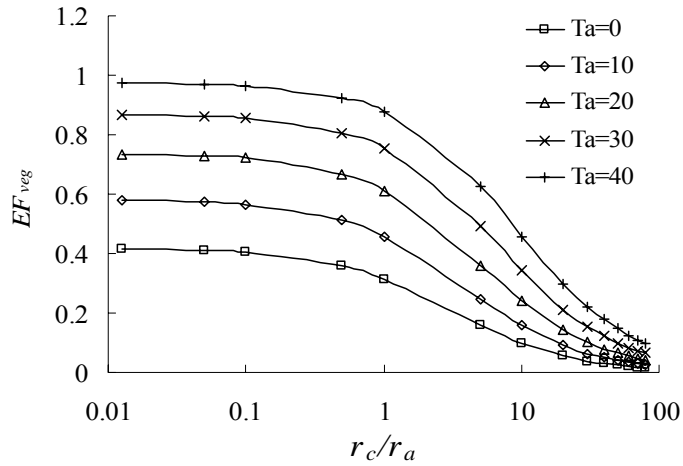


Fig.2-10 Sensitivity analysis of air temperature, canopy resistance (r_c) and aerodynamic resistance (r_a) to EF of vegetation. Assuming r_c and r_a in the possible range of 5-400 s/m, r_c/r_a is within 0.0125-80.

In equation (2), Δ is sensitive to air temperature. When $T_a=0^\circ\text{C}$, $\Delta =33.51 \text{ Pa}/^\circ\text{C}$; when $T_a=40^\circ\text{C}$, $\Delta =231.28 \text{ Pa}/^\circ\text{C}$. From Fig. 2-10, it can be determined that EF for vegetation is linearly sensitive to air temperature when canopy resistance is less than aerodynamic resistance. Additionally, EF for vegetation is not sensitive to resistance when canopy resistance is less than aerodynamic resistance. However, EF for vegetation linearly depends on r_c/r_a when canopy resistance is larger than aerodynamic resistance. It demonstrates that overestimation of wind speed and underestimation of aerodynamic resistance will produce large errors in MOD16. Air temperature is assumed to be equal to the surface temperature of the pixel with the maximum vegetation index in the VI-Ts diagram in MOD16, but the estimated air temperature is sometimes much higher than the observed. Both when the land surface is entirely covered by vegetation and when soil water is supported without deficit, the estimated air temperature is close to the observed (DOY129 and DOY145). In Fig. 2-11, the mean difference between the estimated and the observed air temperatures is about 5°C . Therefore, the estimated air temperature is another potential error source in MOD16. In practice, the quasi-linear relationship between T_s and T_s-T_a can be used to infer air temperature (Bastiaanssen et al., 1998). From Fig. 2-11, T_s-T_a is also related to the vegetation index. Hence, the

vegetation index, such as NDVI, is useful information for the air temperature estimation.

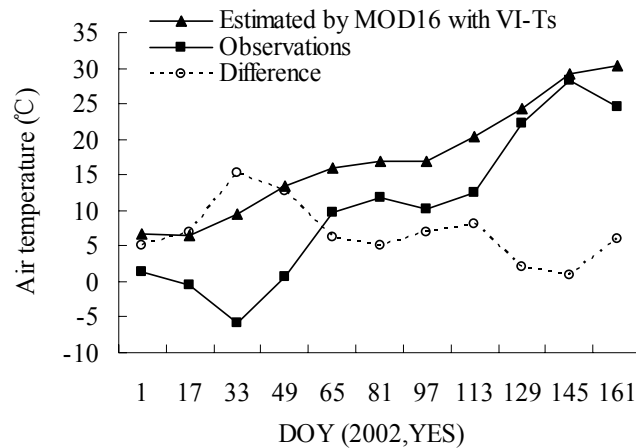


Fig.2-11 Comparison of air temperatures observed and estimated by MOD16 with the VI-Ts method.

Because the evaluation of MOD16 was over a winter wheat field, only *ET* for vegetation was estimated by using equation (2-1) and (2-2). It was compared with the observations of the eddy covariance system and *ET* calculated by the P-M method (Fig. 2-12). In this study, the P-M results were used to evaluate *ET* estimated by MOD16. Almost all *ETs* estimated directly by the original MOD16 algorithm were higher than those estimated by the modified MOD16 algorithm and calculated by the P-M method (Fig. 2-12). Comparing the *ET* estimated directly by the original MOD16 algorithm with the P-M calculated results gave a mean absolute error of 56.84W/m^2 and a mean relative error of 53.6%, while comparing the *ET* estimated by the MOD16 modified algorithm with the P-M calculated results gave a mean absolute error of 21.93W/m^2 and a mean relative error of 21.8%. Their slopes and R^2 of a 1:1 line analysis were 1.29, 0.85 and 1.02, 0.91, respectively (Fig. 2-13). Jiang et al. (2004) summarized the uncertainties in latent heat flux measurement and estimation. His analysis showed that the error was typically on the order of 10–20% or larger for surface sensible and latent heat fluxes. According to this, the results of the modified MOD16 algorithm can be accepted.

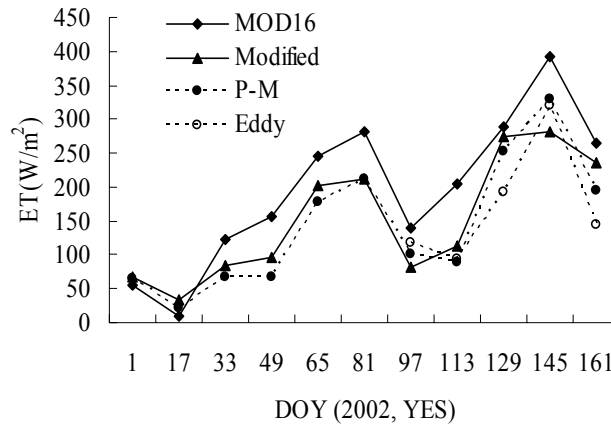


Fig.2-12 Seasonal variations in *ET* estimated from the original (Nishida et al., 2003a,b; MOD16) and modified (this study; Modified) MOD16, P-M calculations based on in-situ measurement variables (P-M) and eddy covariance measurements (Eddy) over a winter wheat field.

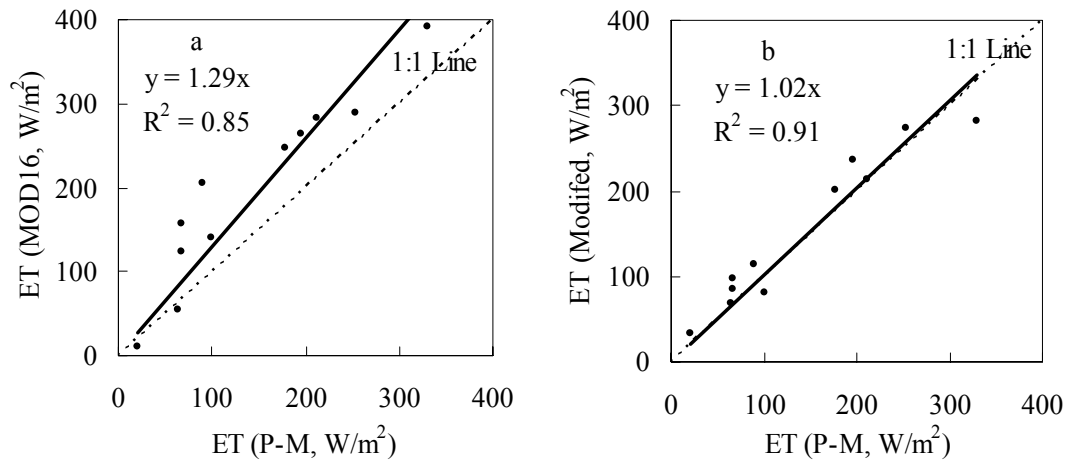


Fig.2-13 Comparisons of *ET* estimated by the original MOD16 algorithm and modified algorithm to *ET* calculated by the P-M method.

2.5 Conclusion

The MOD16 model was evaluated using MODIS and ground observational data in a winter wheat field, as well as its sub-models, the radiation budget on the land surface, canopy resistance and aerodynamic resistance. By comparing with field observations, results showed that the downward shortwave radiation in MOD16 was close to the observations only on cloudless days. Because the vegetation physiological temperatures and minimum canopy resistance were considered as constants, canopy resistance with a larger error was obtained when LAI was less than 2.5 in the winter wheat field. Because strong unstable thermal stratification above dry bare soil surface was ignored, aerodynamic resistance above vegetation surface was underestimated. By using the modified methods, *EF* and *ET* were more consistent with both eddy covariance observations and estimates of the P-M method. This demonstrates that the modified MOD16 algorithm has potential applications for accurate estimations of *EF* and *ET* over a winter wheat field. However, these accurate estimations still depend on ground data, which blocks its wide application in mapping *ET* from a large spatial scale.

References

- Ball, J. T., Woodrow, I. E., & Berry, J. A. (1987). A model predicting stomatal conductance and its contribution to the control of photosynthesis under different environmental conditions. In *Progress in photosynthesis research*, Biggins, I, (ed). Martinus Nijhoff Publishers, Amsterdam, 221-224.
- Bastiaanssen, W. G. M., Meneti, M., Feddes, A., & Holtslag, A. A. M. (1998). A remote sensing surface energy balance algorithm for land (SEBAL) 1. Formulation. *Journal of Hydrology*, 212-213, 198-212.
- Bertrand, C., & Royer, A. (2004). Aerosol optical depth spatio-temporal characterization over the Canadian BOREAS domain. *International Journal of Remote Sensing*, 25(15), 2903-2917.
- Bhaskar, J. C., & Nicolo, E. D. (1998). A biophysical process-based estimate of global land surface evaporation using satellite and ancillary data I. Model description and comparison with observations. *Journal of Hydrology*, 205, 164-185.
- Boegh, E., Soegaard, H., & Thomsen, A. (2002). Evaluating evapotranspiration rates and surface conditions using Landsat TM to estimate atmospheric resistance and surface resistance. *Remote Sensing of Environment*, 79, 329-343.
- Brutsaert, W., & Sugita, M. (1992). Application of self-preservation in the diurnal evolution of the surface energy budget to determine daily evaporation. *Journal of Geophysical Research*, 97(D17), 18, 377-382.
- Businger, J. A., Wyngaard, J. C., Izumi, Y., & Bradley, E. F. (1971). Flux-profile relationships in the atmospheric surface layer. *Journal of Atmospheric Sciences*, 28, 181-189.
- Byun, A. J. (1990). On the analytical solution of flux-profile relationships for the atmospheric surface layer. *Journal Applied Meteorology*, 29, 652-657.
- Carlson, T. N., & Ripley, D. A. (1997). On the relation between NDVI, fraction vegetation cover, and leaf area index. *Remote Sensing of Environment*, 62, 241-252.

- Chander, G., Helder, D. L., Markham, B. L., Dewald, J. D., Kaita, E., Thome, K. J., Micijevic, E., & Ruggles, T. A. (2004). Landsat-5 TM reflective-band absolute radiometric calibration. *IEEE Transactions on Geoscience and Remote Sensing*, 42(12), 2747-2760.
- Choudhury, B. J., Ahmed, N. U., Idso, S. B., Reginato, R. J., & Daughtry, CTM. (1994). Relations between evaporation coefficients and vegetation indices studied by model simulations. *Remote Sensing of Environment*, 50, 1-17.
- Combal, B., Baret, F., Weiss, M., Trubuil, A., Macé, D., Pragnère, A., Myneni, R., Knyazikhin, Y., & Wang, L. (2003). Retrieval of canopy biophysical variables from bidirectional reflectance--Using prior information to solve the ill-posed inverse problem. *Remote Sensing of Environment*, 84(1),1-15.
- Cook, B. I., Smith, T. M., & Mann, M. E. (2005). The North Atlantic oscillation and regional phenology prediction over Europe. *Global Change Biology*, 11(6), 919-926.
- Cox, P. M., Huntingford, C., & Harding, R. J. (1998). A canopy conductance and photosynthesis model for use in a GCM land surface scheme. *Journal of Hydrology*, 212-213, 79-94.
- Crago, R. D. (1996). Conservation and variability of the evaporation fraction during the daytime. *Journal of Hydrology*, 180(1-4), 173-194.
- Dyer, A. J. (1974). A review of flux – profile relationships. *Boundary-Layer Meteorology*, 7, 363-372.
- Gao, S. H. (1995). Agricultural climate productive potential and study on strategy of its exploitation and utilization in the North of China. Science Press, Beijing, 62 (in Chinese).
- Gillies, R. R., & Carlson, T. N. (1995). Thermal remote sensing of surface soil water content with partial vegetation cover for incorporation into climate models. *Journal of Applied Meteorology*, 34, 745-756.
- Hanan, N. P., & Prince, S. D. (1997). Stomatal conductance of West-Central Supersite vegetation in HAPEX-Sahel: measurements and empirical models. *Journal of Hydrology*, 188-189, 536-562.

- Hogstrom, U. (1988). Non-dimensional wind and temperature profiles in the atmospheric surface layer: a re-evaluation. *Boundary-Layer Meteorology*, 42, 55-78.
- Irmak, S., Allen, R. G., & Whitty, E. B. (2003). Daily grass and alfalfa-reference evapotranspiration estimates and alfalfa-to-grass evapotranspiration ratios in Florida. *Journal of Irrigation and Drainage Engineering-ASCE*, 129(5), 360-370.
- Jarvis, P. G. (1976). The interpretation of the variations in leaf water potential and stomatal conductance found in canopies in the field. *Philosophical Transactions of the Royal Society: London; Ser. B(273)*, 593-610.
- Jiang, Z., Huete, A., Chen, J., Chen, Y., Li, J., Yan, G., & Zhang, X. (2006). Analysis of NDVI and scaled difference vegetation index retrievals of vegetation fraction. *Remote Sensing of Environment*, 101 (3), 366-378.
- Jiang, L., Islam, S., & Carlson, T. N. (2004). Uncertainties in latent heat flux measurement and estimation: implications for using a simplified approach with remote sensing data. *Canadian Journal of Remote Sensing*, 30(5), 769-787.
- Jolly, W. M., Nemani, R., Running, S. W. (2005). A generalized, bioclimatic index to predict foliar phenology in response to climate. *Global Change Biology*, 11(4), 619-632.
- Kondo, J. (1994). *Meteorology of Water Environment*. Asakura-shoten: Tokyo, 350.
- Kondo, J. (2000). *Atmospheric Science near the Ground Surface*. University of Tokyo Press: Tokyo, 324.
- Kustas, W. P., Choudhury, B. J., Moran, M. S., Reginato, R. J., Jackson, R. D., Gay, L. W., & Weaver, H. L. (1989). Determination of sensible heat flux over sparse canopy using thermal infrared data. *Agriculture and Forest Meteorology*, 44, 197-216.
- Launiainen, J. (1995). Derivation of the relationship between the Obukhov stability parameter and the bulk Richardson number for flux-profile studies. *Boundary-Layer Meteorology*, 76,165-179.

- Mobley, C. D., Sundman, L. K., Davis, C. O., Bowles, J. H., Downes, T. V., Leathers, R. A., Montes, M. J., Bissett, W. P., Kohler, D. D. R., Reid, R. P., Louchard, E. M., & Gleason, A. (2005). Interpretation of hyperspectral remote-sensing imagery by spectrum matching and look-up tables. *Applied Optics*, *44* (17), 3576-3592.
- Moran, M. S., Kustas, W. P., Bach, L. B., Weltz, M. A., Huete, A. R., & Amer S. A. (1991). Use of remotely sensed spectral data for evaluation of hydrologic parameters in semiarid rangeland. AMS Preprint of the Tenth Conference on Biometeorology and Aerobiology and Special Session on Hydrometeorology, 10-13 September, Salt Lake City, UT, American Meteorological Society, 238-241.
- Nishida, K., Nemani, R. R., & Running, S. W. (2003a). An operational remote sensing algorithm of land surface evaporation. *Journal of Geophysical Research*, *108*(D9), 4270. DOI: 10.1029/2002JD002062.
- Nishida, K., Nemani, R. R., Glassy, J. M., & Running, S.W. (2003b). Development of an evapotranspiration index from Aqua/MODIS for monitoring surface moisture status. *IEEE Transactions on Geoscience and Remote Sensing*, *41*(2), 1-9.
- Prihodko, L., Goward, S. N. (1997). Estimation of air temperature from remotely sensed surface observations. *Remote Sensing of Environment*, *60*, 335-346
- Sakai, R. K., Fitzjarrald, D. R., & Moore, K. E. (1997). Detecting leaf area and surface resistance during transition seasons. *Agricultural and Forest Meteorology*, *84*, 273-284.
- Shen, Y. J., Kondoh, A., Tang, C. Y., Zhang, Y. Q., Chen, J., Li, W., Sakura, Y., Liu, C. M., Tanaka, T., & Shimada, J. (2002). Measurement and analysis of evapotranspiration and surface conductance of a wheat canopy. *Hydrological Processes*, *16*, 2173-2187.
- Shuttleworth, W. J., Gurney, R. J., Hsu, A. Y., & Ormsby, J. P. (1989). FIFE: The variation in energy partition at surface flux sites. *IAHS Publication*, *186*, 67-74.

- Steven, M. D., Malthus, T. J., Baret, F., Xu, H., & Chopping, M. J. (2003). Intercalibration of vegetation indices from different sensor systems. *Remote Sensing of Environment*, 88, 412-422
- Sugita, M., & Brutsaert, W. (1991). Daily evaporation over a region from lower boundary layer profiles measured with radiosondes. *Water Resource Research*, 27, 745-752.
- Van Laake, P. E., & Sanchez-Azofeifa, G. A. (2005). Mapping PAR using MODIS atmosphere products. *Remote Sensing of Environment*, 94, 554-563.
- Van Leeuwen, W. J. D., Huete, A. R., & Laing, T. W. (1999). MODIS vegetation index compositing approach: A prototype with AVHRR data. *Remote Sensing of Environment*, 69(3), 264-280.
- Verseghy, D. L., McFarlane, N. A., & Lazare, M. (1993). CLASS—a Canadian land surface scheme for GCMs. II. Vegetation model and coupled runs. *International Journal of Climatology*, 13, 347-370.
- Wan, Z., Zhang, Y., Zhang, Q., & Li, Z. L. (2004). Quality assessment and validation of the MODIS global land surface temperature. *International Journal of Remote Sensing*, 25(1), 261-274.
- Wang, Q. X., Watanabe, M., & Ouyang, Z. (2005). Simulation of water and carbon fluxes using BIOME-BGC model over crops in China. *Agricultural and Forest Meteorology*, 131, 209-224.

Chapter 3

Development of a Simple Remote Sensing Evapotranspiration Model (Sim-ReSET model): Algorithm and Parameterizations

3.1 Introduction

The accurate estimations of ET and EF in the MOD16 model mainly relate to canopy and aerodynamic resistances whose true values depend on ground data. If the calculations of canopy and aerodynamic resistances are further avoided, ET and EF can be obtained only from remote sensing data. A **Simple Remote Sensing EvapoTranspiration** model (Sim-ReSET) was developed bases solely on remote sensing data in this study. In this model, canopy resistance is avoided while ET is obtained as a residual of the land surface energy balance equation (1-4). Aiming to reduce or avoid the r_a calculation, some researches used a reference site to estimate the regional ET (Bastiaanssen et al., 1998a,b; Bastiaanssen, 2000; Jia et al., 2003; Kustas et al., 1994; Loheide II and Gorelick, 2005; Su, 2002; Qiu et al., 1998; 2006). Aerodynamic resistance is removed by introducing a dry bare soil surface in this study. Other input variables into the Sim-ReSET model include R_n , G and canopy height that can be obtained from remote sensing.

3.2 Algorithm of Sim-ReSET model

If energies stored by canopy, utilized by plant photosynthesis and transferred by advection are ignored, the land surface energy balance can be expressed as,

$$H + ET = R_n - G \quad (3-1)$$

H equals to,

$$H = \rho C_p \frac{T_s - T_a}{r_a} \quad (3-2)$$

Then ET is given as a residual term,

$$ET = R_n - G - \rho C_p \frac{T_s - T_a}{r_a} \quad (3-3)$$

In semiarid or arid areas, dry bare soil can be easily found in the sampling window, whose ET equals 0. Then, the following formula at dry bare soil can be obtained,

$$(R_n - G)_d = \rho C_p \frac{T_{sd} - T_{ad}}{r_{ad}} \quad (3-4)$$

where the subscript d represents parameters at dry bare soil. After changing the form of equation (3-4), it is rewritten as,

$$r_{ad} = \rho C_p \frac{T_{sd} - T_{ad}}{(R_n - G)_d} \quad (3-5)$$

Base on the similarity theory, aerodynamic resistance above dry bare soil can also be expresses as,

$$r_{ad} = \frac{1}{k^2 u(z)_d} \left[\ln\left(\frac{z}{z_{ohd}}\right) - \psi_H\left(\frac{z}{L}\right) \right] \left[\ln\left(\frac{z}{z_{omd}}\right) - \psi_M\left(\frac{z}{L}\right) \right] \quad (3-6)$$

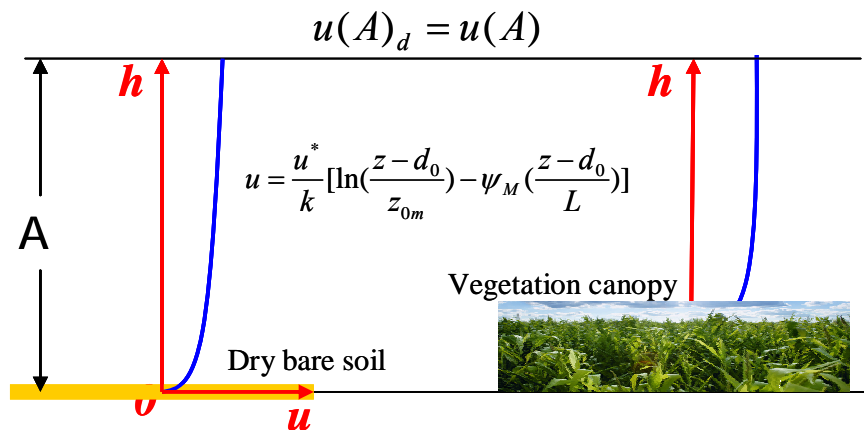


Fig.3-1 The upper boundary of atmospheric surface layer used to remove r_a calculation.

It has been assumed that wind speed at a certain height A above the land surface within a limited sampling window is almost homogeneous due to the existence of a well-mixed layer above this height (Fig. 3-1) (Brutsaert, 1998). This height is the

boundary between atmospheric surface layer (ASL) and atmospheric mixed layer (AML). Brutsaert (1998) suggested that this boundary was on the order of 100 m for neutral or unstable conditions above a uniform surface. The MOS is usually valid within the ASL. The value of 100 m will be tested in Chapter 5. The vertical profile of wind speed is nearly logarithmic with height in the ASL,

$$u = \frac{u^*}{k} \left[\ln\left(\frac{z-d_0}{z_{0m}}\right) - \psi_M\left(\frac{z-d_0}{L}\right) \right] \quad (3-7)$$

Then the ratios of wind speed on land surface to that at the upper boundary of ASL (A) can be obtained as,

$$\frac{u(A)}{u(z)} = \frac{\ln\left(\frac{A-d_0}{z_{0m}}\right) - \psi_M\left(\frac{A-d_0}{L}\right)}{\ln\left(\frac{z-d_0}{z_{0m}}\right) - \psi_M\left(\frac{z-d_0}{L}\right)} \quad (3-8a)$$

$$\frac{u(A)_d}{u(z)_d} = \frac{\ln\left(\frac{A}{z_{0md}}\right) - \psi_M\left(\frac{A}{L}\right)}{\ln\left(\frac{z}{z_{0md}}\right) - \psi_M\left(\frac{z}{L}\right)} \quad (3-8b)$$

When $u(A)_d = u(A)$,

$$\begin{aligned} \frac{u(z)}{u(z)_d} &= \frac{\ln\left(\frac{A}{z_{0md}}\right) - \psi_M\left(\frac{A}{L}\right)}{\ln\left(\frac{z}{z_{0md}}\right) - \psi_M\left(\frac{z}{L}\right)} \bigg/ \frac{\ln\left(\frac{A-d_0}{z_{0m}}\right) - \psi_M\left(\frac{A-d_0}{L}\right)}{\ln\left(\frac{z-d_0}{z_{0m}}\right) - \psi_M\left(\frac{z-d_0}{L}\right)} \\ &= \frac{[\ln\left(\frac{A}{z_{0md}}\right) - \psi_M\left(\frac{A}{L}\right)][\ln\left(\frac{z-d_0}{z_{0m}}\right) - \psi_M\left(\frac{z-d_0}{L}\right)]}{[\ln\left(\frac{A-d_0}{z_{0m}}\right) - \psi_M\left(\frac{A-d_0}{L}\right)][\ln\left(\frac{z}{z_{0md}}\right) - \psi_M\left(\frac{z}{L}\right)]} \end{aligned} \quad (3-9)$$

In equation (3-2), if r_a is calculated using equation (3-6), combining equation (3-5), (3-6), and (3-9), equation (3-2) can be rewritten as,

$$\begin{aligned} H &= \rho C_p \frac{T_s - T_a}{r_a} \\ &= (R_n - G)_d \frac{T_s - T_a}{T_{sd} - T_a} \frac{[\ln\left(\frac{z}{z_{ohd}}\right) - \psi_h\left(\frac{z}{L}\right)][\ln\left(\frac{A}{z_{0md}}\right) - \psi_m\left(\frac{A}{L}\right)]}{[\ln\left(\frac{z-d_0}{z_{oh}}\right) - \psi_h\left(\frac{z-d_0}{L}\right)][\ln\left(\frac{A-d_0}{z_{0m}}\right) - \psi_m\left(\frac{A-d_0}{L}\right)]} \end{aligned} \quad (3-10)$$

$f(H)$ is defined as an sensible heat flux transfer function while $(R_n-G)_d$ can be considered as the maximum sensible heat flux,

$$f(H) = \frac{T_s - T_a}{T_{sd} - T_a} \frac{[\ln(\frac{z}{z_{ohd}}) - \psi_h(\frac{z}{L})][\ln(\frac{A}{z_{0md}}) - \psi_m(\frac{A}{L})]}{[\ln(\frac{z-d_0}{z_{oh}}) - \psi_h(\frac{z-d_0}{L})][\ln(\frac{A-d_0}{z_{0m}}) - \psi_m(\frac{A-d_0}{L})]} \quad (3-11)$$

If the atmospheric stratification corrections are ignored under neutral or weak unstable conditions, equation (3-11) is simplified as,

$$f(H) = \frac{T_s - T_a}{T_{sd} - T_a} \frac{\ln(\frac{z}{z_{ohd}}) \ln(\frac{A}{z_{0md}})}{\ln(\frac{z-d_0}{z_{oh}}) \ln(\frac{A-d_0}{z_{0m}})} \quad (3-12)$$

For bare soil, equation (3-12) can be further simplified, which is the same to the model developed by [Qiu et al. \(2006\)](#),

$$f(H)_{soil} = \frac{T_s - T_a}{T_{sd} - T_a} \quad (3-13)$$

here $T_a \ll T_s \ll T_{sd}$, $0 \ll f(H) \ll 1$.

In this study, a dual-source model was developed if a pixel could be assumed as a mixture of vegetation and bare soil, and equations are shown as follows,

$$ET = f_{veg} ET_{veg} + (1 - f_{veg}) ET_{soil} \quad (3-14a)$$

and,

$$f_{veg} = \left(\frac{VI - VI_{min}}{VI_{max} - VI_{min}} \right)^2 \quad (3-14b)$$

$$ET_{veg} = (R_n - G)_{veg} - (R_n - G)_d f(H)_{veg} \quad (3-14c)$$

$$ET_{soil} = (R_n - G)_{soil} - (R_n - G)_d f(H)_{soil} \quad (3-14d)$$

where $f(H)_{veg}$ and $f(H)_{soil}$ are calculated respectively using equation (3-12) and (3-13).

3.3 Parameterizations in Sim-ReSET model

The Sim-ReSET model mainly requires 5 input parameters, net radiation, soil heat flux, surface temperature, air temperature, and canopy height. All these parameters

can be obtained from remote sensing. The methods for determining air temperature and surface temperature will be described in Chapter 4.

3.3.1 Net radiation

Based on the land surface radiation balance, net radiation is the difference between the incoming and outgoing radiation,

$$R_n = R_S^\downarrow - R_S^\uparrow + R_L^\downarrow - R_L^\uparrow = (1 - \alpha)R_S^\downarrow + \sigma(\varepsilon_a T_a^4 - \varepsilon_s T_s^4) \quad (3-15)$$

In this study, a simple scheme proposed by [Bisht et al. \(2005\)](#) was used to estimate instantaneous net radiation for cloud-free days only using remote sensing observations. Because the information regarding transmittance by Reyleigh scattering, mixed gases, water vapor, aerosols and zone is not readily available, downward solar radiation is estimated using the method of [Zillman \(1972\)](#),

$$R_S^\downarrow = S_0 \cos^2 \theta / d \quad (3-16)$$

where $d = 1.085 \cos \theta + e_0(2.7 + \cos \theta) \times 10^{-3} + 0.1$. The solar zenith angle θ is calculated using the information of geographic latitude, day of year, hour angle. In equation (3-15), air emissivity is estimated using the equation proposed by [Prata \(1996\)](#),

$$\varepsilon_a = 1 - (1 + \xi) \exp[-(1.2 + 3\xi)^{1/2}] \quad (3-17)$$

where $\xi = 46.5e_0 / T_a$.

3.3.2 Soil heat flux

Soil heat flux can be estimated by multiplying net radiation by a ratio. This ratio is closely related to vegetation cover. From [Fig. 3-2](#), the ratio of soil heat flux to net radiation reaches the minimum when LAI reaches the peak. Therefore, the vegetation cover fraction weighted equation was used to estimate this ratio in many previous studies (*e.g.*, [Boegh et al., 2002](#))

$$G / R_n = \Gamma = f_{veg} \Gamma_{veg} + (1 - f_{veg}) \Gamma_{soil} \quad (3-18)$$

where Γ_{veg} and Γ_{soil} are the ratios for vegetation and soil.

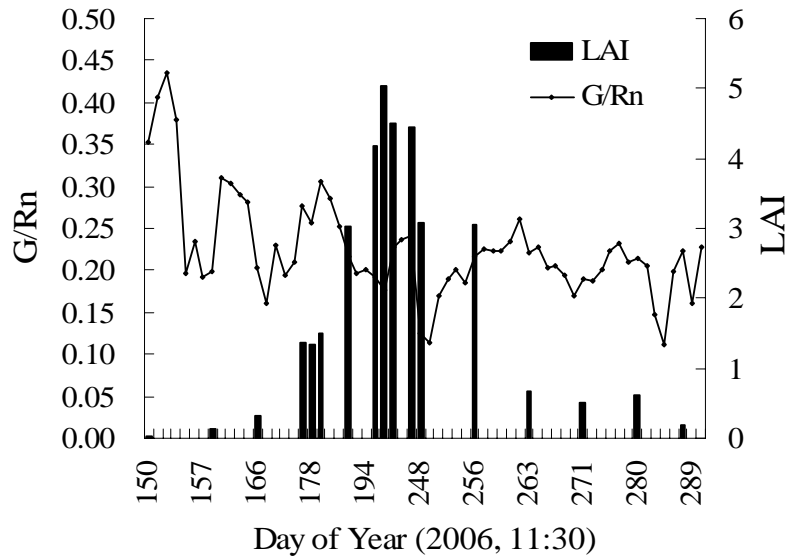


Fig.3-2 Seasonal variations of leaf area index (LAI) and the ratio of soil heat flux to net radiation in Yucheng Experimental Station in 2006.

However, it is noted that the ratio of G/R_n varies with soil water content over bare soil (Fig. 3-3). In my study area, soil field capacity is about 30%, and soil wilting point is about 10%. From Fig. 3-3, it can be found that the ratio of G/R_n also reaches the minimum when soil water content is larger than soil field capacity.

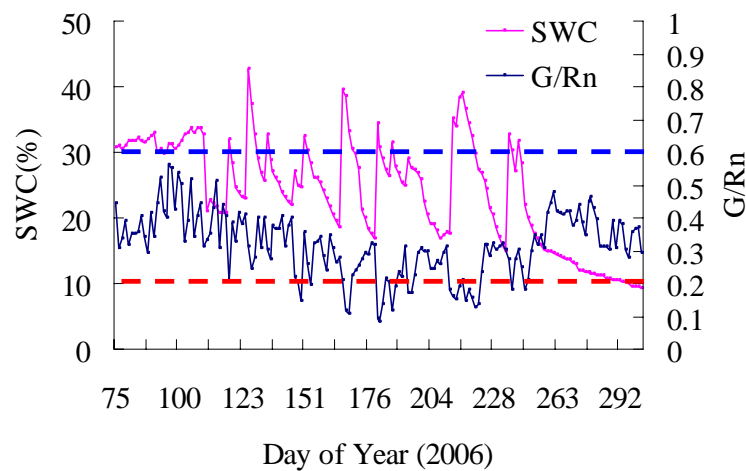


Fig.3-3 Seasonal variations of soil water content (SWC) and the ratio of soil heat flux to net radiation observed over bare soil in Yucheng Experimental Station in 2006.

The Sim-ReSET model is a dual-source model, thus soil heat fluxes for both soil and vegetation are required. Based on our experimental observations, the ratio of G/R_n for vegetation is 0.1; the ratio of G/R_n for soil can be scaled between the ratios

for dry soil and wet soil using a scaled temperature. This scaled temperature between air temperature and dry surface temperature of bare soil can be considered as an indicator of land surface moisture status (Sandholt et al., 2002).

$$\Gamma_{soil} = \frac{T_{soil} - T_a}{T_{soil-dry} - T_a} \Gamma_{soil-dry} + \left(1 - \frac{T_{soil} - T_a}{T_{soil-dry} - T_a}\right) \Gamma_{soil-wet} \quad (3-19)$$

where the ratio of G/R_n for wet soil is the same as that for vegetation, and the ratio of G/R_n for dry soil is 0.5. If albedo and emissivity are unavailable for the Sim-ReSET model input, vegetation albedo and emissivity can be considered as constants, and soil albedo and emissivity can also be estimated approximately by means of the scaled temperature in equation (3-19) where albedo and emissivity of dry bare soil are 0.25 and 0.89, and those of wet bare soil are 0.1 and 0.98, respectively.

$$\alpha_{soil} = \frac{T_{soil} - T_a}{T_{soil-dry} - T_a} \alpha_{soil-dry} + \left(1 - \frac{T_{soil} - T_a}{T_{soil-dry} - T_a}\right) \alpha_{soil-wet} \quad (3-20)$$

$$\varepsilon_{soil} = \frac{T_{soil} - T_a}{T_{soil-dry} - T_a} \varepsilon_{soil-dry} + \left(1 - \frac{T_{soil} - T_a}{T_{soil-dry} - T_a}\right) \varepsilon_{soil-wet} \quad (3-21)$$

3.3.3 Roughness length, zero plane displacement height and canopy height

In the Sim-ReSET model, roughness length for bare soil surface z_{0d} is approximate to 0.005 m. For plant canopies, z_{0m} and d_0 can be estimated by $z_{0m} = 0.13h$, $d_0 = 0.63h$, where h is canopy height. z_{0h} is calculated using the value of $kB^{-1} = \ln(z_{0m}/z_{0h}) = 2$, which is fairly constant (~ 2) for many vegetated surfaces. Vegetation canopy height is an important parameter for the estimations of land surface aerodynamic characters. In the last decades, some active sensors were developed to obtain consistent estimates of vegetation canopy height, including Light Detection and Ranging (LiDAR) (e.g., Dubayah & Drake, 2003) and Synthetic Aperture Radar (SAR) (e.g., Kellndorfer & Ulaby, 2003). From the latest research result by Walker et al. (2007), an average error of absolute height was 2.1 m for regional- to continental- scale estimates of vegetation canopy height using interferometric

synthetic aperture radar (InSAR) and passive optical remote sensing. Based on the present technologies, hence, vegetation canopy height may not be obtained with accuracy better than the absolute error of 2.1 m. For the simple and clear manner in the Sim-ReSET model, a look-up table (LUT) was adopted according to the land cover types released by the International Geosphere-Biosphere Programme (IGBP) (Table 3-1). Generally, the heights of forest and shrubland don't change with seasons, but grass and crop are the annual plants, thus their canopy heights vary with time in their whole lifecycles. In this study, it is noted that the crops' heights have linear relationships with LAI before their height reach the maximum (Fig. 3-4). Therefore, the following equation can be used to estimate the heights for crop and grass approximately,

$$h = h_{\max} f_{veg} \tag{3-22}$$

Table 3-1 The look-up table for vegetation canopy height based on the IGBP land cover classifications.

ID (IGBP)	Land cover	Height (m)
1, 2, 3, 4, 5	forests	15
6, 7	shrublands	2.5
8, 9	savannas	1
10, 16	grassland	0.5
12, 14	cropland	1
13, 15, 254	urban and built-up, permanent snow	No value

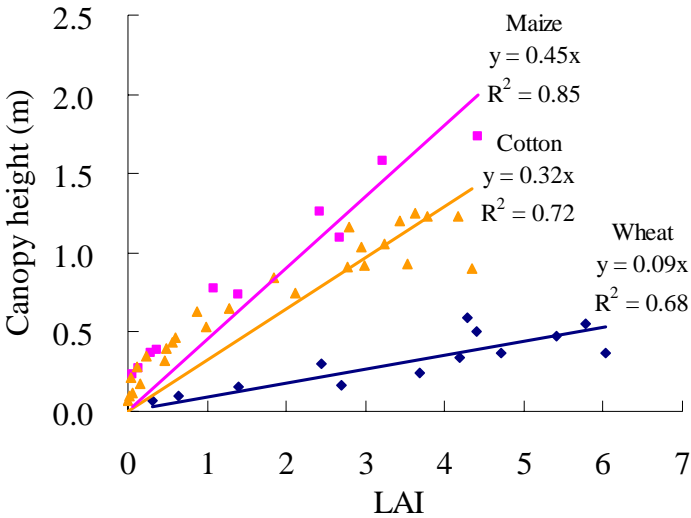


Fig.3-4 Linear relationship between canopy heights and LAI.

3.4 Conclusion

A new dual-source *ET* model was developed, named as the Sim-ReSET model. Requirements of canopy and aerodynamic resistances were avoided in the Sim-ReSET model. *ET* can be estimated by the Sim-ReSET only using remote sensing data. In order to keep the Sim-ReSET model simple and practical, the atmospheric stratification corrections were ignored in the model. There usually exists an unstable atmospheric stratification above dry bare soil surface in the daytime because air temperature near soil surface is larger than that in the higher atmospheric layers. Based on the results in Chapter 2, it can be predicted that ignoring the atmospheric stratification corrections may result in *ET* overestimation in the Sim-ReSET model.

References

- Bastiaanssen, W. G. M., Menenti, M., Feddes, R. A., & Holtslag, A. A. M. (1998a). A remote sensing surface energy balance algorithm for land (SEBAL) 1. Formulation. *Journal of Hydrology*, 212-213, 198-212.
- Bastiaanssen, W. G. M., Pelgrum, H., Wang, J., Ma, Y., Moreno, J. F., Roerink, G. J., & van der Wal, T. (1998b). A remote sensing surface energy balance algorithm for land (SEBAL) 2. Validation. *Journal of Hydrology*, 212-213, 213-229.
- Bastiaanssen, W. G. M. (2000). SEBAL-based sensible and latent heat fluxes in the irrigated Gediz Basin, Turkey. *Journal of Hydrology*, 229, 87-100.
- Bisht, G., Venturini, V., Islam, S., & Jiang L. (2005). Estimation of the net radiation using MODIS (Moderate Resolution Imaging Spectroradiometer) data for clear sky days. *Remote Sensing of Environment*, 97, 52-67.
- Boegh, E., Soegaard, H., & Thomsen, A. (2002). Evaluating evapotranspiration rates and surface conditions using Landsat TM to estimate atmospheric resistance and surface resistance. *Remote Sensing of Environment*, 79, 329-343.
- Brutsaert, W. (1998). Land-surface water vapor and sensible heat flux: spatial variability, homogeneity, and measurement scales. *Water Resources Research*, 34 (10), 2433-2442.
- Dubayah, R. O., & Drake, J. B. (2003). Lidar remote sensing for forestry. *Journal of Forestry*, 98, 44-46.
- Jia, L., Su, Z., van den Hurk, B., Menenti, M., Moene, A., De Bruim, H. A. R., Yrisarry, J. J. B., Ibanez, M., & Cuesta, A. (2003). Estimation of sensible heat flux using the surface energy balance system and ATSR measurements. *Physics and Chemistry of the Earth*, 28, 75-88.
- Kellndorfer, J. M., & Ulaby, F. T. (2003). Forest biomass inversion from SAR using object oriented image analysis techniques. *IEEE Geoscience and Remote Sensing Symposium, Toulouse*, 6, 3465-3467.
- Kustas, W. P., Perry, E. M., Doraiswamy, P. C., & Moran, M. S. (1994). Using satellite remote sensing to extrapolate evapotranspiration estimates in time and

- space over a semiarid rangeland basin. *Remote Sensing of Environment*, 49, 275-286.
- Loheide II, S. P., & Gorelick, S. M. (2005). A local-scale, high-resolution evapotranspiration mapping algorithm (ETMA) with hydroecological applications at riparian meadow restoration site. *Remote Sensing of Environment*, 98, 182-200.
- McGauley, M., C Zhang. and N. A. Bond (2004). Large-scale characteristics of the atmospheric boundary layer in the Eastern Pacific cold tongue – ITCZ region. *Journal of Climate*, 17, 3907-3920.
- Prata, A. J. (1996). A new long-wave formula for estimating downward clear-sky radiation at the surface. *Quarterly Journal of the Royal Meteorological Society*, 122, 1127-1151.
- Qiu, G. Y., Yano, T., & Momii, K. (1998). An improved methodology of measure evaporation from bare soil based on comparison of surface temperature with a dry soil surface. *Journal of Hydrology*, 210, 93-105.
- Qiu, G.Y., Shi, P.J., & Wang, L.M. (2006). Theoretical analysis of a remotely measurable soil evaporation transfer coefficient. *Remote Sensing of Environment*, 101, 390-398.
- Sandholt, I., Rasmussen, K. & Andersen, J. (2002). A simple interpretation of the surface temperature/vegetation index space for assessment of surface moisture status. *Remote Sensing of Environment*, 79, 213-224.
- Su, Z. (2002). The surface energy balance system (SEBS) for estimation of turbulent heat fluxes. *Hydrology and Earth System Sciences*, 6 (1), 85-99.
- Walker, W. S., Kellndorfer, J. M., LaPoint, E., Hoppus, M., & Westfall, J. (2007). An empirical InSAR-optical fusion approach to mapping vegetation canopy height. *Remote Sensing of Environment*, 109, 482-499.
- Zillman, J. W. (1972). A study of some aspects of the radiation and heat budgets of the southern hemisphere oceans. *Meteorol. Studyl 26, Bur. Of Meteorol..* Canberra, Australia: Dept. of the Inter.

Chapter 4

A New Method to Obtain “Dry and Wet Points” for Sim-ReSET Model Using Subpixel Information

4.1 Introduction

The VI-Ts diagram determined by the scatter points of remotely sensed vegetation index (VI) and land surface temperature (Ts) has been widely used to retrieve information on the partitioning of available surface energy (Boegh et al., 2002; Nishida et al., 2003; Venturini et al., 2004) and surface moisture status (Smith and Choudhury, 1991; Nemani et al., 1993; Moran et al., 1994; Carlson et al., 1995; Gillies et al., 1997; Sandholt et al., 2002). All these applications are under the condition of homogenous atmospheric forcing such as solar radiation and air temperature over a sampling window for the definition of a VI-Ts diagram, so the size of the sampling window can not be too large. If the sampling window covers full ranges of land surface moisture (from dry to well-watered) and VI (from bare soil to closed canopy), the VI-Ts diagram typically represents a right triangle when canopy temperature is assumed to be equal to Ts of well-watered bare soil (Nishida et al., 2003; Gillies et al., 1997; Sandholt et al., 2002; Prihodko and Goward, 1997) (Fig. 4-1). The triangular VI-Ts diagram has been widely applied in previous studies (Nishida et al., 2003; Venturini et al., 2004; Smith and Choudhury, 1991; Nemani et al., 1993). The key point in these applications is how to define an ideal VI-Ts diagram, while the key point in the definition of the VI-Ts diagram is how to determine a dry edge in the VI-Ts diagram. Two automatic methods were proposed to define the dry edge in previous studies (Nemani et al., 1993; Sandholt et al., 2002; Verstraeten et al., 2005). However, these two traditional methods require

enough pixels that cover full ranges of land surface moisture and VI. Practically, it is difficult to find enough ideal pixels within a limited sampling window, especially when using a satellite data with coarse resolution, such as 1 km MODerate-resolution Imaging Spectroradiometer (MODIS) data. Generally, a natural land surface at the scale of 1 km is usually a mixture of vegetation, water and soil. If the component Ts information of vegetation and bare soil within a 1 km pixel can be obtained, the two extreme surface conditions, dry bare soil (dry point) and closed vegetation (wet point), will be found with more possibilities at subpixel scale. From Fig. 4-1, the VI-Ts diagram will be readily defined if the dry and wet points are determined.

The MODIS and the Advanced Spaceborne Thermal Emission Reflection Radiometer (ASTER) are onboard the NASA's Earth Observation System (EOS)-Terra satellite launched in 1999, both of which can provide high quality observations of land surface. MODIS was designed to collect observational data over a wide range at moderate resolutions (250 m, 500 m and 1000 m) with almost daily coverage of the Earth (<http://modis.gsfc.nasa.gov/>). ASTER captures high spatial resolution data in 14 bands, from the visible (15 m) to the thermal infrared (90 m) wavelengths, and provides a capability of stereo viewing (30 m) for the digital elevation model creation (<http://asterweb.jpl.nasa.gov/>). As the "zoom lens" for Terra, ASTER data can be used by other Terra and space-borne instruments for validation and calibration. Since both MODIS and ASTER are on the same satellite, ASTER provides an opportunity to validate MODIS observational data.

The purposes of this chapter were as followings: (1) to propose a new practical method to define a VI-Ts diagram using subpixel information from vegetation and bare soil within an 1 km - MODIS pixel; (2) to validate the proposed method by using ASTER data; (3) to compare the proposed method with the traditional method by using MODIS data across a semiarid agricultural region in the North China Plain through 2003.

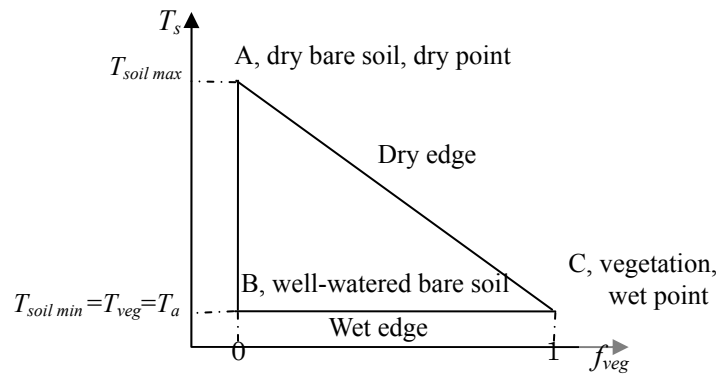


Fig.4-1 The concept of a triangular VI-Ts diagram. Point A is called dry point, and Point C is called wet point in the VI-Ts diagram. AC is named as dry edge, and BC is named as wet edge.

4.2 Methods

4.2.1. Study area and ground data collection

The North China Plain (NCP) is one of main food production regions in China. There is a typical continental monsoon climate over the NCP. The yearly mean air temperature is 13.1°C, and the annual precipitation is about 610 mm, of which about 70% falls between June and August. Therefore, the NCP is zoned as a semiarid agricultural region. Our study area (30 km × 30 km) locates at the center of the NCP (Fig. 4-2). The light, temperature and water conditions support a 1-year 2-harvest cropping system (winter wheat (Oct.-Jun.) - summer maize (Jul.-Sep.)) in this study area. Winter wheat is mainly dependent on irrigation. Usually, about four irrigations are required in the whole growing season of winter wheat. The Yucheng Experimental Station (YES, Latitude 36°50'N, Longitude 116°35'E, 26m altitude) of the Chinese Academy of Sciences locates in the study area.

Regular meteorological data recorded at the time when the EOS-Terra satellite overpassed our study area were collected from a flux station in the YES through 2003 including air temperature, humidity, wind speed, precipitation, downward and upward shortwave solar radiation, and downward and upward long-wave radiation (Wang et al., 2005). The bulk temperature of an infinitely thick vegetation canopy is close to ambient air temperature (Prihodko and Goward, 1997). Hence, observed air temperature was used to validate Ts of wet points (Ts_wet) in this study.

Assuming that the latent heat flux is 0 over the surface of dry point, the T_s of dry point (T_{s_dry}) can be obtained based on the land surface energy balance (Moran et al., 1994; Loheide and Gorelick, 2005; Zhang et al., 2005)

$$T_{s_dry} = \frac{(R_n - G)(r_a + r_{excess})}{\rho_a C_p} + T_a \quad (4-1)$$

The methods of r_a and r_{excess} calculations are the same to those in previous literatures (Moran et al., 1994; Loheide and Gorelick, 2005; Zhang et al., 2005). In this study, T_s of dry points estimated based on the ground data were used to validate those derived from remote sensing data.

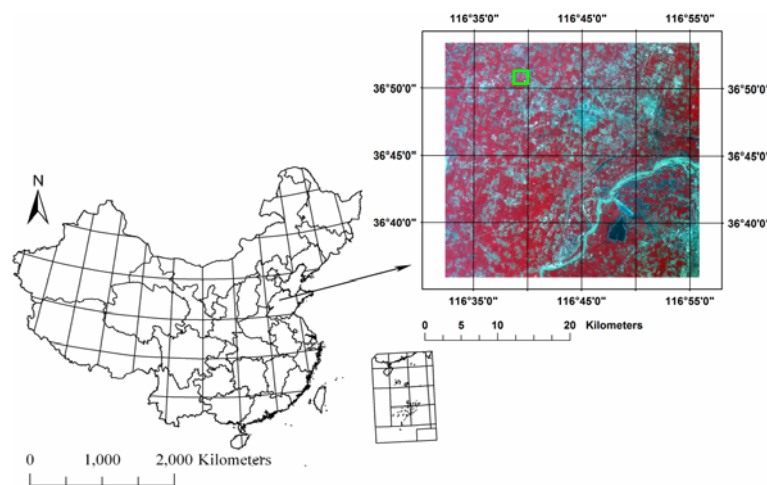


Fig.4-2 Study area. On the right is the ASTER false-color image (UTM-N50, WGS-84, 15 m, Band 3, 2, 1). The red part is vegetation, mainly winter wheat. The green rectangle in the ASTER image is the Yucheng Experimental Station (YES).

4.2.2 Satellite data collection and processing

Two level-2 data products of ASTER (projection: UTM-50N; datum: WGS-84) over our study area on May 9 2003 were collected from the Japanese Ground Data System (http://www.gds.aster.ersdac.or.jp/gds_www2002/index_e.html): AST07 - the atmospheric corrected surface reflectance (resolution: 15 m), and AST08 - the surface temperature qualitatively assessed by cloud mask (resolution: 90 m). The AST08 is produced using the Temperature Emissivity Separation (TES) algorithm that yields accuracies around 0.01 for surface emissivity and 1 K for radiometric temperature, respectively (Gillespie et al., 1998). At the same observational time to ASTER (about 11:00 am of local standard time on May 9 2003), two MODIS data

products (projection: Sample IS; datum: WGS-84; resolution: 1 km) were also collected from the EOS data gateway (<http://edcimswww.cr.usgs.gov/pub/imswelcome/>): MOD11 - the daily land surface temperature and emissivity masked by clouds, and MOD09 - the atmospheric corrected surface reflectance. The MOD11 product has been validated in South America, and results showed that the accuracy was better than 1°C in the range from -10°C to 50°C (Wan et al., 2004). Both MODIS and ASTER products are georegistered in their making processes. The accuracy of MODIS geolocation approximates 50 m at the nadir (Wolfe et al., 2002). The hand-to-hand registration accuracy of ASTER is better than 0.2 pixels (Iwasaki and Fujisada, 2005). The reflectances of red and near-infrared bands were used to calculate the Normalized Difference Vegetation Index (MODIS_NDVI and ASTER_NDVI). ASTER_Ts was resampled to the resolution of 1 km from 90 m by averaging pixels in order to compare the system difference between MODIS and ASTER sensors. The projection of MODIS data was transferred from Sample IS to UTM-50N. The statistics of above datasets were listed in Table 1. It is found that both maximum and range of MODIS_NDVI are greater than those of ASTER_NDVI, which is consistent with the report in (Buheosier et al., 2003). Due to the pixel-average scaling effect (Jacob et al., 2004; Liu et al., 2006), 1km_ASTER_Ts has a larger minimum and a smaller maximum, and then a narrow range compared to the 90 m ASTER_Ts. The comparison of 1 km_ASTER_Ts with MODIS_Ts reveals that Ts observed by ASTER is a little larger than that by MODIS (Fig. 4-3a). The root mean square error (RMSE) of the difference between 1 km_ASTER_Ts and MODIS_Ts is 3.61°C. From Table 4-1, only the minimum 1 km_ASTER_Ts is close to the minimum MODIS_Ts, and other statistical items show larger differences between 1 km_ASTER_Ts and MODIS_Ts. This is caused by the difference of their respective retrieval algorithms (Gillespie et al., 1998; Wan et al., 2004; Jacob et al., 2004). In order to make MODIS_Ts comparable to 1 km_ASTER_Ts, 1 km_ASTER_Ts was normalized based on their relationship in Fig. 4-3a,

$$ASTER_Ts = 1.25 \times MODIS - 2.33$$

$$ASTER_Ts_N = MODIS_Ts = (ASTER_Ts + 2.33) / 1.25 \quad (4-2)$$

where $ASTER_Ts_N$ is the normalized $ASTER_Ts$. The RMSE of difference between the normalized 1 km $ASTER_Ts$ and $MODIS_Ts$ is reduced to 0.98°C (Fig. 4-3b). The 90 m $ASTER_Ts$ was also normalized using equation (4-2) to remove the effects caused by the difference between their respective algorithms, and the spatial variability and scaling issues.

Table 4-1 Statistics of the ASTER and MODIS datasets related to Ts and NDVI on May 9 2003.

Dataset	Resolution	Size (pixel×pixel)	Min.	Max.	Mean	Stdev*	Range
15 m $ASTER_NDVI$	15 m	2336×2158	0.03	0.74	0.40	0.11	0.71
$MODIS_NDVI$	1000 m	35×33	0.07	0.85	0.44	0.09	0.78
90 m $ASTER_Ts$ ($^\circ\text{C}$)	90 m	390×359	17.85	46.85	25.97	2.29	29.00
1 km $ASTER_Ts$ ($^\circ\text{C}$)	1000 m	35×33	20.40	34.37	26.19	1.63	13.97
$MODIS_Ts$ ($^\circ\text{C}$)	1000 m	35×33	20.05	27.15	22.81	0.86	7.10

* Stdev is the standard deviation.

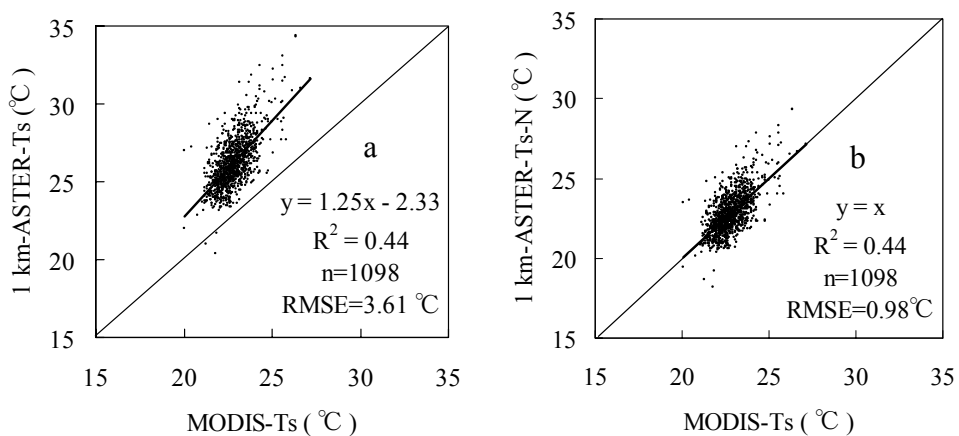


Fig.4-3 Comparisons of (a) 1 km $ASTER_Ts$ and (b) normalized 1km $ASTER_Ts$ with $MODIS_Ts$.

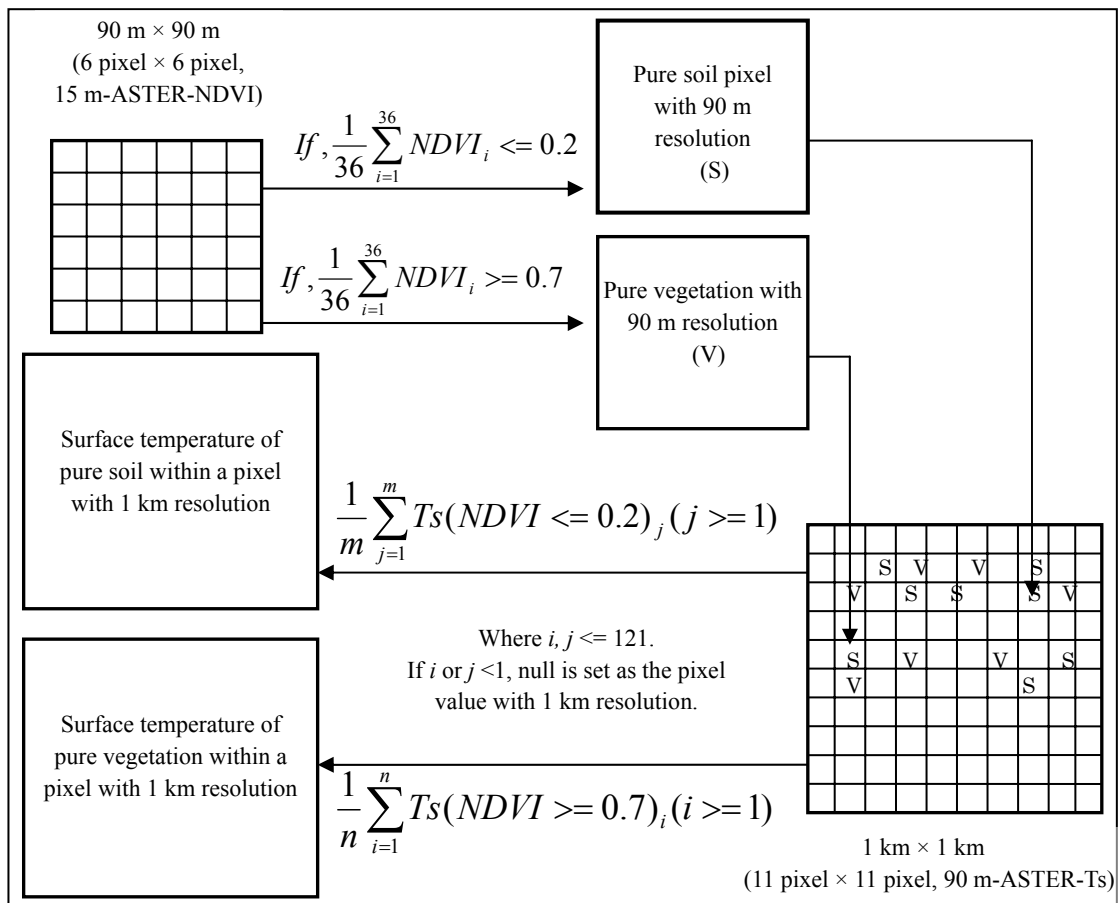


Fig.4-4 Procedure scheme of identifying the ASTER 90 m-pixels of pure soil and vegetation and obtaining Ts of pure soil and vegetation within a pixel with 1 km resolution.

In this study, MODIS_Ts was decomposed to the component Ts of vegetation and soil, and then the retrieved component Ts were evaluated by comparing with Ts of pure vegetation and soil retrieved from 15m_ASTER_NDVI and normalized 90m_ASTER_Ts. The detailed process of obtaining Ts of pure soil and vegetation was shown in Fig. 4-4. Firstly, pure vegetation and soil pixels were identified using their respective ASTER_NDVI thresholds, and then were resampled from 15 m to 90 m. Based on a histogram analysis and viewing-identification on 15 m ASTER_NDVI, we found that NDVI of pure soil pixels was less than 0.20, while NDVI of pure vegetation pixels was greater than 0.7. These values are consistent with those proposed in a previous study (Jiménez-Muñoz et al., 2006). Then, Ts of pure vegetation and soil pixels with 90 m resolution were averaged within a pixel with 1 km resolution.

In order to further compare the VI-Ts diagrams defined respectively using the MODIS pixel and subpixel information, MODIS_Ts and MODIS_NDVI on other 12 cloud-free days through 2003 were also collected (Table 4-2). Here, MODIS_NDVI was calculated using the MOD09 reflectance product.

Table 4-2 Statistics of MODIS_NDVI and MODIS_Ts on 12 cloud-free days in 2003.

Year/Month/Day	MODIS_NDVI					MODIS_Ts (°C)				
	Min.	Max.	Mean	Stdev	Range	Min.	Max.	Mean	Stdev	Range
2003-3-27	0.05	0.49	0.3	0.07	0.44	11.79	25.91	21.05	1.85	14.12
2003-4-25	0.1	0.86	0.46	0.11	0.75	17.95	24.49	20.63	0.93	6.54
2003-4-30	0.1	0.81	0.48	0.11	0.7	19.95	27.63	23.42	0.82	7.68
2003-5-13	0.15	0.75	0.5	0.1	0.6	24.79	35.17	28.17	1.19	10.38
2003-6-24	0	0.66	0.31	0.05	0.66	29.61	38.35	35.18	1.46	8.74
2003-6-28	0	0.44	0.32	0.05	0.44	30.29	40.55	36.13	1.58	10.26
2003-7-26	0.18	0.93	0.76	0.11	0.75	28.35	32.85	30.19	0.44	4.5
2003-9-21	0.17	0.87	0.69	0.12	0.7	24.13	30.81	26.23	0.93	6.68
2003-10-21	0.03	0.61	0.29	0.06	0.59	18.35	22.79	20.99	0.68	4.44
2003-10-23	0	0.55	0.27	0.06	0.55	14.67	19.63	16.95	0.94	4.96
2003-11-22	0.01	0.52	0.27	0.05	0.51	6.45	8.97	7.74	0.4	2.52
2003-12-26	0	0.46	0.24	0.05	0.46	2.55	7.89	4.94	1.12	5.34

4.2.3 Estimating the component surface temperatures of vegetation and soil

A given pixel can be approximately considered as a mixture of vegetation and bare soil in our study area. If the dry and wet points are determined using the minimum component Ts of vegetation and the maximum component Ts of bare soil within a sampling window, a triangular VI-Ts diagram will be easily defined based solely on these two points. Therefore, the key work in our proposed method for defining the VI-Ts diagram is to estimate the component Ts of vegetation and soil. Several methods have been proposed to estimate component Ts in previous studies (Nishida et al., 2003; Zhang et al., 2005; Cain, 2004; Dozier, 1981; Xu et al., 2001; Zhang et al., 2003). In these previous studies, at least two equations are required to estimate the component surface temperatures of vegetation (T_{veg}) and soil (T_{soil}) within a pixel. One equation can be obtained based on the energy balance emitted from land surface (Zhang et al., 2005; Cain, 2004; Dozier, 1981; Xu et al., 2001; Zhang et al., 2003; Heilman et al., 1981),

$$\sigma \varepsilon_s T_s^4 = f_{veg} \sigma \varepsilon_{veg} T_{veg}^4 + (1 - f_{veg}) \sigma \varepsilon_{soil} T_{soil}^4 \quad (4-3)$$

where ε_{veg} and ε_{soil} are the emissivities of vegetation and soil within a pixel; and ε_s is the emissivity of a mixed pixel surface (a mixture of vegetation and soil). Hence, ε_s can be approximately estimated using ε_{veg} , ε_{soil} and f_{veg} (Jiménez-Muñoz et al., 2006),

$$\varepsilon_s = f_{veg} \varepsilon_{veg} + (1 - f_{veg}) \varepsilon_{soil} \quad (4-4)$$

After combining equations (4-3) and (4-4), equation (4-3) can be rewritten as,

$$(f_{veg} \varepsilon_{veg} + (1 - f_{veg}) \varepsilon_{soil}) T_s^4 = f_{veg} \varepsilon_{veg} T_{veg}^4 + (1 - f_{veg}) \varepsilon_{soil} T_{soil}^4 \quad (4-5)$$

where T_s and f_{veg} can be obtained from remote sensing images, and ε_{veg} and ε_{soil} can be considered as constants, 0.98 for vegetation and 0.89 for soil in this study.

The other equation was obtained using different information in previous studies, e.g., multi-channel data of thermal infrared radiometer (Cain, 2004; Dozier, 1981), multi-angle observations of thermal infrared radiometer (Xu et al., 2001), thermal inertia information (Zhang et al., 2003), and the isoline of land surface moisture in a VI-Ts diagram (Nishida et al., 2003; Zhang et al., 2005). If the variation of vegetation surface temperature is considered, the VI-Ts diagram is similar to a trapezoid in Fig. 1-1. Within all pixels on an isoline of land surface moisture, soil and vegetation surface moisture statuses are homogeneous (Fig. 4-5). Because the atmospheric forcing is required to be homogeneous over the sampling window, it can be assumed that surface temperatures of soil and vegetation are respectively homogeneous within pixels on the same isoline of land surface moisture, and that surface temperature variation of pixels on the isoline of land surface moisture is caused by vegetation cover fraction. Therefore, based on two similar triangles (ΔACE and ΔBCD in Fig. 4-5), an equation can be obtained,

$$\frac{1 - f_{veg}}{1 - 0} = \frac{T_s - T_{veg}}{T_{soil} - T_{veg}} \quad (4-6)$$

Combining equations (4-6) and (4-5), component temperatures of soil and vegetation can be obtained.

$$T_{soil} = \frac{T_s - f_{veg} T_{veg}}{1 - f_{veg}} \quad (4-7)$$

$$T_{soil} = [((f_{veg} \epsilon_{veg} + (1 - f_{veg}) \epsilon_{soil}) T_s^4 - f_{veg} \epsilon_{veg} T_{veg}^4) / (1 - f_{veg}) \epsilon_{soil}]^{1/4} \quad (4-8)$$

It should be noted that equation (4-8) is a nonlinear one, and right side of it includes T_{veg} . Thus an iteration solution with a step of 0.2°C is required to obtain T_{veg} . A test showed that equation (4-8) was convergent, and that the calculations could be finished within some iterations.

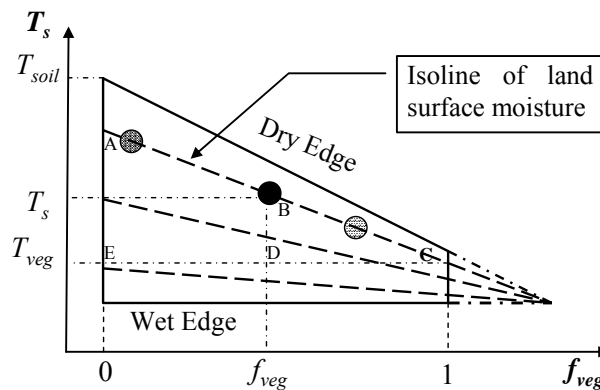


Fig.4-5 The trapezoidal VI-Ts diagram for obtaining surface temperatures of soil and vegetation.

4.3 Results

4.3.1 Validating the MODIS_ T_{veg} and MODIS_ T_{soil} using the normalized 90m_ASTER_ T_s

The component surface temperatures, MODIS_ T_{veg} (vegetation) and MODIS_ T_{soil} (soil), were obtained from MODIS data by using the method described in section 4.2.3. Surface temperatures of pure soil and vegetation pixels were also obtained from the normalized 90 m_ASTER_ T_s according to the procedure shown in Fig. 4-4. Results show that MODIS_ T_{veg} agrees well with 90 m_ASTER_ T_{veg_N} . The differences of statistic items between MODIS_ T_{veg} and 90 m_ASTER_ T_{veg_N} are all less than 1°C (Table 4-3). The means of MODIS_ T_{soil} and 90 m_ASTER_ T_{soil_N} are also close. Their difference is less than 2°C . Compared with 90 m_ASTER_ T_{soil_N} , however, MODIS_ T_{soil} has a narrower range because of the

inherent bias between MODIS_Ts and ASTER_Ts although ASTER_Ts has been normalized. These accuracies of MODIS_T_{veg} and MODIS_T_{soil} estimations are similar to those reported in (Xu et al., 2001; Archer and Jones, 2006), especially for the estimation of MODIS_T_{veg}.

Table 4-3 Comparisons of MODIS_T_{veg} and MODIS_T_{soil} with the normalized 90 m_ASTER_Ts of pure vegetation and soil on May 9 2003.

	Pixels	Mean	Stdev	Range	Min.	Max.
90 m_ASTER_T _{veg_N} (°C)	356	20.72	0.68	5.36	19.42	24.78
MODIS_T _{veg} (°C)	356	21.09	0.78	5.13	19.8	24.93
90 m_ASTER_T _{soil_N} (°C)	549	24.78	2.05	12.17	17.28	29.45
MODIS_T _{soil} (°C)	549	23.16	0.76	6.49	21.26	27.75

4.3.2 Comparing the proposed and traditional methods with results obtained from the normalized 90 m_ASTER_Ts

Results of three triangular VI-Ts diagrams defined by different methods are shown in Fig. 4-6. In Fig. 4-6a, the maximum 90 m_ASTER_T_{soil_N} and minimum 90 m_ASTER_T_{veg_N} were used to determine dry and wet points, then to define a triangular VI-Ts diagram on May 9 2003. This VI-Ts diagram based on the normalized 90 m_ASTER_Ts is considered as a “true” VI-Ts diagram in this study. In Fig. 4-6b, the minimum MODIS_T_{veg} and maximum MODIS_T_{soil} were also used to define a triangular VI-Ts diagram based on the subpixel information of MODIS. In Fig. 4-6c, the triangular VI-Ts diagram was defined using the traditional method based on the pixel information of MODIS. The traditional method is a combination of two previous automatic methods (Nemani et al., 1993; Sandholt et al., 2002; Verstraeten et al., 2005). Firstly, the pixels with maximum temperatures within each small VI interval are selected from the VI-Ts scatter plot. Then, some selected pixels far from the upper boundary of the VI-Ts scatter plot are excluded. Finally, the dry edge is defined by a linear regression on the available selected pixels.

The VI-Ts diagram in Fig. 4-6b is similar to that in Fig. 4-6a, but the VI-Ts diagram in Fig. 4-6c is far from that in Fig. 4-6a. The wet point in Fig. 4-6b is very

close to that in Fig. 4-6a because the difference between the minimum 90 m-ASTER- T_{veg-N} and the minimum MODIS- T_{veg} is less than 1°C . However, the dry point in Fig. 4-6b is a little lower than that in Fig. 4-6a because the T_{s_dry} in Fig. 4-6b is 1.34°C lower than that in Fig. 4-6a. If this shift of dry point between Fig. 4-6a and 4-6b resulted from the T_s bias between MODIS and ASTER is ignored, the VI- T_s diagrams are very close between two figures. However, the T_{s_dry} in Fig. 4-6c (26.84°C) is lower, and the T_{s_wet} (21.56°C) is higher by than those in Fig. 4-6a. This results in a VI- T_s triangle far from the “true” VI- T_s diagram in Fig. 4-6a. The reason of higher T_{s_wet} in Fig. 4-6c is due to few pixels for determining the dry edge within the range between 0.5 and 1.0 of vegetation cover fraction. This weakness cannot be avoided by the traditional method because it depends on both the full ranges of vegetation cover fraction and land surface moisture. From the comparisons in Fig. 4-6, it is indicated that the proposed method has a similar capability to define the VI- T_s diagram using a coarse-resolution MODIS data just like using a fine-resolution ASTER data.

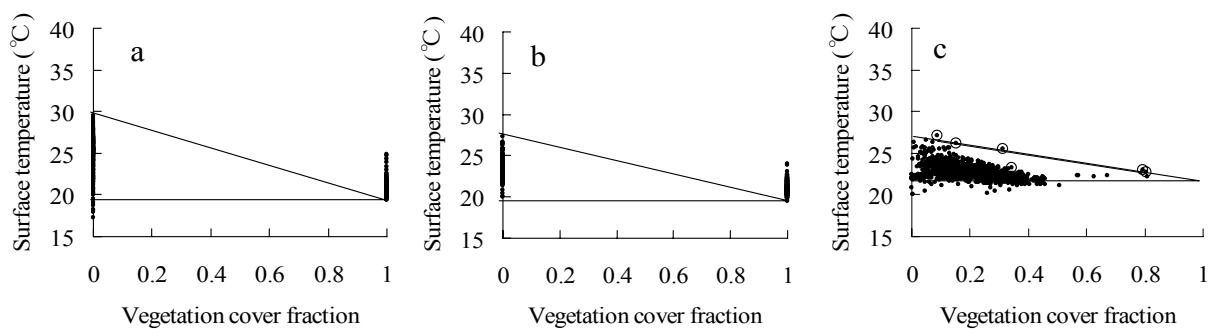


Fig. 4-6 The VI- T_s diagrams on May 9 2003 (a) defined using the 90 m_ ASTER_ T_s of pure vegetation and soil, (b) defined by the proposed method using MODIS data, and (c) defined by the traditional method using MODIS data. In Fig. 4-6a and 4-6b, yellow and green points are component T_s of soil and vegetation, respectively. In Fig. 4-6c, yellow circles (o) are pixels for defining the dry edge.

4.3.3 Comparing the proposed and traditional methods for defining the VI-Ts diagram based on MODIS data through the whole year of 2003

The proposed and traditional methods were also tested using other 12 MODIS datasets on cloudless days through 2003. Results were listed in [Table 4-4](#) (including results on May 9 2003), and the VI-Ts diagrams were shown in [Fig. 4-7](#). The absolute differences between Ts_{dry} estimated based on the ground data and Ts_{dry} estimated by the proposed method are all less than 1.66°C through 2003. The average of differences through the whole year is 0.95°C . As for the traditional method, the average of absolute differences of Ts_{dry} is 1.62°C . From [Fig. 4-7](#), it is obviously shown that this larger error is mainly caused by the large differences on Jul. 26 (5.63°C) and Sep. 21 (4.81°C). From July to September is the rainy season in the NCP. There were 63.5 mm and 11 mm rainfalls in the half month just before Jul. 26 ([Fig. 4-8a](#)) and Sep. 21 ([Fig. 4-8b](#)) in 2003, respectively. Both soil and vegetation had been watered before the EOS-Terra satellite overpassed on Jul. 26 and Sep. 21, so the Ts of bare soil pixels were close to the Ts of vegetation pixels, and the ranges of Ts were only 4.5°C and 6.68°C over the study area, respectively. Therefore, it was very difficult to find the true dry point using the traditional method at the 1-km pixel scale in the rainy season, although the concrete, asphalt or some bare soil surfaces within pixels had become dry after the sunrise. In contrast, the proposed method could obtain the dry points with good accuracies based on subpixel information in the rainy season. The absolute biases were reduced to 1.41°C and 1.03°C on Jul. 26 and Sep. 21, respectively.

From [Table 4-4](#), the maximum absolute difference between Ts_{wet} based on the ground data and Ts_{wet} estimated by the proposed method is 2.68°C . The average of absolute differences through 2003 is 0.82°C . As for the traditional method, the average of absolute differences of Ts_{wet} through the whole year is 3.99°C . This larger error is mainly caused by the large differences of Ts_{wet} on Mar. 27 (13.82°C , before the re-growing of winter wheat), Jun. 28 (11.79°C , after the harvest of winter wheat) and Dec. 26 (10.71°C , in winter). In [Fig. 4-7](#), the ranges

of MODIS_NDVI were all narrower than 0.5 on these three days, so less information on Ts of vegetation pixels contributed to dry edges, and thus resulted in large errors on dry edges. In the proposed method, however, wet points could be obtained using the minimum Ts within a sampling window even in the case of narrow range of NDVI. The absolute biases were reduced to 0.30°C, 0.88°C and 0.16°C on Mar. 27, Jun. 28 and Dec. 26, respectively.

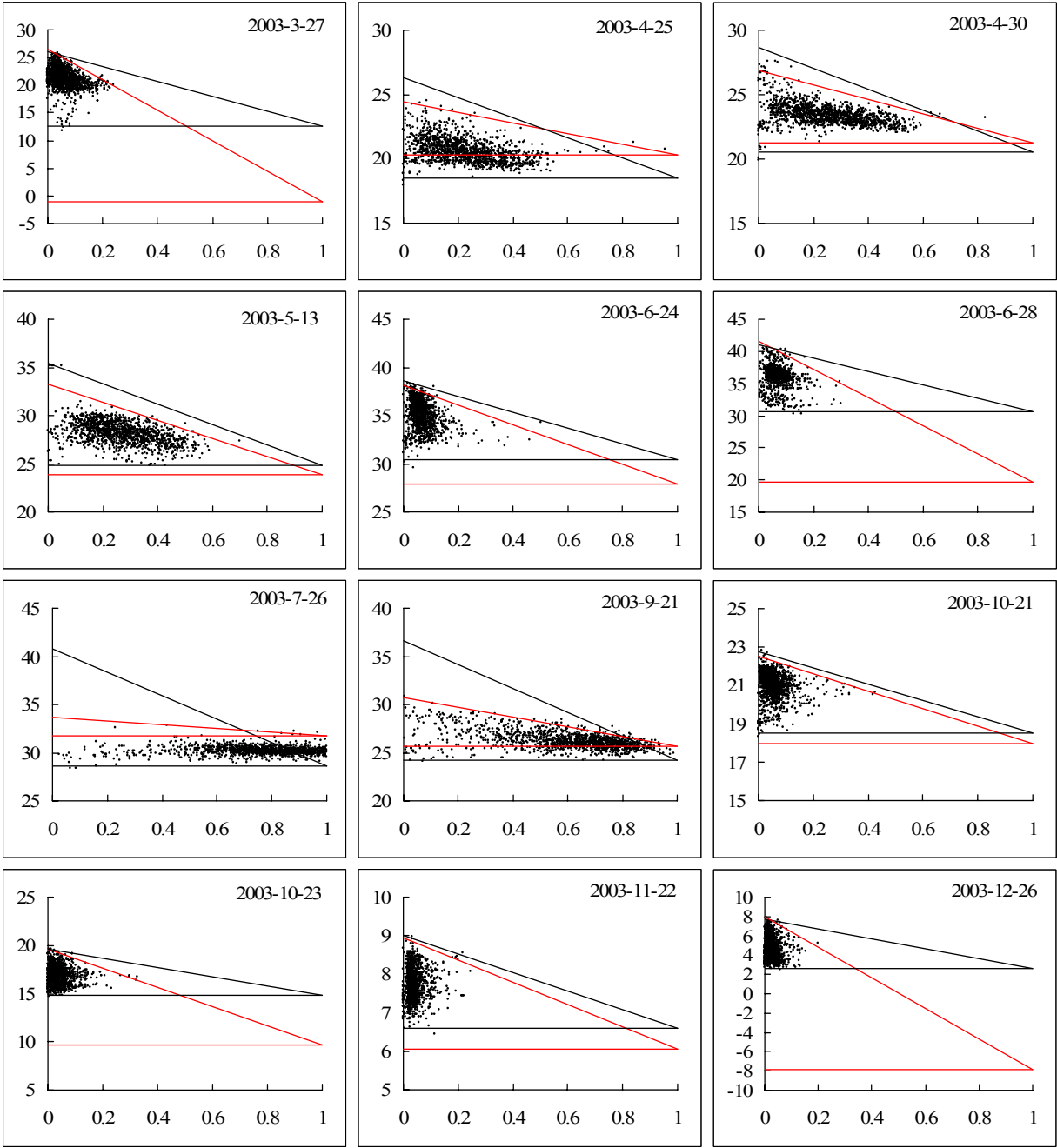


Fig. 4-7 The VI-Ts diagrams defined by the proposed (black) and traditional (red) methods using MODIS data through 2003. The horizontal axis is vegetation cover fraction, and the vertical axis is surface temperature in °C.

Table 4-4 Surface temperatures of dry and wet points from the ground data, the proposed and the traditional methods using MODIS data, respectively.

Year/Month/Day	Based on the ground data		Proposed method using MODIS data				Traditional method using MODIS data			
	Ts_dry (°C)	Ts_wet (°C)	Ts_dry (°C)	*Absolute bias of Ts_dry (°C)	Ts_wet (°C)	Absolute bias of Ts_wet (°C)	Ts_dry (°C)	Absolute bias of Ts_dry (°C)	Ts_wet (°C)	Absolute bias of Ts_wet (°C)
2003/3/27	24.51	12.85	26.16	1.66	12.55	0.30	26.56	2.06	-0.97	13.82
2003/4/25	25.26	18.80	26.33	1.07	18.49	0.31	24.41	0.85	20.31	1.51
2003/4/30	27.29	21.95	28.68	1.39	20.50	1.45	26.90	0.38	21.29	0.66
2003/5/9	28.51	19.19	27.45	1.06	20.23	1.04	26.84	1.67	21.56	2.37
2003/5/13	36.33	22.60	35.41	0.92	24.88	2.28	33.28	3.05	23.82	1.22
2003/6/24	38.31	30.34	38.63	0.31	30.46	0.12	38.12	0.19	27.86	2.48
2003/6/28	41.78	31.52	41.00	0.78	30.64	0.88	41.62	0.16	19.73	11.79
2003/7/26	39.36	31.27	40.77	1.41	28.59	2.68	33.72	5.63	31.72	0.45
2003/9/21	35.56	24.20	36.60	1.03	24.25	0.05	30.75	4.81	25.71	1.51
2003/10/21	22.55	17.77	22.77	0.22	18.54	0.77	22.52	0.04	17.97	0.20
2003/10/23	20.86	14.29	19.63	1.22	14.83	0.54	19.63	1.23	9.61	4.68
2003/11/22	8.99	6.54	9.02	0.03	6.61	0.07	8.96	0.03	6.06	0.48
2003/12/26	9.00	2.81	7.75	1.24	2.65	0.16	8.01	0.99	-7.90	10.71
Average				0.95		0.82		1.62		3.99

*Absolute bias is the absolute difference between ground-based value and MODIS-based value.

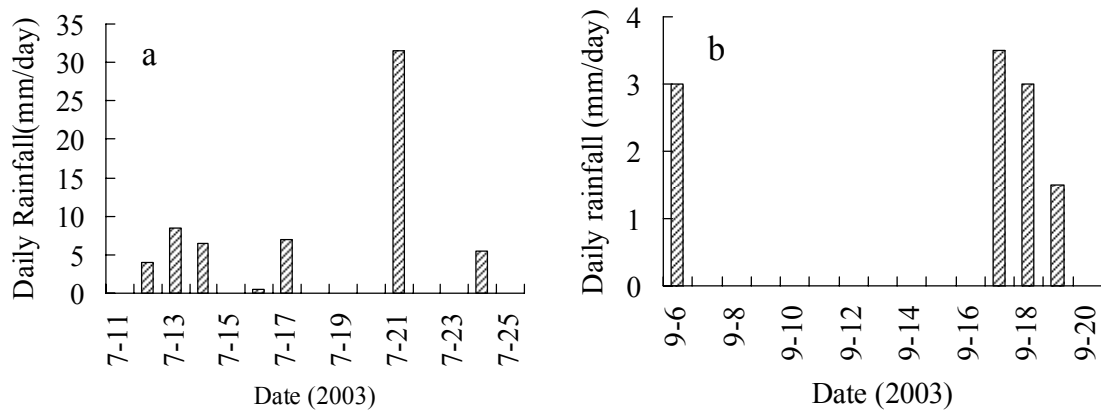


Fig. 4-8 Daily rainfall within the half month just before Jul. 26 (a), and Sep. 21 (b) in 2003.

4.4 Discussions

4.4.1 Issues about the Bias between MODIS_Ts and ASTER_Ts

MODIS_Ts and ASTER_Ts retrievals were compared by considering the spatial variability of the 11×11 aggregated ASTER pixel (90 m) values inside the corresponding MODIS pixel (1 km) in a previous study (Jacob et al., 2004). They took 2.5°C as a given threshold. If the standard deviation of radiometric temperature was larger than 2.5°C , the MODIS and ASTER pixels were not considered, and then their results showed that selected MODIS_Ts and scaled ASTER_Ts retrievals were in good agreement. In order to compare all MODIS_Ts and ASTER_Ts over our study area, the threshold of Ts standard deviation was not used to exclude pixels. From Fig. 4-3a, MODIS_Ts is lower than 1 km_ASTER_Ts. The first reason comes from their respective algorithms (Gillespie et al., 1998; Wan et al., 2004; Jacob et al., 2004), and the second reason is probably that the spatial variability and scaling issues are not considered (Jacob et al., 2004; Liu et al., 2006). In order to remove these effects, ASTER_Ts was normalized in this study. MODIS_Ts is then relatively consistent with the normalized 1 km_ASTER_Ts (Fig. 4-3b), but MODIS_Ts is still a little lower than 1 km_ASTER_Ts_N, especially for pixels with higher Ts (see points in the upper of scatter plot in Fig. 4-3b). This results in a small shift of dry point in Fig. 4-6. If this shift is ignored, the VI-Ts diagrams are very close between Fig. 4-6a and 4-6b.

4.4.2 Issues about obtaining dry and wet points

In the proposed method, the key process is to obtain T_{veg} and T_{soil} , and then to determine dry and wet points. In equation (4-2), a pixel is considered as a mixture of vegetation and soil where non-vegetation components are all simplified as soil. T_{veg} can be considered as a “true” value of vegetation. However, T_{soil} may be not the “true” value of soil but of other components such as roads, house roofs and water surface. In this study, dry point is defined as a surface without vegetation cover and evaporation. Water surface can be excluded because of its low T_s and strong evaporation, but the impervious surfaces such as roads, house roofs satisfy the definition of dry point. It is well known that impervious surfaces and soils have a heating effect through absorbing and holding solar energy, so T_s of them are usually higher than T_s of vegetation and water. Analysis of ASTER images for examining the relationship between urban thermal features and biophysical descriptors in Indianapolis (Indiana, USA) showed that T_s of impervious surfaces in urban areas were relatively higher than that of dry soil surface in agricultural areas (Lu and Deng, 2006; Small, 2006). This was also validated using ASTER images in our study area, and results show that T_s of impervious surfaces in urban areas are 2-6°C higher than that of dry soil surface in agricultural areas on May 9 2003. Further analysis on the VI- T_s diagram from 90 m ASTER_ T_s and ASTER_NDVI shows that some scatter points near the position of dry point in the VI- T_s diagram correspond to urban areas. Therefore, there may be several subpixel can all meet the conditions of dry points in a VI- T_s diagram, especially in or near urban areas (Fig. 4-9). If several dry points occur in the same VI- T_s diagram, the dry point defined by our proposed method must be the point (dry point 1) with the maximum T_s (e.g., roads, house roofs), and the true dry point (dry point 3, e.g., bare soil) will be excluded. This is the reason why the average absolute error of dry point estimation (0.95°C) using our proposed method is relatively larger than that of wet point estimation in this study. However, this error is not significant because our study area is an agricultural landscape. In order to identify the true dry point in or near urban areas, the technology of spectral mixture analysis (Lu and Deng,

2006; Small, 2006) is suggested to distinguish bare soil and impervious surfaces (e.g., roads and house roofs) in further studies. In practices, alternatively, dry point can be determined using the average of several maximum T_{soil} in order to reduce the effects from impervious surfaces.

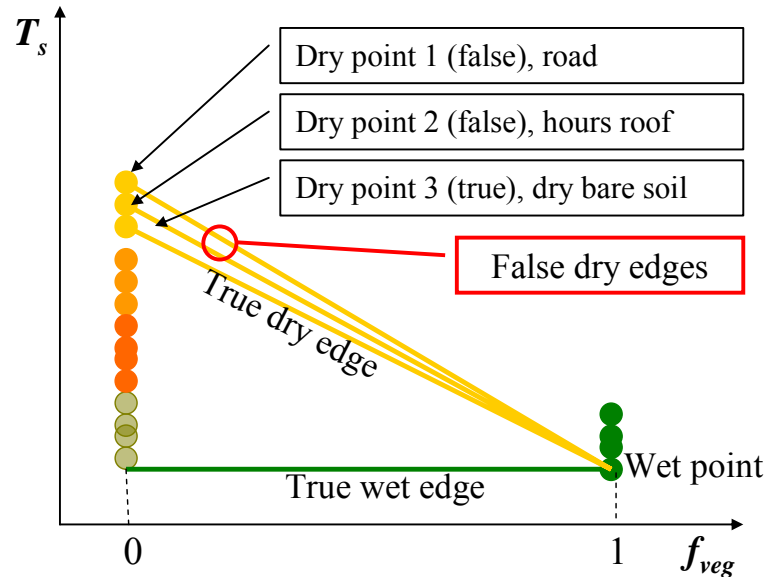


Fig.4-9 Description of several dry points in the same VI-Ts diagram

4.4.3 Limitations of the Proposed Method

To define an ideal VI-Ts diagram, the traditional method requires the full and continuous ranges of land surface moisture and VI (Nemani et al., 1993; Sandholt et al., 2002; Verstraeten et al., 2005). It needs enough heterogeneity of land surface moisture and vegetation cover within a limited sampling window. Sometimes, however, these conditions are difficult to meet in practice. For example, narrow ranges of VI resulted in large errors of T_{s_wet} by the traditional method on Mar. 27, Jun. 28 and Dec. 26 in 2003 in this study. The advantage of our proposed method is that it can relax the above limitations. If vegetation and soil information at a subpixel scale within a sampling window can be obtained, the nearly “true” dry and wet points will be found, and then a VI-Ts diagram will be easily defined. However, the proposed method will be helpless to define a VI-Ts diagram if the land cover is entirely homogenous within the sampling window, such as continuous bare soil (e.g., North African and Mid-Asian deserts) and vegetation (e.g., tropical and boreal forests) regions. In these regions, all pixels within the

sample window will cluster near dry or wet points (no wet point in desert regions, no dry point in forest regions). In applications, if such a cluster occurs in the VI-Ts diagram, it will also contribute to studies about land surface energy balance. The cluster near dry point indicates almost no latent heat partitioned from land surface available energy, while the cluster near wet point indicates almost no sensible heat partitioned from land surface available energy. Even if the land surface is a mixture of bare soil and vegetation, the sampling window should still cover dry bare soil. Vegetation such as forest, grass and crop can be easily found from a mixed land surface. Dry bare soil is also easily found in arid or semiarid areas. However, if the land surface is fully wet across the entire sampling window, such as in humid areas, it is impossible to find dry soil even at subpixel scale. In this case, the VI-Ts scatter plot looks like a horizontal line (no dry point in humid areas), and Ts of all pixels within the sampling window are close to air temperature (Prihodko and Goward, 1997). Almost all available energy of land surface is transferred to latent heat in such a case. In brief, our proposed method cannot define a triangular VI-Ts diagram without dry and wet points. Our study area is a typical semiarid agricultural landscape (a mixture of bare soil and crop), so our proposed method can obtain dry and wet points with good accuracies through the whole year in this study.

4.5 Conclusion

The traditional method can not always define a reasonable VI-Ts diagram within a limited sampling window. It is invalid in two cases of rainy season and narrow range of VI. In this study, therefore, a new method was proposed to define a VI-Ts diagram using dry and wet points from the subpixel information of vegetation and soil. The VI-Ts diagram defined by the proposed method is close to that defined using the ASTER_Ts of pure vegetation and soil. The proposed method can obtain “true” dry and wet points with respective average accuracies of 0.95 °C and 0.82 °C through the whole year of 2003 in our study area. This indicates that our proposed method can define “true” VI-Ts diagrams in our study area through the whole year, even in two cases of rainy season and narrow range of vegetation index. In applications, two limitations of the proposed method should be noted. A triangular VI-Ts diagram cannot be obtained if one of dry and wet points is absent. The other is that some false dry points may be involved in or near urban areas.

References

- Archer, N. A. L., & Jones, H. G. (2006). Integrating hyperspectral imagery at different scales to estimate component surface temperatures. *International Journal of Remote Sensing*, 27 (11), 2141-2159.
- Boegh, E., Soegaard, H., & Thomsen, A. (2002). Evaluating evapotranspiration rates and surface conditions using Landsat TM to estimate atmospheric resistance and surface resistance. *Remote Sensing of Environment*, 79 (2-3), 329-343.
- Buheaosier, Tsuchiya, K., Kaneko, M., & Sung, S. J. (2003). Comparison of image data acquired with AVHRR, MODIS, ETM+ and ASTER over Hokkaido, Japan. *Advance Space Research*, 32 (11), 2211-2216.
- Cain, S. (2004). Bayesian-based subpixel brightness temperature estimation from multichannel infrared GOES radiometer data. *IEEE Transactions on Geoscience and Remote Sensing*, 42 (1), 188-201.
- Carlson, T. N., Gillies, R. R., & Schmugge, T. J. (1995). An interpretation of methodologies for indirect measurement of soil water content. *Agricultural and Forest Meteorology*, 77, 191-205.
- Dozier, J. (1981). A method for satellite identification of surface temperature fields of subpixel resolution. *Remote Sensing of Environment*, 11, 221-229.
- Gillespie, A., Rokugawa, S., Matsunaga, T., Cothorn, S., Hook, S., & Kahle, A. (1998). A temperature and emissivity separation algorithm for Advanced Spaceborne Thermal Emission and Reflection radiometer (ASTER) images. *IEEE Transactions on Geoscience and Remote Sensing*, 36, 1113-1126.
- Gillies, R. R., Carlson, T. N., Cui, J., Kustas, W. P., & Humes, K. S. (1997). A verification of the 'triangle' method for obtaining surface soil water content and energy fluxes from remote measurements of the Normalized Difference Vegetation Index (NDVI) and surface radiant temperature. *International Journal of Remote Sensing*, 18 (15), 3145-3166.
- Heilman, J. L., Heilman, W. E., & Moore, D. G. (1981). Remote sensing of canopy temperature at incomplete cover. *Agronomy Journal*, 73, 403-406.

- Iwasaki, A., & Fujisada, H. (2005). ASTER geometric performance. *IEEE Transactions on Geoscience and Remote Sensing*, 43(12), 2700-2706.
- Jacob, F., Petitcolin, F., Schmugge, T., Vermote, É., French, A., & Ogawa, K. (2004). Comparison of land surface emissivity and radiometric temperature derived from MODIS and ASTER sensors. *Remote Sensing of Environment*, 90, 137-152.
- Jiménez-Muñoz, J. C., Sobrino, J. A., Gillespie, A., Sabol, D., & Gustafson, W. T. (2006). Improved land surface emissivities over agricultural areas using ASTER NDVI. *Remote Sensing of Environment*, 103, 474-487.
- Liu, Y., Hiyama, T., & Yamaguchi, Y. (2006). Scaling of land surface temperature using satellite data: A case examination on ASTER and MODIS products over a heterogeneous terrain area. *Remote Sensing of Environment*, 105, 115-128.
- Loheide II, S. P., & Gorelick, S. M. (2005). A local-scale, high-resolution evapotranspiration mapping algorithm (ETMA) with hydroecological applications at riparian meadow restoration site. *Remote Sensing of Environment*, 98, 182-200.
- Lu, D., & Weng, Q. (2006). Spectral mixture analysis of ASTER images for examining the relationship between urban thermal features and biophysical descriptors in Indianapolis, Indiana, USA. *Remote Sensing of Environment*, 104, 157-167.
- Moran, M. S., Clarke, T. R., Inoue, Y., & Vidal, A. (1994). Estimating crop water deficit using the relation between surface-air temperature and spectral vegetation index. *Remote Sensing of Environment*, 49, 246-263.
- Nemani, R. R., Pierce, L., Running, S. W., & Goward, S. (1993). Developing satellite-derived estimates of surface moisture status. *Journal of Applied Meteorology*, 32 (3), 548-557.
- Nishida, K., Nemani, R. R., Running, S. W., & Glassy, J. M. (2003). An operational remote sensing algorithm of land surface evaporation. *Journal of Geophysical Research*, 108 (D9), 4270, DOI: 10.1029/2002JD002062.

- Prihodko, L., & Goward, S. N. (1997). Estimation of air temperature from remotely sensed surface observations. *Remote Sensing of Environment*, 60 (3), 335-346.
- Sandholt, I., Rasmussen, K., & Andersen, J. (2002). A simple interpretation of the surface temperature/vegetation index space for assessment of surface moisture status. *Remote Sensing of Environment*, 79, 213-224.
- Small, C. (2006). Comparative analysis of urban reflectance and surface temperature. *Remote Sensing of Environment*, 104, 168-189.
- Smith, R. C. G., & Choudhury, B. J. (1991). Analysis of normalized difference and surface temperature observations over southeastern Australia. *International Journal of Remote Sensing*, 12 (10), 2021-2044.
- Venturini, V., Bisht, G., Islam, S., & Jiang, L. (2004). Comparison of evaporative fractions estimated from AVHRR and MODIS sensors over South Florida. *Remote Sensing of Environment*, 93, 77-86.
- Verstraeten, W. W., Veroustraete, F., & Feyen, J. (2005). Estimating ET of European forests from NOAA-imagery at satellite overpass time: Towards an operational processing chain for integrated optical and thermal sensor data products. *Remote Sensing of Environment*, 96, 256-276.
- Wan, Z., Zhang, Y., Zhang, Q., & Li, Z. (2004). Quality assessment and validation of the MODIS global land surface temperature. *International Journal of Remote Sensing*, 25(1), 261-274.
- Wang, Q., Watanabe, M., & Ouyang, Z. 2005. Simulation of water and carbon fluxes using BIOME-BGC model over crops in China. *Agricultural and Forest Meteorology*, 131, 209-224.
- Wolfe, R. E., Nishihama, M., Fleig, A. J., Kuyper, J. A., Roy, D. P., Storey, J. C., & Patt, F. S. (2002). Achieving sub-pixel geolocation accuracy in support of MODIS land science. *Remote Sensing of Environment*, 83 (1-2), 31-49.
- Xu, X., Chen, L., & Zhuang, J. (2001). Genetic inverse algorithm for retrieval of component temperature of mixed pixel by multi-angle thermal infrared remote sensing data. *Science in China, D*, 44 (4), 363-372.

- Zhang, R., Sun, X., & Liu, J. (2003). Determination of regional distribution of crop transpiration and soil water use efficiency using quantitative remote sensing data through inversion. *Science in China, D*, 46 (1), 10-22.
- Zhang, R., Sun, X., Wang, W., Xu, J., Zhu, Z., & Tian, J. (2005). An operational two-layer remote sensing model to estimate surface flux in regional scale: Physical background. *Science in China, Series D Earth Science*, 48 supplement, 225-244.

Chapter 5

Mapping *ET* from Satellite Data by Sim-ReSET Model and *in situ* Validation

5.1 Introduction

Once air temperature and a dry bare soil pixel are obtained from the VI-Ts diagram, the Sim-ReSET model can run based solely on remote sensing data. The MODIS datasets used in Chapter 4 were reused for mapping *ET* by the Sim-ReSET model in the North China Plain in 2003. Ground data were also collected for the sensitivity analysis and validation of the Sim-ReSET model in the Yucheng Experimental Station. In order to compare with previous *ET* models based on remote sensing, *ET* was also estimated using the original MOD16 model and the same MODIS datasets in 2003.

5.2 Mapping *ET* from satellite data by the Sim-ReSET model

5.2.1 Study area and data

Excluding remote sensing images with cloud cover above the Yucheng Experimental Station, 12-day remote sensing data were selected over the North China Plain through 2003, including MOD11A1-instantaneous T_s and MOD09-reflectance data on DOY 86, 115, 120, 129, 133, 175, 179, 264, 294, 296, 326, and 360, where DOY stands for day of year. MOD12-land cover of the study area was also collected in 2003. MOD09, MOD11A1 and MOD12 data were downloaded from the Land Processes Distributed Active Archive Center (<http://edcimswww.cr.usgs.gov/pub/imswelcome/>). NDVI was calculated using

MOD09-reflectance data. Albedo was obtained from MOD09 reflectance data using the method proposed by Liang (2000).

5.2.2 Mapping *ET*

Fig. 5-1 is the flowchart of mapping *ET* using the Sim-ReSET model. Albedo and vegetation index can be obtained directly from MOD34 and MOD13 products. In this study, albedo and NDVI were calculated using narrow band reflectances. In order to keep the Sim-ReSET model simple and practical, air vapor pressure was assumed as a constant of 60% although it can be collected from MOD07-atmospheric profile.

R_n , G , ET and EF were obtained as the outputs of the Sim-ReSET model over the North China Plain through 2003. Examples of R_n , G , ET and EF on DOY133 of 2003 over the North China Plain were shown in this chapter (Fig. 5-2; Fig. 5-3; Fig. 5-4; Fig. 5-5).

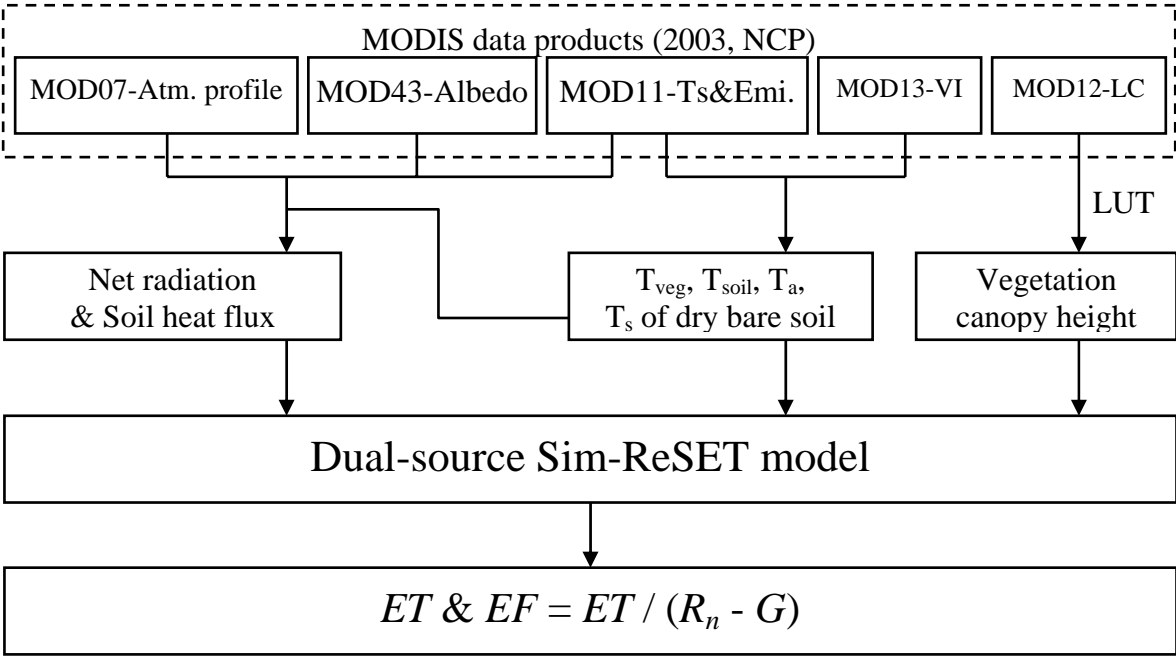


Fig.5-1 Flowchart of the Sim-ReSET model.

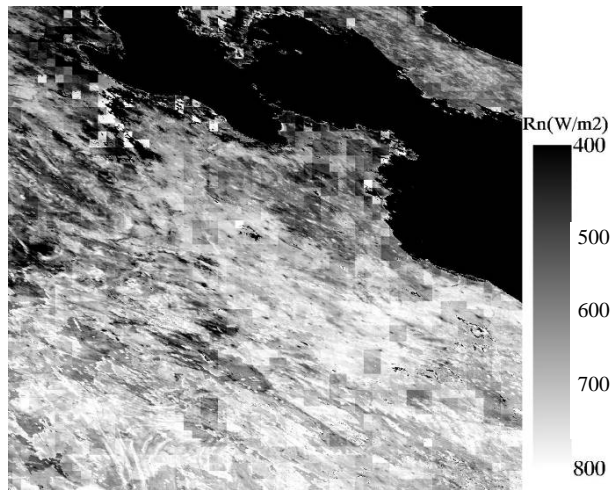


Fig.5-2 Net radiation map over the North China Plain on DOY133 of 2003.

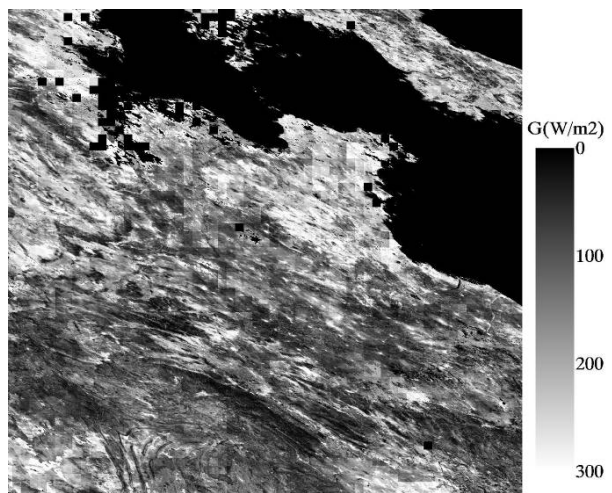


Fig.5-3 Soil heat flux map over the North China Plain on DOY133 of 2003.

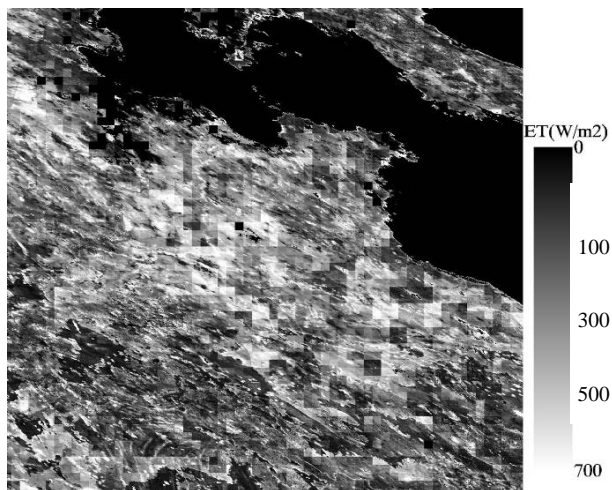


Fig.5-4 Evapotranspiration map over the North China Plain on DOY133 of 2003.

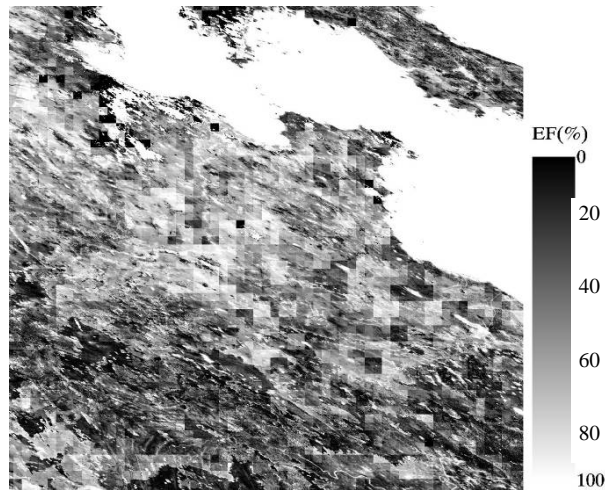


Fig.5-5 Evaporation fraction map over the North China Plain on DOY133 of 2003.

5.3 Sensitivity analysis and validation

Although land surface temperature, emissivity and reflectance have been well retrieved from remote sensing, there are still some errors due to the atmospheric effect. With the purposes of sensitivity analysis and mechanism evaluation of the Sim-ReSET model without the effect of potential errors from RS data, firstly, only intensive ground data were used to validate the Sim-ReSET model. Then, remote sensing-based outputs of the Sim-ReSET model were validated using ground observations.

5.3.1 Dry point experiment and data used for validation without using remote sensing data

A dry point is required in the Sim-ReSET model. In this study, a dry point was designed in the Yucheng Experimental Station. A 20 m × 20m bare soil surface was plotted for the experiment. A pole was set at the center of this plot that was 500 m west to the APEIS-Flux station. The membrane of poly-chlorothene was spread at 5 cm soil depth around the pole in order to cut the upgoing soil water (Fig. 5-6). Downward and upward shortwave radiation, downward and upward long wave radiation, soil heat flux, surface temperature, and soil surface water content were measured from March 2006 to April 2007. The datasets were shown in Fig. 5-7, 5-8, and 5-9, and all the datasets were collected with good qualities.

From Fig. 5-9, soil surface water content was close to the wilting point continuously during the period of DOY 263-319, 2006. The measurements during this period were selected for validation as well as the same datasets (plus air temperature, and sensible and latent heat flux by eddy covariance system) collected from the APEIS-flux station in the cotton field.

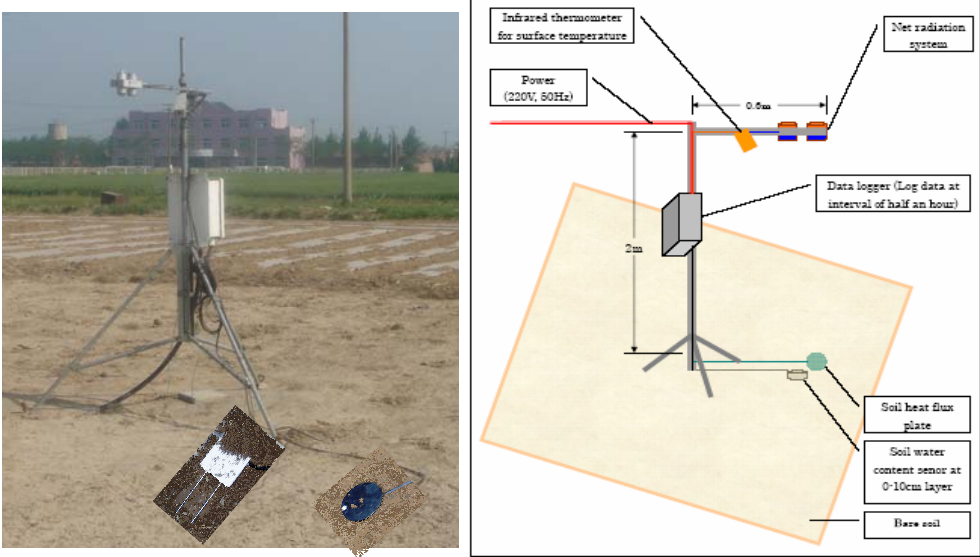


Fig.5-6 Dry point experiment design.

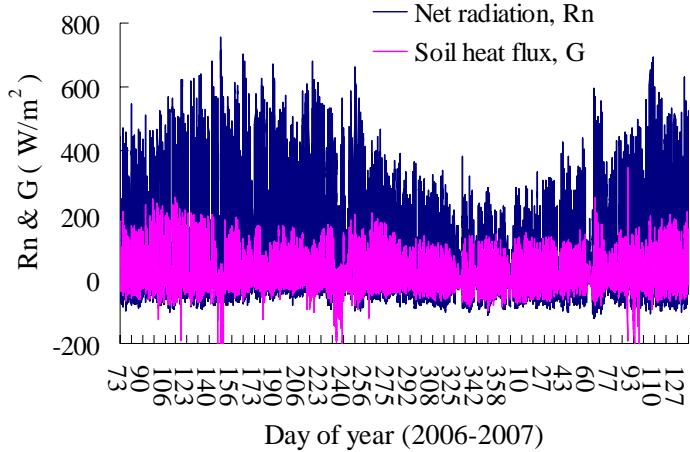


Fig.5-7 Time series of net radiation and soil heat flux.

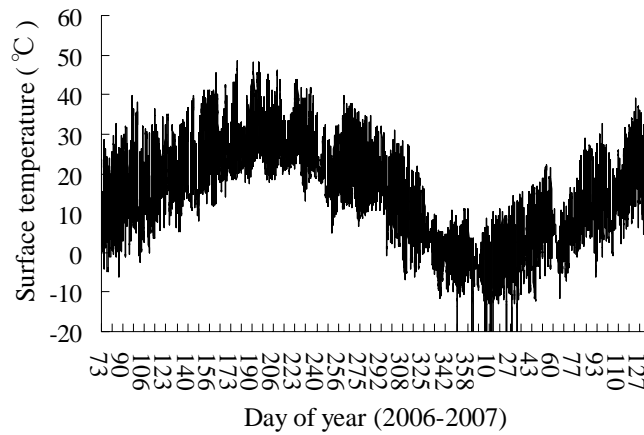


Fig.5-8 Time series of surface temperature.

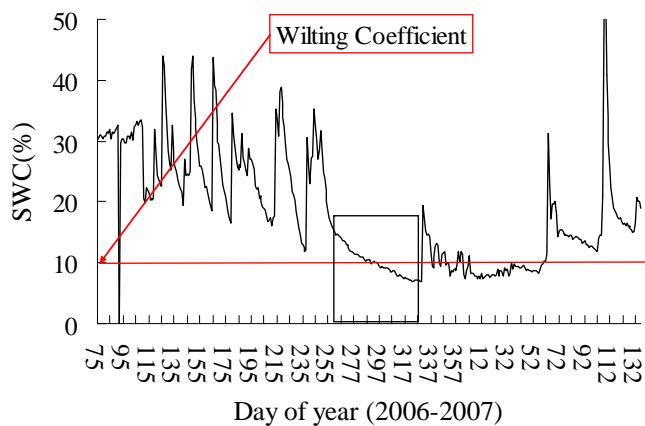


Fig.5-9 Time series of soil surface water content.

5.3.2 Validation without using remote sensing data

Using equation (3-12) and (3-14c) with two input datasets:

- (1) Dry point – net radiation, soil heat flux, and surface temperature;
- (2) APEIS-Flux station – net radiation, soil heat flux, surface temperature, air temperature, and cotton canopy height; *ET* (or latent heat flux) can be obtained over cotton canopies around the APEIS-Flux station (Fig. 5-10). By the analysis of the relationship between the upper boundary of the ASL (*A*) and the sensible heat transfer function (Fig. 5-11), it was found that the sensible heat transfer function became nearly stable when *A* was greater than 100 m. Further more, the MOS theory is only valid within the ASL (Brutsaert, 1998). In the calculations, therefore, *A* was set as 100 m. The cotton canopy height was set as 1.25 m according to the measurement. By comparing the ground-based *ET* estimations to the *ET*

measurements from the eddy covariance system (Fig. 5-12), the result showed that the estimations by the Sim-ReSET model agreed well with the measurements by the eddy covariance system, and that the root mean square error (RMSE) was 48.94 W/m^2 . This error is due probably to measurement errors of observational sensors, the ignorance of atmosphere atmospheric stratification corrections, and the inconsistency between the flux fetch and the sensed fields of micrometeorological factors.



Fig.5-10 The APEIS-Flux station in the cotton field.

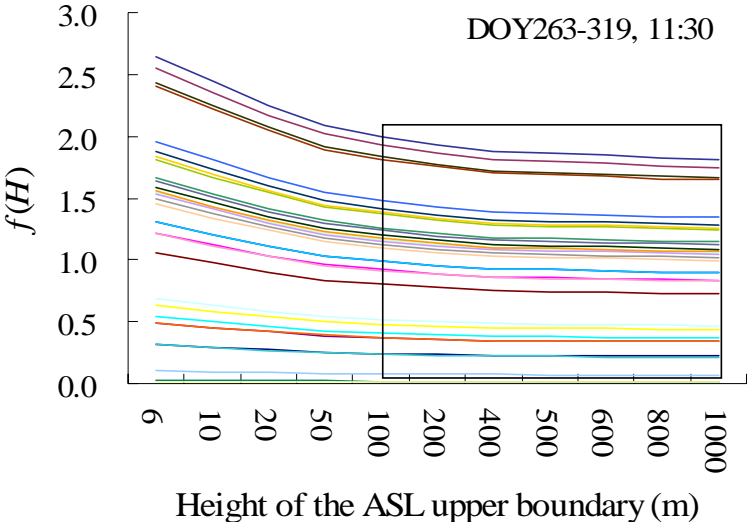


Fig.5-11 Relationship between the height of the upper boundary of the ASL and the sensible heat transfer function. One line of $f(H)$ was estimated using the dataset at 11:30 of one day from DOY263-319.

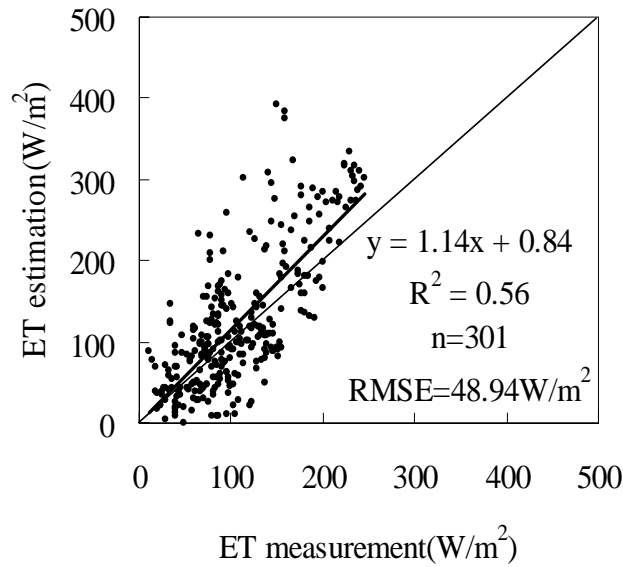


Fig.5-12 Comparison of *ET* between the measurements by the eddy covariance system and the estimations using the Sim-ReSET model and ground data.

5.3.3 Sensitivity analysis

There are eight key variables in Sim-ReSET model. The sensitivities of these variables were tested using the ground data during the period of DOY 263-319, 2006. The strategy of sensitivity analysis is to compare *ET* estimations without any changed variable to those while only one variable for the sensitivity analysis is changed by $\pm 10\%$. The results are shown in [Table 5-1](#) and [Fig. 5-13](#). The variables related to temperature had high sensitivities for *ET* estimations. A small change of temperature resulted in a large change of *ET* estimation. In equation (3-12) and (3-13), T_a and T_{sd} were obtained based on T_s while T_s was retrieved from remote sensing, so probable errors from sensor deviation, atmospheric effect and retrieving algorithm of T_s will be the same for T_a , T_{sd} and T_s . These probable errors can be avoided because T_a , T_{sd} and T_s are used in a difference-ratio form, $(T_s - T_a)/(T_{sd} - T_a)$, in equation (3-12) and (3-13). Hence, potential error sources related to temperature mainly come from the determinations of T_a , T_{sd} , and the VI-Ts diagram.

Net radiation is the energy source of evapotranspiration, so its accuracy relates to the *ET* accuracy. From [Table 5-1](#), $\pm 10\%$ changes of net radiation resulted in -23.15% and 38.68% changes of *ET* estimation. From [Fig. 5-13](#), it was found that *ET*

estimations were insensitive to canopy height and soil heat flux. Therefore, the potential error of canopy height obtained from a look-up table will not influence the *ET* accuracy significantly.

Table 5-1 Results of sensitivity analyses for variables in Sim-ReSET model.

Input Variables	Increase/decrease 10%	Ratio (%)
<i>h</i>	+10%	-6.35
	-10%	11.26
<i>T_s</i>	+10%	-81.59
	-10%	180.27
<i>T_a</i>	+10%	149.52
	-10%	-78.54
<i>T_{sd}</i>	+10%	61.86
	-10%	-24.17
<i>R_{nd}</i>	+10%	-14.69
	-10%	35.02
<i>G_d</i>	+10%	14.51
	-10%	-6.93
<i>R_n</i>	+10%	38.68
	-10%	-23.15
<i>G</i>	+10%	-4.97
	-10%	8.17

Ratio = 100 % × (*ET* with one changed variable – *ET* without any changed variable) / *ET* without any changed variable

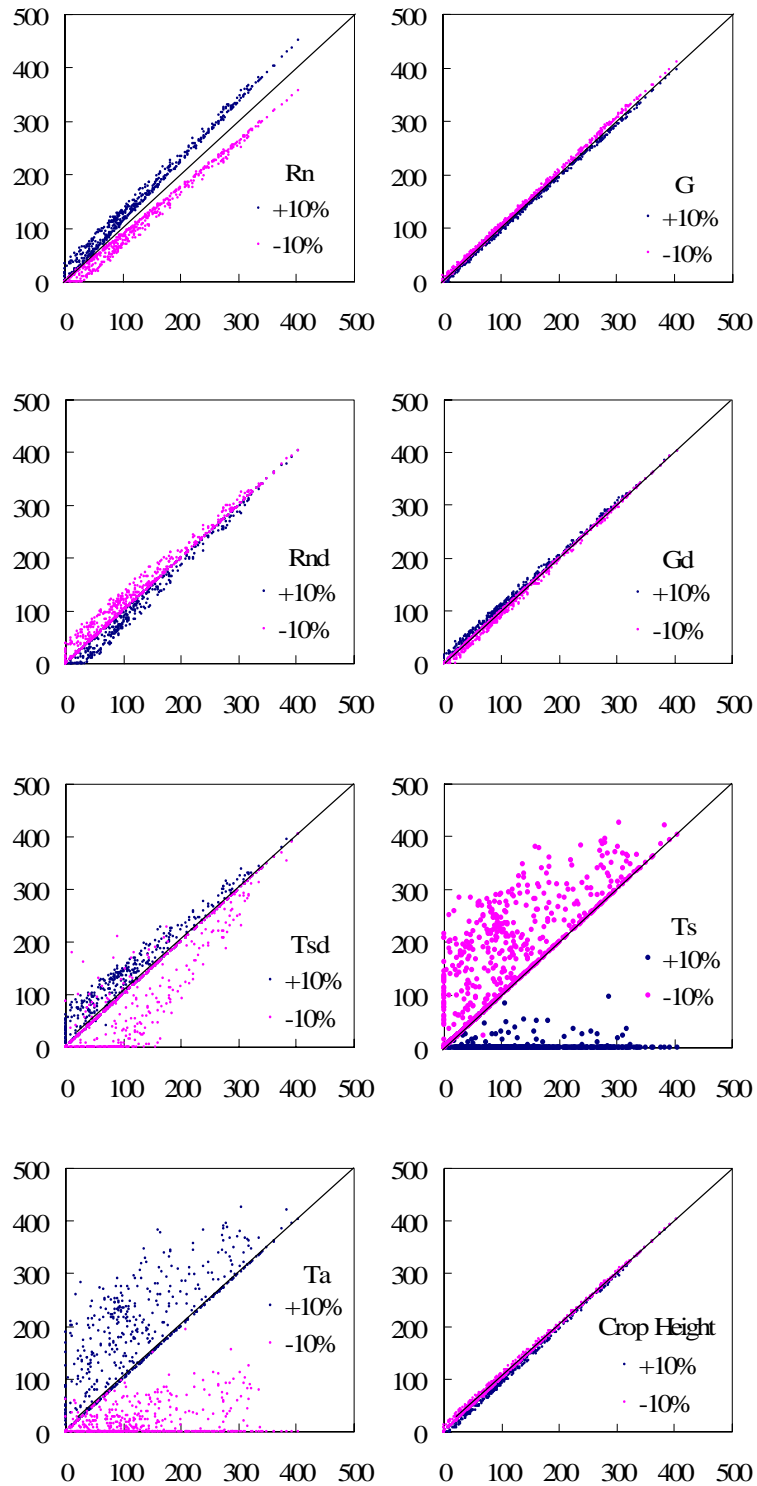


Fig.5-13 Sensitivity analyses of key variables in the Sim-ReSET model. X-axis is ET without changing any variable. Y-axis is ET while changing only one variable.

5.3.4 Validation using remote sensing and ground data

R_n , G , ET and H were collected from the APEIS-Flux station in the Yucheng Experimental Station according to the date and time when remote sensing data were observed in 2003 (Table 4-2). The Terra satellite passes over the study area

near 11:00 of local standard time. A 3 pixels \times 3 pixels window corresponding to the geographic location of the Yucheng Experimental Station was used to average the estimations of R_n , G , ET and EF from the Sim-ReSET model, and the estimations of ET and EF from the MOD16 model. Then the averaged values were compared with ground observations.

Net radiation — R_n

From Fig. 5-14, net radiation estimated by Sim-ReSET model was close to that observed on the ground. R^2 between them was 0.93, and RMSE was 45.54 W/m^2 . This estimation accuracy was consistent with the results in previous studies (Jacobs et al., 2000; Ma et al., 2002; Norman et al., 2002; Bisht et al., 2005). In a simple manner, 60% of relative humidity was assumed in the Sim-ReSET model. If the true values of relative humidity were used, a better net radiation would be obtained.

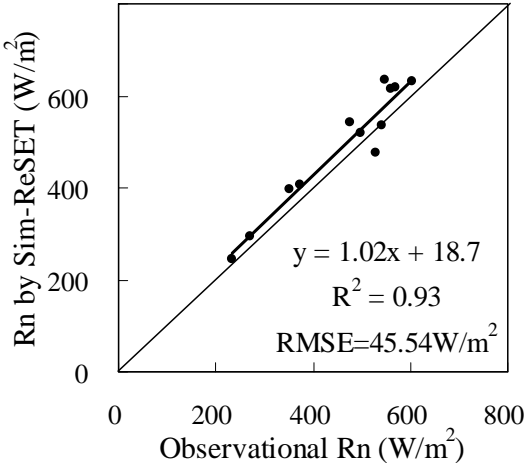


Fig.5-14 Comparison of net radiation estimated by the Sim-ReSET model and that measured on the ground.

Soil heat flux — G

From Fig. 5-15, soil heat flux estimated by the Sim-ReSET model was close to that observed on the ground. R^2 between them was 0.84, and RMSE was 29.67 W/m^2 .

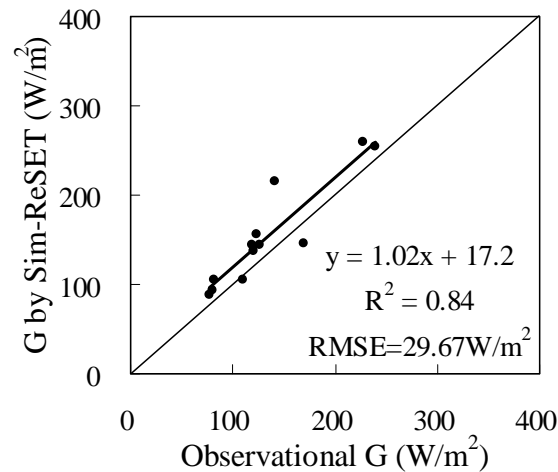


Fig.5-15 Comparison of soil heat flux estimated by the Sim-ReSET model and that measured on the ground.

Evapotranspiration — *ET*

From Fig. 5-16a, *ET* estimated by the Sim-ReSET model agreed with that observed on the ground. R^2 between them was 0.92, and RMSE was 58.74 W/m². Jiang et al. (2004) summarized the potential error sources in *ET* estimations, and the results showed that the error was typically from 20 W/m² to 70 W/m² for *ET* estimations. Hence, *ET* estimated by the Sim-ReSET model was comparable. R^2 and RMSE between *ET* estimated by the original MOD16 model and the observational *ET* were 0.84 and 65.48 W/m² (Fig. 5-16b). This result was not as good as that of the Sim-ReSET model mainly because canopy resistance was largely overestimated ($f_1(T_a) \rightarrow 0$ in equation (2-4), then $r_c \rightarrow 100000$ m/s in equation (2-3)), and then *ET* was largely underestimated over winter wheat fields by the MOD16 model in winter.

In Fig. 5-16, there were a few positive biases of *ET* estimations from both the Sim-ReSET model and the MOD16 model. From Chapter 2, it was known that *ET* was easily overestimated by the MOD16 model because the unstable atmospheric stratification correction was not considered. In order to keep the Sim-ReSET model simple and practical, the atmospheric stratification correction wasn't considered presently. Therefore, *ET* was also a little overestimated by the simple version of the Sim-ReSET model, and a positive bias was caused in Fig. 5-16a.

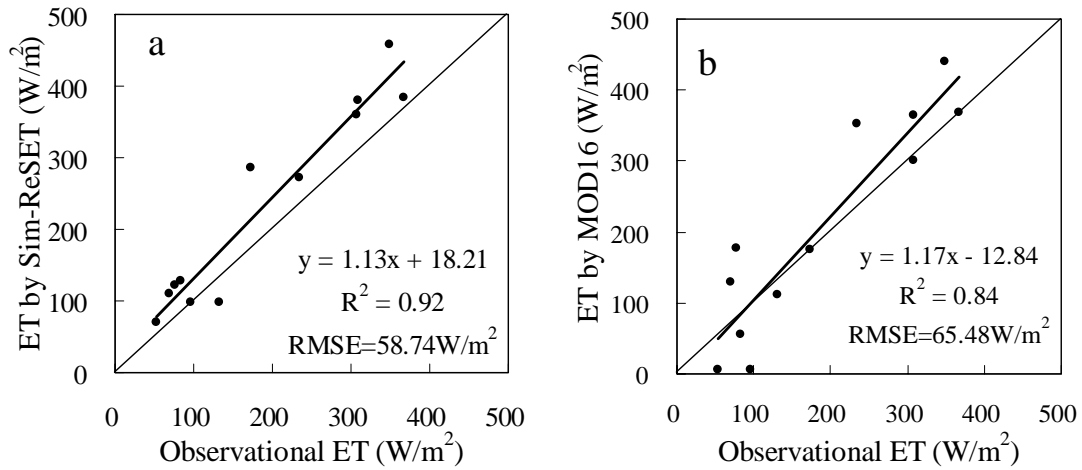


Fig.5-16 Comparison of *ET* estimated by Sim-ReSET model (a) and by the MOD16 model (b) using the measured *ET* on the ground.

Evaporation fraction — *EF*

From Fig. 5-17a, *EF* estimated by the Sim-ReSET model was also in good agreement with that observed on the ground. R^2 between them was 0.81, and RMSE was 10.82%. For *EF* estimated by the MOD16 model, R^2 between them was 0.74, and RMSE was 15.95%. From Fig. 5-17b, two points were far from 1: 1 line because canopy resistance of winter wheat was largely overestimated by the MOD16 in winter.

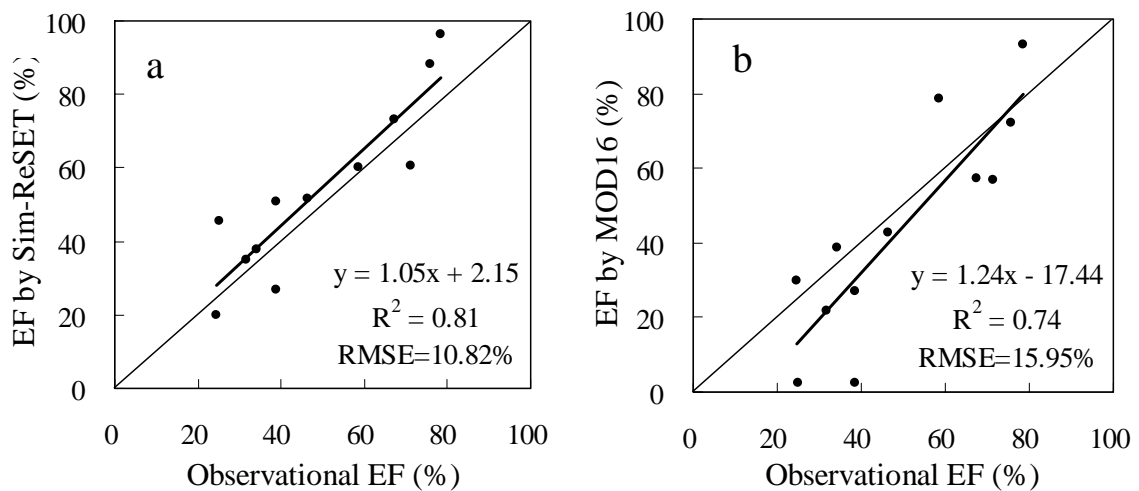


Fig.5-17 Comparison of *EF* estimated by the Sim-ReSET model (a) and by the MOD16 model (b) using the measured *EF* on the ground.

5.4 Conclusions

The Sim-ReSET model was validated using the ground observations and MODIS remote sensing data. It was also compared with the MOD16 model in the study area in 2003. The results showed that output accuracies of the Sim-ReSET model were close to those of other models or algorithms depending on ground data, and that the MOD16 could not obtain the true ET over winter wheat fields in winter because canopy resistance was largely overestimated. In addition, the results of sensitivity analyses showed that the most sensitive variables were temperatures in the Sim-ReSET model, and that vegetation canopy height had a negligible effect on the model. With the purpose of keeping the Sim-ReSET model simple and practical, atmospheric stratification corrections were not considered, and then *ET* showed a few overestimations in the Sim-ReSET model, especially when solar radiation and air temperature were high (Fig. 5-16 and 5-17). In future studies, this simple version of the Sim-ReSET model can be revised to combine atmospheric stratification corrections according to the requirements of applications.

References

- Bisht, G., Venturini, V., Islam, S., & Jiang L. (2005). Estimation of the net radiation using MODIS (Moderate Resolution Imaging Spectroradiometer) data for clear sky days. *Remote Sensing of Environment*, 97, 52-67.
- Brutsaert, W. (1998). Land-surface water vapor and sensible heat flux: spatial variability, homogeneity, and measurement scales. *Water Resources Research*, 34 (10), 2433-2442.
- Jacobs, J. M., Myers, D. A., Anderson, M. C., & Diak, G. R. (2000). GOES surface insolation to estimate wetlands evapotranspiration. *Journal of Hydrology*, 266, 53-65.
- Jiang, L., Islam, S., & Carlson, T. N. (2004). Uncertainties in latent heat flux measurement and estimation: implications for using a simplified approach with remote sensing data. *Canadian Journal of Remote Sensing*, 30(5): 769-787.
- Liang, S. L. (2000). Narrowband to broadband conversions of land surface albedo: I Algorithms. *Remote Sensing of Environment*, 76, 213-238.
- Ma, Y., Su, Z., Li, Z., Koike, T., & Menenti, M. (2002). Determination of regional net radiation and soil heat flux over a heterogeneous landscape of the Tibetan Plateau. *Hydrological Processes*, 16, 2963-2971.
- Norman, J. M., Anderson, M. C., Kustas, W. C., French, A. N., Mecikalski, J., Torn, R., et al. (2003). Remote sensing of surface energy fluxes at 10¹-m pixel resolutions. *Water Resources Research*, 39(8), 1221.

Chapter 6

General Conclusions

Satellite remote sensing can regularly provide unprecedented coverage data for *ET* estimation on large spatial scales. If some models or algorithms without using ground data are available, a real-time routine *ET* will be obtained. For this purpose, firstly, a previous remote sensing *ET* model (MOD16) was evaluated in this study. The MOD16 model minimized the use of ground data, but its accurate *ET* estimation still depended on ground data. Thus a new *ET* model (Sim-ReSET) only using remote sensing data was developed, and then was validated in the NCP. Air temperature and a dry bare soil pixel were required in the Sim-ReSET model, which were obtained by a new proposed method using subpixel information of surface temperature.

(1) Evaluation of a previous evapotranspiration model over winter wheat fields in the NCP (MOD16)

Intensive ground data were used to evaluate the MOD16 model and its sub models in winter wheat fields in the NCP in 2002, including the radiation budget on the land surface, canopy resistance and aerodynamic resistance. By comparing with field observations, it was found that downward shortwave radiation in the original model was close to the observations only on cloud-free days. Because vegetation physiological temperatures and minimum canopy resistance were considered as constants, a larger error of canopy resistance was produced when LAI is less than 2.5 in winter wheat fields. Because strong unstable thermal stratification above dry

bare soil surface was ignored, wind speed above bare soil surface with maximum surface temperature was overestimated, and aerodynamic resistance above vegetation surface was underestimated. If canopy resistance and net radiation on cloudy days were estimated using ground data, and if aerodynamic resistance was estimated using sophisticated equations and ground data, EF and ET became more consistent with both observations from the eddy covariance system and estimations from the Penman-Monteith method. The mean absolute error of EF is 0.1, the mean relative error is 26% and the correlation coefficient is 0.88. The mean absolute error of ET is 21.93 W/m^2 , the mean relative error is 21.8% and its slope and R^2 of a 1:1 line analysis are 1.02 and 0.91, respectively. These results show that the MOD16 model performs well when mapping ET if the ground data are available.

(2) Development of Sim-ReSET model: algorithm & parameterizations

A dual-source model, Sim-ReSET, was developed based solely on remote sensing data. A dry point was introduced to remove the requirement of aerodynamic resistance by means of two hypotheses in the model. Canopy resistance was also avoided by estimating ET as a residual of the land surface energy balance equation. Therefore, input requirements for the Sim-ReSET model are only net radiation, soil heat flux, canopy height, surface temperature (T_s), air temperature, and parameters related to dry point that all can be obtained from RS observations. In the Sim-ReSET model, net radiation was estimated by an existing simple method; bare soil heat flux was estimated using a scaled temperature; and canopy height was obtained from a look-up table based on the IGBP classification. Dry point and air temperature were obtained from the VI- T_s diagram. Air temperature is assumed to be close to T_s of wet point in the VI- T_s diagram.

(3) A new method to obtain “dry & wet points” for Sim-ReSET model

If both dry and wet points can be obtained, a right triangle of VI-Ts diagram can be readily defined, and air temperature and surface temperature of dry point are also available for the Sim-ReSET model. The traditional method cannot define a correct VI-Ts diagram in both cases of rainy season and narrow range of VI. A new method based on subpixel information of MODIS Ts was proposed to define the VI-Ts diagram in this study. This method was tested in a 30 km×30 km area in the NCP through 2003 using ground data and MODIS RS data. Wet and dry points obtained from the proposed method were compared with those obtained from ground data. The results showed that the proposed method could obtain nearly true dry and wet points, and VI-Ts diagrams throughout the whole year, even for both cases of rainy season and narrow range of VI.

(4) Mapping *ET* from satellite data by Sim-ReSET model and *in situ* validation

The result of validation without using remote sensing data showed that the Sim-ReSET model could obtain *ET* with RMSE of 48.94 W/m² over a cotton field. Additionally, the results of sensitivity analyses showed that the most sensitive variables were temperatures in the Sim-ReSET model, and that vegetation canopy height had a negligible effect on the model. The Sim-ReSET model and the original MOD16 model were used to map *ET* over the NCP through 2003 using MODIS products. Pixel-based *ET* was validated using the ground flux data obtained from the eddy covariance system. Results showed that the accuracy of the Sim-ReSET model was close to those of other models or algorithms depending on ground data. *ET* RMSE of the Sim-ReSET model was 58.74 W/m² while *ET* RMSE of the original MOD16 model was 65.48 W/m².

(5) Limitations and application scopes of the Sim-ReSET model

The purpose of this study is to develop a simple and practical *ET* model to obtain a real-time routine *ET* only using remote sensing data. Therefore, atmospheric stratification corrections were ignored in the Sim-ReSET model, which resulted in a few overestimations of *ET*, especially when solar radiation and air temperature were high. However, these biases were relatively small in this study. In future studies, this simple version of the Sim-ReSET model can be updated to combine atmospheric stratification corrections according to the requirements of applications. *ET* was very sensitive to air temperature and surface temperature of dry bare soil in the Sim-ReSET model. If both of them are not correctly determined in the VI-Ts diagram, a false *ET* will be obtained. In this study, a new method was proposed to find dry and wet points, and then to define the VI-Ts diagram using subpixel information. In some cases, however, dry and wet points are not easily found even at subpixel scale, such as desert and rain forest. If the Sim-ReSET model is directly used in these cases, the results must be false. In the program of the Sim-ReSET model, a strategy was proposed to solve this problem using subpixel information. If the difference of surface temperatures between wet and dry points are less than 2°C, *ET* equals to 0 when both VI and the range of VI are less than 0.2; *ET* equals to the potential *ET* when the range of VI is less than 0.2, and VI is great than 0.8. Here, VI is vegetation cover fraction. My study area was in a semiarid agricultural region, and dry and wet points were easily found at pixel or subpixel scales, so these extreme cases were not met in this study.

The main inputs to the Sim-ReSET model are surface temperature and vegetation index. On cloudy days, surface temperature cannot be observed by sensors onboard the satellite. Furthermore, solar radiation is not readily estimated on cloudy days, too. Therefore, the Sim-ReSET method can be used only on cloud-free days.

(6) Future studies

The Sim-ReSET model described in this dissertation is a simplified version for *ET* and *EF* estimations on cloud-free days. It was validated only in the North China Plain, a semiarid agricultural region. My final purpose is to develop a robust and practical model for global *ET* and *EF* estimations independent of ground data. Therefore, several further studies should be done in the future.

- (i) To integrate a simple scheme of atmospheric stratification corrections into the Sim-ReSET model. As described in Chapter 2, atmospheric stratification corrections require many intensive ground data, such as air temperature profile, wind speed and canopy height. If these sophisticated atmospheric stratification corrections are used in the Sim-ReSET model, the model must depend on ground data, which will hamper its broad applications. Hence, a simple scheme of atmospheric stratification corrections is required. In this dissertation, canopy height was estimated using a LUT, air temperature profile was replaced by the difference of surface temperature and air temperature, and wind speed was avoided based on a reference dry point. However, wind speed is required again for atmospheric stratification corrections. In future, the study on this simple scheme of atmospheric stratification corrections should focus on the simplification of wind speed - related algorithms.
- (ii) To validate the Sim-ReSET model using more intensive ground data across diverse land covers. Presently, the Sim-ReSET model was validated only over crop fields in a semiarid agricultural region. In the future, other ground data will be collected for the model's validation from other 4 APEIS-Flux stations covering grassland, sparse shrub land, paddy and forest. These APEIS-Flux stations are running from 2002, which provide intensive micrometeorological data and eddy covariance data at a 30-minute interval.

- (iii) To consider an alternative method of *ET* and *EF* estimations in cloudy days. Only cloud-free estimates of *ET* and *EF* were generated and validated in my study. However, many water resource, agricultural and forest managements require routine *ET* even in cloudy and rainy days. Compared to the visible and infrared, microwaves have special properties that are important for remote sensing. Longer wavelength microwave radiation can penetrate through cloud cover, haze, dust, and all but the heaviest rainfall as the longer wavelengths are not susceptible to atmospheric scattering which affects shorter optical wavelengths. This property allows detection of microwave energy under almost all weather and environmental conditions so that data can be collected at any time. Future attempt is to use microwave technologies to retrieve land surface moisture and *ET* in cloudy days. Such studies have been included in the proposed HYDROS mission of NASA (<http://hydros.gsfc.nasa.gov/>).
- (iv) To output routine *ET* and *EF* from the Sim-ReSET model. Some satellite sensors, such as MODIS, can provide daily global coverage data. This is a reliable data source for routine *ET* estimations. After the Sim-ReSET model is intensively validated across diverse land covers, routine *ET* and *EF* are expected to be outputted from the Sim-ReSET model using MODIS data across East Asia.